UNIVERSITA' DEGLI STUDI DI PARMA
Dottorato di ricerca in
Scienza e Tecnologia dei Materiali Innovativi
Ciclo XXVI

New glycosylated materials for lectin inhibition, detection and targeting

Coordinatore:
Prof. Enrico Dalcanale

Tutor:
Prof. Alessandro Casnati
Dott. Francesco Sansone

Dottorando: Paola Fezzardi

2010-2013

Contents

Chapter 1:

Introduction

1.1 Glycobiology

Glycobiology is an interdisciplinary science, crossing the fields of chemistry, biology and medicine studying all the aspects of the structure, biosynthesis and functions of glycans widely distributed in nature. A very broad spectrum of functions have been assigned to glycans, besides the well-known, energetic and structural role they have.[1] Nowadays is well known that carbohydrates, together with nucleotides and amino acids, are one of the most important class of biomolecules in nature. In fact, they not only have an important structural and protecting role and are the main energy reserves of cells, but they are also involved in many important cellular processes thanks to specific interactions with different chemical or biological species as, for example, viruses, bacteria, proteins, nucleic acids, hormones and acting as mediators for cell-cells communication[2] (fig. 1.1). In most of such processes a carbohydrate ligand usually binds to a protein receptor.[3,4] Therefore there is an increasing interest in the synthesis of new neoglycoconjugates or high affinity mimics of native saccharides which could interfere in these recognition processes; such compounds have potential therapeutic value in the treatment of infections and of a wide range of human tumours. The study and understanding of protein–carbohydrate interactions is, for these reasons, really important.

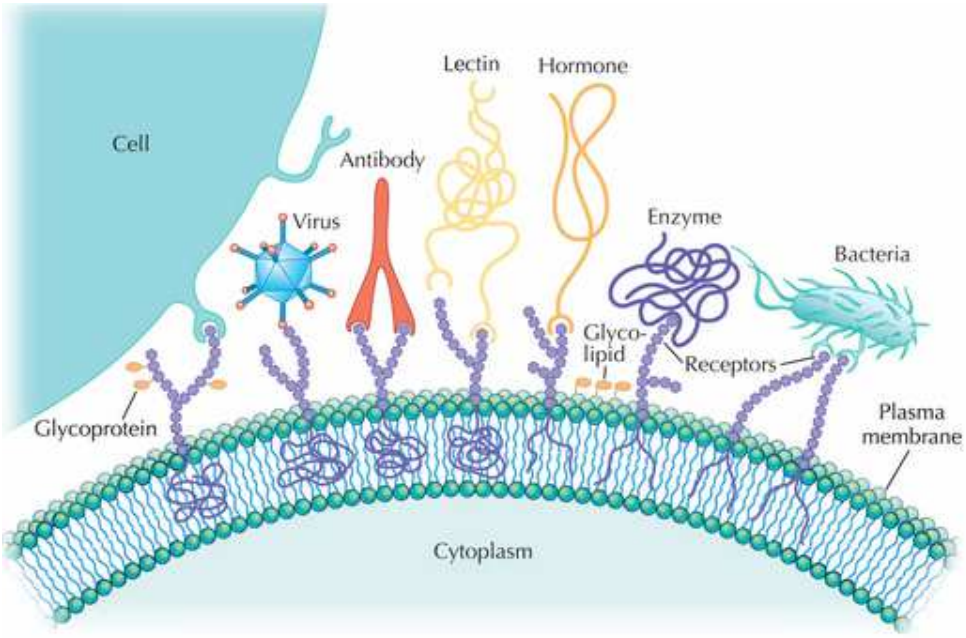

Figure 1.1 Representation of some of the possible interactions between membrane glycans and protein receptors of different biological entities.[5]

A complete understanding of all the roles that carbohydrates have in the so many physiological and pathological events of the cell is a quite difficult challenge. One reason lies in the structural complexity of oligosaccharides. In fact, while the other two classes of biopolymer, nucleic acids and proteins, have a linear arrangement of repeating units, carbohydrate building blocks have multiple points of attachment, leading to highly branched and stereochemically differentiated structures[6] (fig. 1.2). This structural complexity is further increased by post–synthetic modifications: hydroxyl groups can be sulphated, phosphorylated, acetylated, oxidized or replaced with other functional groups, especially those containing nitrogen in order to tune distinct biological activities.[7]

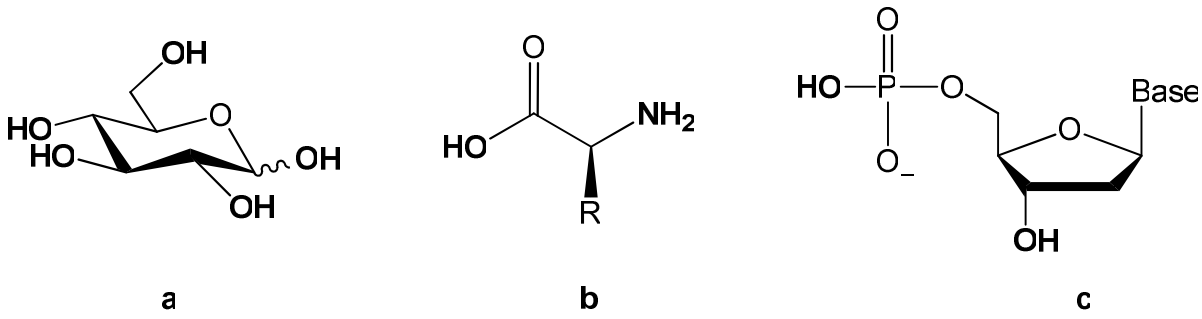

Figure 1.2 Building blocks of oligosaccarides (a), proteins (b) and nucleic acids (c), with evidenced in bold the groups potentially involved in oligomerization processes.

This incredibly high structural diversity which can be generated by these oligosaccharides, called Sugar Code,[8] stores detailed biochemical information which can be translated by suitable sugar binding proteins.

A second difficulty in studying carbohydrate-protein interactions is that binding affinities are weak, with dissociation constants in the milli-micromolar range;[3] however, the efficiency and selectivity of the *in vivo* control of events mediated by protein–carbohydrate binding requires significantly greater affinity. Nature overcomes this limitation by combining multiple simultaneous interactions between two or more carbohydrates of the glycoproteins organised in domains on the cell surface and a corresponding multimeric protein (fig. 1.1). These multivalent interactions have several mechanistic and functional advantages over their monovalent counterparts, the most relevant one probably being the ability to increase the specificity of binding. It is not surprising therefore that nature uses carbohydrates to mediate and encode the information for many biochemical processes,

exploiting the high specificity in the ligand-receptor interactions. Immunological response,[9,10,11] tumour metastasis,[12] fertilization[13] and inflammation[14] are just some examples of the processes in which carbohydrates take part. Besides they act as mediators in diverse cellular activities, such as recognition, growth and apoptosis.[15,16]

1.2 Carbohydrate binding proteins: Lectins

The initial contact between two cells or a cell and a pathogenic agent, often starts with a carbohydrate-protein recognition process. The outer surface of cells shows a complex set of carbohydrates, called glycocalyx, usually belonging to oligo-, poly-saccharides, glycolipids and glycoproteins. The proteins which non-covalently interact with carbohydrates are generally called carbohydrate binding proteins (CBP). In nature, there are several families of these kind of proteins, such as carbohydrate-specific enzymes and anti-carbohydrate antibodies. A very important class of CBP that has recently raised the interest are lectins:[17,18,19] proteins able to bind carbohydrates but without any catalytic or immunogenic activity. Furthermore lectins appear as more and more attractive targets for new diagnostic and therapeutic strategies, since it was demonstrated, in the second half of the last century, their involvement in physiological and pathological phenomena, from cell differentiation to cancer.[20] The study of lectins and their role in cell recognition processes, as well as the application of these proteins to the study of carbohydrates in solution and on cell surfaces, are giving important contributions to the advancement of glycobiology.[21]

Lectins are divided, according to their origin, in microbial, plant or animal[18] lectins. Initially they were classified, into five groups, depending on the specificity to the monosaccharide for which they exhibit the highest affinity:

- D-mannose,
- D-galactose/*N*-acetyl-D-galactosamine,
- *N*-acetyl-D-glucosamine,
- L-fucose,
- *N*-acetylneuraminic acid.

Relevant for the biological activities of lectins is the fact that notwithstanding the numerous monosaccharides found in nature, only those listed above are typical

constituents of surfaces of eukaryotic cells. The classification of lectins according to their monosaccharide specificity, however, masks the fact that they often exhibit an exquisite specificity for di-, tri-, and tetrasaccharides (with association constants up to 1000-fold higher as compared with the monosaccharide) and that certain lectins interact only with oligosaccharides. Moreover, lectins of the same specificity group may differ markedly in their affinities for different oligosaccharides. However, also thanks to the high-resolution X-ray crystallography of lectins and their complex with carbohydrates it was possible to identify the carbohydrate recognition domain (CRD): therefore, the more accepted current classification of lectins is based on the homology of their CRD (Table 1.1).

Lectin Family	**Cation dependency**	**Carbohydrate specificity**
C-type	Yes	variable (Man, Gal, Fuc)
I-type	No	variable (Man, GlcNAc, α(2,3)/α(2,6)-Sia)
S-type (Galectins)	No	β-Gal
F-type	Yes	Fuc
P-type	Variable	Man-6-P
R-type	No	β-Gal

Table 1.1 Current categories for classification of various animal lectins.

Other families of animal lectins, which include pentraxines (pentameric subunit arrangement), ganglioside binding proteins, sulfoglucoronosyl lipid-binding proteins and others, resist to this classification because of differences in their CRD that do not allow to find sequence homologies or evolutionary relation.

A very important class of animal lectins are galectins. They recognize glycoconjugates presenting a terminal β-galactose residue and show a conserved amino acid sequence consisting of approximately 130 residues for the carbohydrate binding domain.[22] Galectins are mainly located in the nucleus and cytoplasm, although they can be found also at cell surface or within the extracellular matrix where they can interact with glycosylated compounds.[23,24]

Considering their importance in a number of biological processes, it is not surprising that galectins have recently been under intense investigations. They take part in the cell-cell

communication, adhesion and cell migration processes. They also have a role in embryonic development, differentiation and RNA splicing.[25] Moreover, galectins are involved in inflammatory processes (for example Galectin-1 acts as anti-inflammatory agent,[26] oppositely to Galectin-3 which instead shows pro-inflammatory activity[27]), apoptosis (for example Galectin-1 induces apoptosis of activated human T cells and human T leukemia cell lines,[28] while Galectin-3 contributes in preventing this mechanism[29]), tumor growth and metastasis.[30, 31, 32] Currently, fifteen members of this family have been identified in mammals.[33] Because of the lack of human counterparts of Galectins -5, -6, -11, -14 and -15, there are only 10 types of human Galectins. However, based on their structure, Galectins can be also divided into three subgroups: proto-type, tandem-repeat-type and chimera-type (fig. 1.3).

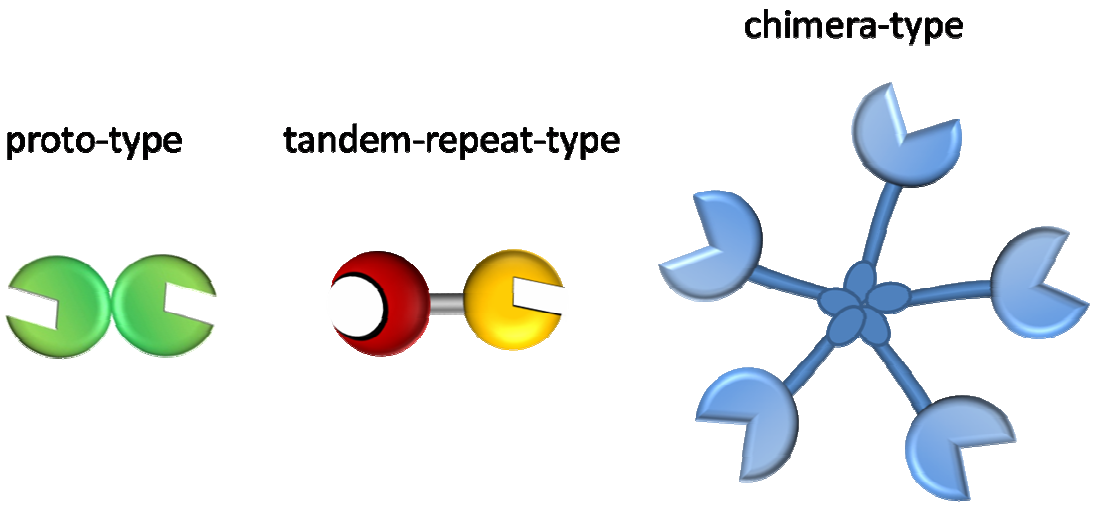

Figure 1.3 The schematic representation of the three different structures of human Galectins

Proto-type Galectins (-1, -2, -5, -7, -10, -11, -13, -14 and -15) contain one carbohydrate recognition domain (about 15 kDa) and they can be in the form of monomers or homodimers; tandem-repeat-type Galectins (-4, -6, -8, -9 and -12) present two distinct CRDs in a single peptide chain; chimera-type, whose only member is Galectin-3 (about 30 kDa), is constituted by one CRD with a non lectin part directly connected to it, which is responsible for the oligomerization,[34] usually pentamerization. Due to the simultaneous presence of several CRDs, when binding to multivalent glycosylated substrates Galectins can form lattices and undergo agglutination.

1.3 Multivalency

Even if Galectins bind saccarides with high specificity, a single carbohydrate-protein interaction shows rather weak binding, with dissociation constants in the milli-micromolar range. In order to enhance the binding affinity and overcome this limitation, nature exploits a powerful tool, the multivalency,[35] that in case of proteins binding to carbohydrates is also named "glycoside cluster effect".[3,36] It consists in the ability of a multimeric receptor to interact with a multivalent ligand via several, simultaneous, noncovalent recognition events (fig. 1.4) giving rise to an overall free energy of binding (ΔG°_{multi}) that is higher than the simple sum of the free energy of the single monovalent interactions (ΔG°_{mono}).

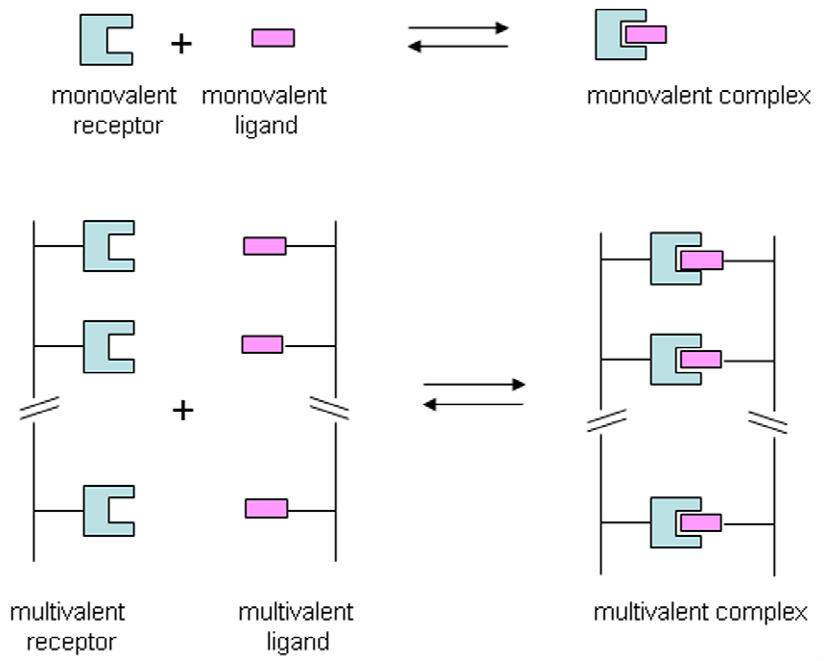

Figure 1.4 Example of monovalent *vs* multivalent complexes.[37]

Multivalent interactions usually result in high specificity and thermodynamic and kinetic stability.

Sometimes the concept of multivalency is associated with the one of *cooperativity*, that on the contrary is generally intended as the influence of the binding of one ligand on the receptor's affinity toward further binding.[38] However, as elegantly pointed out by Ercolani,[39] cooperativity in multivalent systems is usually extremely scarce and rare.

Moreover, cooperativity can be easily and rigorously assessed by using Hill or Scatchard plots for the binding of monovalent ligands to a multivalent receptor, as in the binding of four O_2 molecules to tetrameric haemoglobin. Much more difficult is to prove its existence when a multivalent ligand interacts with a multivalent receptor.

Initially, when a multivalent receptor and a multivalent ligand start to bind to each other, the first possible interaction is obviously intermolecular, but then a competition between inter- and intra-molecular binding events can take place. If the former are predominant, intermolecular aggregates of variable stoichiometry are the result of the binding, otherwise, if the latter are preponderant, the formation of a 1:1 receptor-ligand multivalent complex will be obtained (fig. 1.5).

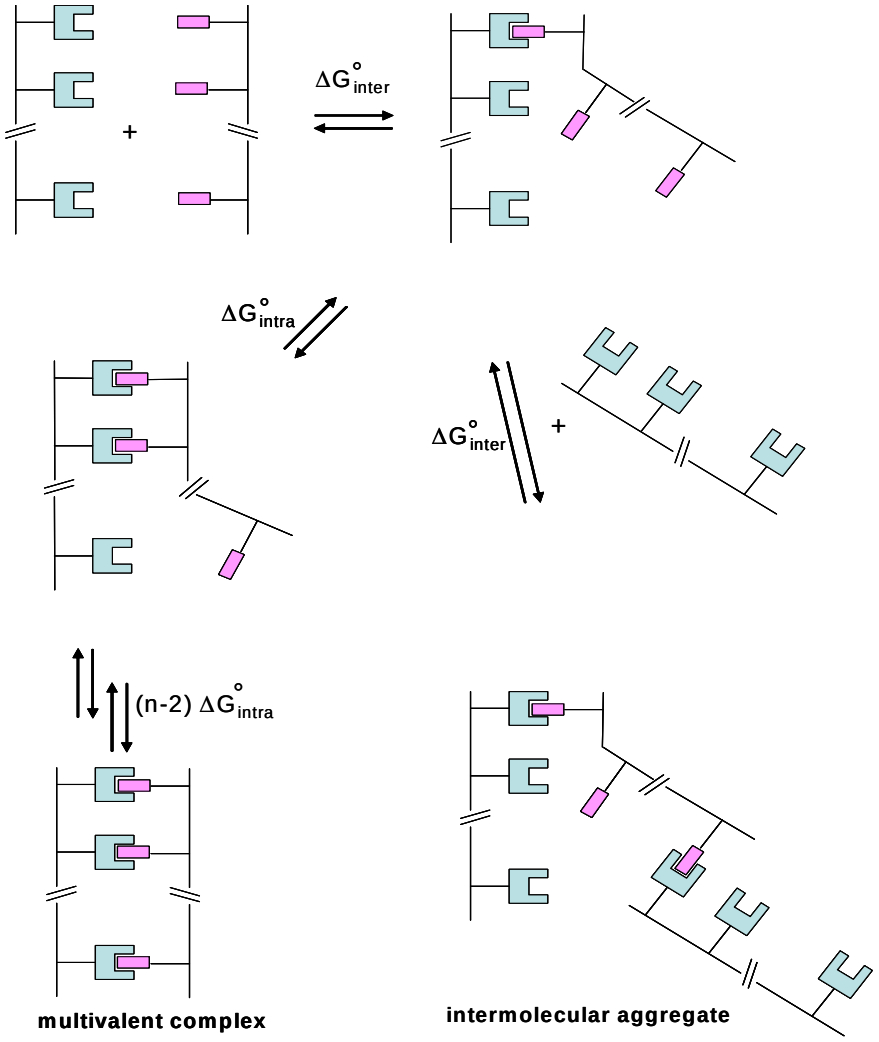

Figure 1.5 Intermolecular and intramolecular processes for the formation of a multivalent complex or of an intermolecular aggregate.[37]

In general, to describe multivalent binding, an approach based on the additivity of the free energies[40] can be used. The standard binding free energy for multivalent binding ΔG°_{multi} is

$$\Delta G^{\circ}_{multi} = n\Delta G^{\circ}_{mono} + \Delta G^{\circ}_{interaction}$$

where ΔG°_{mono} is the standard binding free energy of the corresponding monovalent interaction, n is the valency of the complex and $\Delta G^{\circ}_{interaction}$ is the balance between favourable and unfavourable effects of tethering. Multivalency is obviously observed when $\Delta G^{\circ}_{interaction}$ is favourable to binding ($\Delta G^{\circ}_{interaction} < 0$).

A rather qualitative but often useful parameter, β, has been introduced by Whitesides et al.,[35] as

$$\beta = K_{multi}/K_{mono}$$

where K_{multi} and K_{mono} are the association constants for the multivalent and monovalent complexes, respectively. The parameter β, named *enhancement factor*, has been often used in the literature to compare the efficiency of multivalent ligands having different topology and/or valency: molecules with high β values are efficient ligands/inhibitors. Sometimes, if the valency n of the complex is know, this enhancement factor can be normalised to n, giving rise to the parameter β/n. Similarly, another way to evaluate the presence of multivalent effect is based on *relative potency* (rp), been defined as

$$rp = IC_{50mono}/IC_{50multi}$$

where IC_{50} are values of the multivalent ($IC_{50multi}$) and monovalent (IC_{50mono}) inhibition. Also rp can be normalised to the valency n giving rise to rp/n, *relative potency per ligating unit (sugar).*

More rigorous approaches have been proposed by Kitov and Bundle[41] to quantitatively describe the multivalent binding process. They developed a model, adapting the one from Jenks,[40] where the standard free energy of multivalent interaction, $\Delta G^{\circ}_{avidity}$, is a function of three terms ΔG°_{inter}, ΔG°_{intra} (binding free energies for the first intermolecular and the second intramolecular process, respectively, fig. 1.5) and a statistical term $\Delta S^{\circ}_{avidity}$, namely

avidity entropy, calculated on the basis of the topology of the complex and representing the probability of association and dissociation of individual arms. The avidity entropy can grow rapidly with the valency of the complex, always favouring binding of a multivalent ligand to a multimeric receptor. This explains why multivalency can overcome the loss of conformational entropy. By a nonlinear fitting of the measured binding energies for a series of multivalent ligands, ΔG°_{inter} and ΔG°_{intra} can be determined, thus allowing to design and maximise the avidity of multivalent ligands.

1.4 Multivalent glycosylated ligands

This discovery of functional lectin–carbohydrate interactions and the possibility to inhibit them by using small polyglycosylated molecules offer enormous potential to the design of new drugs which could interfere with several pathological events.

In the last decade, Supramolecular Chemistry became more and more interested in applying the multivalency concept to the recognition of biological important molecules and to nanotechnology and for this reason molecular design became essential. In fact an appropriate spatial disposition of ligands is the prerequisite to obtain the perfect matching between the protein receptor site and ligand binding functionalities.

Multivalent ligands (fig. 1.6) can be of different type, but usually they have some common features that consist of a main core, called *scaffold*, bearing several covalent connections, the *linkers* or *spacers*, and the peripheral *ligating* (binding) units.

Any multivalent scaffold can in principle be used, from those having low valency such as benzene derivatives, monosaccharides, transition metal complexes, azamacrocycles, cyclodextrins or calixarenes to high valency ones such as dendrimers, polymers, peptoids, proteins, micelles, liposomes, and self-assembled monolayers (SAMs) on nanoparticles or plane surfaces.

Once the core structure where to anchor the binding moieties is fixed, two fundamental parameters for the ligand design are the nature and lenght of the spacers. In fact, they can influence the type and strength of the resulting interaction with the multivalent receptor.[35,42]

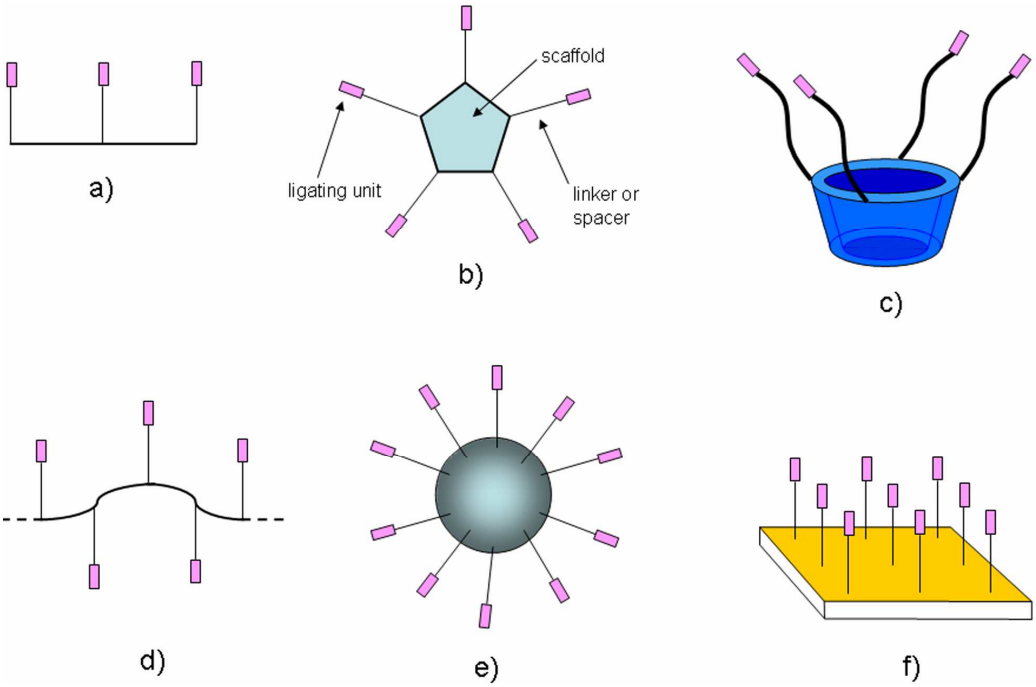

Figure 1.6 Different topologies of multivalent ligands. a) 1-D linear arrangement, b) 2-D cyclic/macrocyclic; c) 3-D cavity containing scaffolds (cyclodextrins/calixarenes); d) polymers/peptoids; e) nanoparticles/dendrimers/liposomes; f) 2-D

Since multivalency can be explained mainly through entropic effects a positive entropic factor, able to favour intramolecular binding, can be obtained through the use of spacers of proper length. Spacers that are too short cannot allow the simultaneous interaction of all the ligating units with the receptor sites, while spacers that are too long can lead to an useless loss of roto-translational degrees of freedom. In both cases intermolecular binding would result favoured instead of the multivalent complex formation.

1.5 Calix[n]arenes

Many polyglycosylated molecules have been prepared as multivalent ligands to study multivalent carbohydrate-protein interactions.[43] Calixarenes,[44,45] the cyclic oligomers obtained by the condensation of phenols and formaldehyde (fig. 1.7), are ideal scaffolds for the construction of multivalent glycosylated ligands with unique properties. In fact, the valency of the calix[n]arene scaffold can be properly varied ($4 < n < 8$) by choosing the desired dimensions of the macrocycle. The even-numbered macrocycles ($n = 4, 6, 8$), aside from being commercially available, are also easily obtained, even in kilogram scale, using

cheap reagents through well-consolidated synthetic procedures.[22] The odd-numbered homologues (n = 5, 7, 9), although known in the literature, can be obtained through more demanding syntheses, especially in terms of separation protocols, and are only rarely used. Glycoclusters with a lower valency (2 and 3) can also be readily prepared by selectively functionalising especially calix[4]arenes.

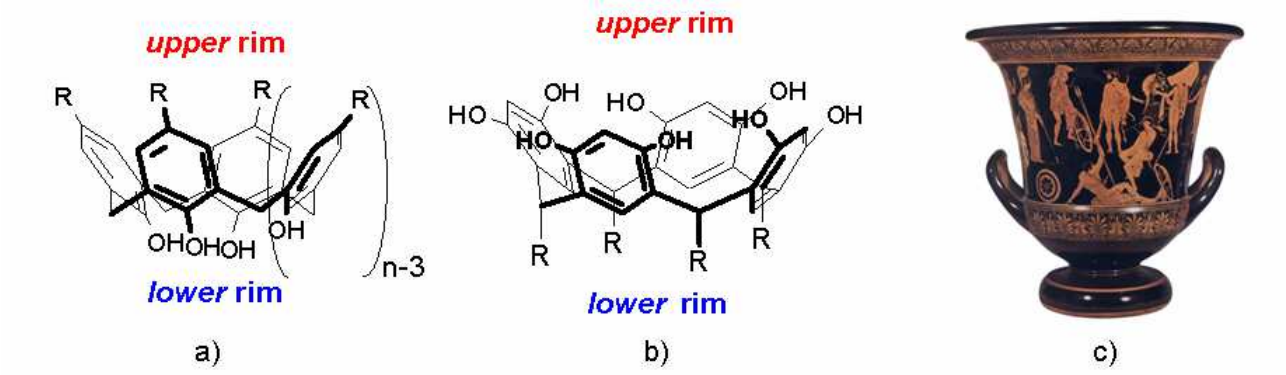

Figure 1.7 a) CH_2-bridged calix[n]arenes or simply calix[n]arenes with notation of the number *n* of repeating -ArCH_2- units and b) resorcarenes, also belonging to the family of the calixarenes; (c) a picture of a Greek vase (*calyx krater*), whose shape inspired the name of the molecule.

An important peculiarity of calix[n]arenes is the dual possibility to keep them conformationally mobile to exploit an induced-fit binding, or, on the contrary, to finely lock them in a specific structure more preorganized for binding. Especially in the case of the calix[4]arene, for instance, while the tetramethoxy- (fig. 1.8, R = Me) and tetraethoxy derivatives (fig. 1.8, R = Et) are conformationally mobile, the introduction of groups larger than ethyl, via efficient stereoselective procedures, can lock the macrocycle into one of the four possible structures (fig. 1.8) named by Gutsche as cone, partial cone, 1,3-alternate and 1,2-alternate,[44] that are characterised by a remarkably different orientation of the phenolic units into the space.

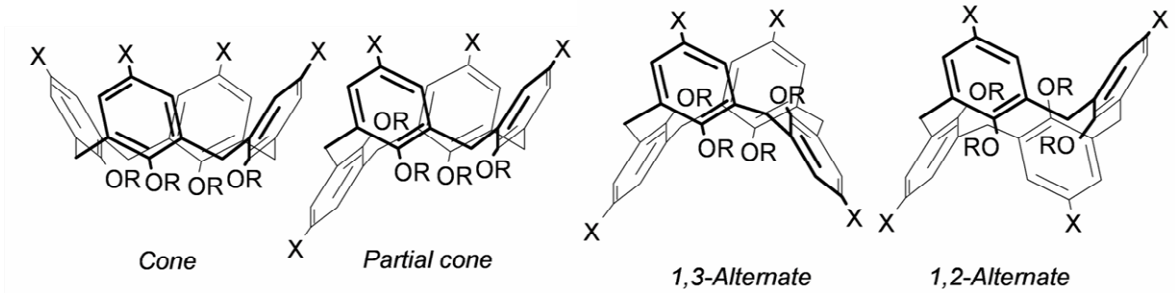

Figure 1.8 The four limiting conformations of calix[4]arenes, when R > Et.

In larger calix[n]arenes (n > 5), the conformational control becomes more difficult; the macrocycle is usually present as a mixture of conformers that possess similar energies and rapidly interconvert from one to another (conformationally mobile derivatives). Extensive bridging at the upper or lower rim is needed to fix these calix[n]arenes in one particular structure.[44]

1.5.1 Glycocalixarenes

Carbohydrates can be efficiently introduced on calixarenes, through a proper spacer, both at the phenolic oxygen atoms (*lower rim*, fig. 1.7) and/or at the para position (with respect to the OH group) on the aromatic nuclei (*upper rim*, fig. 1.7), giving rise to glycoclusters with quite different characteristics. Therefore, the considerable success met by calixarenes as scaffolds for the construction of multivalent ligands is due to a combination of different factors, such as the ease to modulate the valency, size, structure and topology of the binding group presentation together with their straightforward preparation and ease of functionalization. Currently, the chemistry of calixarenes is, in fact, well consolidated, and different and effective methods are known for the introduction of chains, both at the lower and at the upper rim, of variable length and containing most of the functional groups (-CHO, -COOH, -NH_2, -NCS, -N_3, -C=CH …etc) that are frequently used for the conjugation of ligating units. [46,47]

For the synthesis of polyglycosylated structures, such as glycocalixarenes, very efficient reactions have to be used to connect glycosides or glycosylated arms to the desired scaffold and an excellent control of the stereochemistry, if the anomeric carbon atom is involved in the reaction. Only if these conditions are satisfied, it is possible to obtain the desired polyglycosylated compounds in good yields, fully glycosylated and with the correct stereochemistry.[46] The first successful attempt to functionalize a calixarene structure with sugars was achieved using a Mitsunobu reaction at the phenolic hydroxyl groups of the macrocycle lower rim, though this strategy demonstrated the difficulties in controlling the stereoselectivity. On the contrary, a total stereoselectivity was observed, obtaining only the β-glycoside bond, in the reaction at the upper rim with thioethyl

glycosides and copper(II) triflate. In this case the yields after removal of benzoyl protecting groups was around 70%.[48,49]

In order to prevent the formation of complicated mixtures of diasteroisomers, saccarides units are equipped, in general, with linkers terminating with reactive group, used for the conjugation with the multivalent scaffold.

Reaction belonging to the so called "Click Chemistry"[50,51] are largely used: the conjugation between amines and isothiocyanate groups to give thiourea units, and the 1,3-dipolar cycloaddictions catalyzed by copper(II) salts, called copper-catalyzed azide-alkyne cycloaddiction (CuAAC). [52]

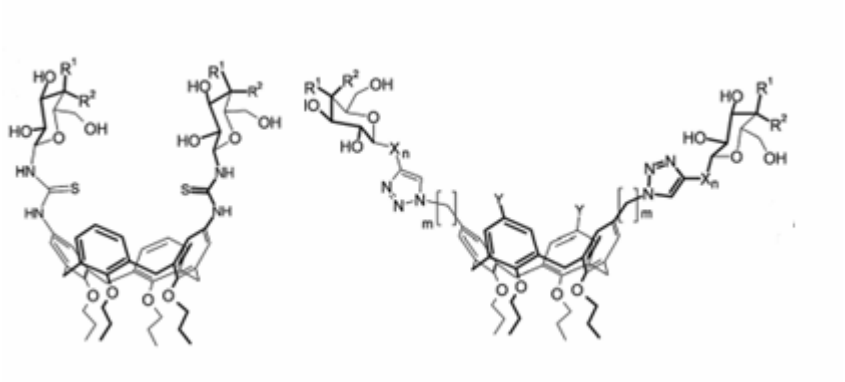

Figure 1.9 Examples of "Click Chemistry" obtained glycocalixarenes.

The conjugation via amine-isothiocyanate condensation is carried out in mild condition, giving high yields and lack of byproduct of partial functionalization or poisoning metal catalysts.[53] For what concerns the CuAAC the formation of the 1,3-disostituted triazole ring is selective and allows the formation of glycocalixarenes such the one in figure 1.9.[54,55] This reaction takes place between a calixarene adorned with alkyne or azide groups at the end of variable chains and saccharide bearing azide or alkyne moiety. The use of microwaves activation was demonstrated to have positive effect on yields and reduction of both reaction time and byproducts. [54,55]

The ability to interact with lectins is the origin of most biological activity of glycocalixarenes.[46,47] These multivalent carbohydrate-binding proteins preserve their ability to selectively recognise the natural saccharide ligands, although the latter ones are offered to the lectin in a rather crowded display, often even hindered by the presence of the macrocyclic structure.

Particularly useful is the possibility to obtain calixarenes of different sizes for studying the multivalent recognition processes of natural macromolecules such as lectins, because it makes it relatively easy to get small libraries of glycocalixarenes that possess different conformational properties and valency. This allows to evaluate how a different number and presentation geometry of the sugar affect the binding activity. This effect has been well and extensively shown in a series of galactosyl- and lactosylthioureido calix[n]arenes (fig. 1.10) synthesized and studied as inhibitors of VAA plant toxin and human Galectins, specifically Galectin-1, -3 and -4 belonging to the three different sub-groups, in the order proto-type, chimera-type and tandem-repeat-type, respectively.[56]

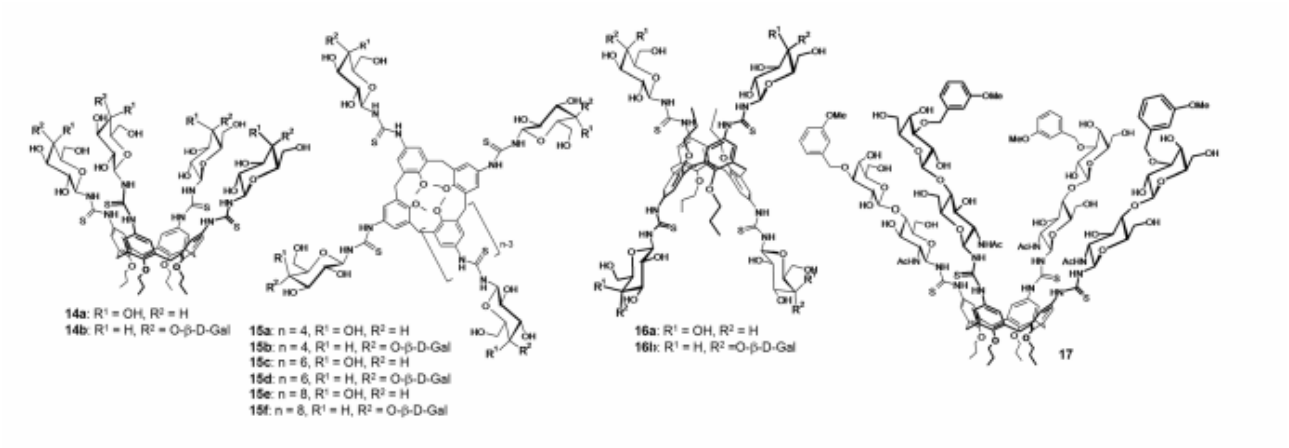

Figure 1.10 Schematic representation of glycocalixarenes (adapted from ref. 46)

The inhibition efficiency was proved to be strongly dependent on the structure of the glycocalixarene scaffold. In fact, through fluorescence assisted cell sorting test, it was observed that the larger and more conformationally mobile lactosyl calixarenes (**f** and **h**) are very efficient toward Galectin-4. Furthermore the 1,3-alternate derivative **j** resulted to be the best inhibitor for Galectin-1, and the cone glycocalixarene **b**, having the same valency but different presentation of lactoside units, is the worst inhibitor. The exact opposite situation was found toward Galectin-3 for the two tetravalent compounds, being the cone isomer **b** the best and the 1,3-alternate isomer **j** the worst inhibitor. These results strongly support the idea that calixarenes offer unique opportunities in design glycoclusters for the effective and selective binding of Galectins.

1.6 Magnetic Nanoparticles

Magnetic materials, based on metals such as iron, cobalt and nickel or metal oxides, have been involved in different ways in the development of modern nanotechnology.

In most cases, magnetic nanoparticles (MNPs) smaller than the single domain limit (around 20 nm for iron oxide) exhibit superparamagnetism at room temperature. Meaning that the MNPs lose their magnetism below their Curie temperature and that are composed of a single magnetic domain. The superparamagnetism has in particular applications in ferrofluids due to the tunable viscosity, in data analysis and in medicine. All these disciplines need to be provided with specific kind of MNPs, stable in different conditions and with different geometries and physical properties. In this context, nanotechnology allows for controlled synthesis and functionalization of materials at nanometre scale.[57]

The microscopic origin of magnetic properties in matter lies in the orbital and spin motions of electrons,[58] whose spin and angular momentum are associated with a magnetic moment. The interaction between the magnetic moments of atoms from the same material causes magnetic order below a certain critical temperature. We can classify bulk materials on the basis of these interactions and their influence on the material behaviour in response to magnetic fields at different temperatures (e.g. ferromagnetism, ferrimagnetism, etc.).[59]

Bulk magnetic materials are composed of magnetic domains, that are regions within which there is an alignment of the magnetic moments. If, as in the case of MNPs, the volume of the material is reduced, the magnetic properties are no longer similar to bulk materials because a situation in which just one domain is reached occurs.

Due to their small volume, MNPs usually present superparamagnetic behaviour, meaning that the thermal energy may be enough to change spontaneously the magnetisation within each MNP. In other words, the magnetic moment of each MNP will be able to rotate randomly just because of the temperature influence. For this reason, in the absence of an electromagnetic field the net magnetic moment of a system containing MNPs will be zero at high enough temperatures (fig. 1.11). However, in the presence of a field, there will be a net statistical alignment of magnetic moments, analogous to what happens to paramagnetic materials, except that now the magnetic moment is not that of a single atom

but of the MNPs containing various atoms which can be up to 10^4 times larger than that of a paramagnetic material.[57]

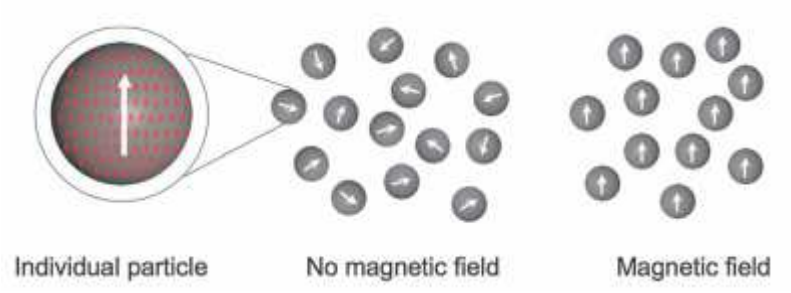

Figure 1.11 Schematic representation of a superparamagnetic particle.[57]

This property, marked by the lack of remanent magnetisation after removal of external fields, enables the MNPs to maintain their colloidal stability and avoid agglomeration, which is important for biomedical applications. [57]

The main parameters to characterize magnetic properties such as coercivity (Hc) and susceptibility (w) are: composition, crystallographic structure, vacancies and defects, and magnetic anisotropy. Additionally for MNPs on the nanoscale range, the shape and size also determine their magnetic behaviour. The magnetic anisotropic energy barrier from the spin-up state to the spin-down state of the magnet is proportional to the product of the magnetic anisotropy constant (K) and the volume of the magnet. Therefore, superparamagnetism depends on the size of the MNP. In general, smaller is the size of the MNP, lower its transition temperature from ferromagnetic to superparamagnetic behaviour will be. Size reduction so reflects in the enhancement of the relative contribution of surface effects. [60] Besides size effects, the MNP shape is known to strongly influence K and again the magnetic anisotropic barrier and the whole magnetic properties of the nanomaterial. In general, large magnetic moments are preferred for most applications, as this would reduce the amount of MNPs needed. However, when dealing with biological applications, biocompatibility reaches great importance, as the accumulation or toxic effects of the MNPs need to be reduced as much as possible. Therefore, most of the time a balance between larger magnetic moments and biocompatibility needs to be reached. This is why iron-based MNPs are often preferred compared to others based on more toxic transition metals. [61]

The MNP coating is also a key element in order to specifically bind other compounds to the MNPs or to prevent agglomeration, but it will also affect the magnetic properties of the MNPs due to the high specific surface area and the large amount of atoms at the surface. In fact, the differences in the nature of the coupling agent and in the type of interaction between the ligand and the MNP surface would explain the differences in the magnetisation values.

The application of an external alternating magnetic field (AMF) to MNPs leads to the production of energy, in the form of heat, if the magnetic field is able to reorient the magnetic moments of the MNPs.[62] Such an effect can be exploited to use MNPs as mediators in magnetic hyperthermia. In bigger multidomain MNPs, this reorientation is produced through the movement of domain walls, while in small mono-domain MNPs, the reorientation of the magnetic moments can occur due to the rotation of the moment within the MNP, overcoming their anisotropy energy barrier (Ne'el loss), or the mechanical rotation of the MNPs that will create frictional losses with the environment (Brown loss).[47]

Magnetic ferrites for biomedical use are most commonly prepared by hydrolytic synthesis, with particular reference to coprecipitation techniques. A widespread approach relies on the Massart method,[63] where magnetite is obtained by alkaline coprecipitation of stoichiometric amounts of ferrous and ferric salts (usually chlorides). The experimental parameters affecting this process, which involves the formation of intermediate hydroxyl species, such as temperature, pH, concentration of the cations and nature of the base, have been studied in order to vary the average MNP size in the range from 3 to 20 nm.

The coprecipitation approach offers a wide range of advantages including: the use of cheap chemicals and mild reaction conditions, the possibility to perform direct synthesis in water, the ease of scale-up.

The application of MNPs in biology requires their stability in solutions containing high concentrations of proteins and salts, as well as in cell culture media. MNPs suitable for this application can be synthesized following different approaches that will lead to hydrophilic surfaces. The two possible approaches to render MNPs surface hydrophilic are: to exchange the surfactant for another ligand molecule that on the one end carries a functional group that is reactive toward the MNP surface and on the other end a

hydrophilic group, or to add a second layer of an amphiphilic molecule or polymer that is solely stabilized around the first layer by hydrophobic effects. The latter method is more universal and agglomeration during the coating process is almost avoided though on the other hand, the hydrodynamic radius is inevitably increased.[56]

In literature, it is possible to find some examples on MNPs covalently functionalized with different biomolecules in order to achieve different results. For example, MNPs can be coated with a thick dextran layer stabilized by crosslinking and functionalized with amino groups, useful to covalently anchor affinity ligand creating nanoswitches, as was explained by Weissleder at al. in 1999.[64] Those nanoswitches have the ability to undergo reversible assembly in presence of specific molecules that are selectively recognized by the affinity ligands immobilized on the surface. This approach was used later to quantitatively determine analytes of different nature, such as glucose[65] or calcium[66] in solution, attaching proper affinity ligands.

It is also possible to detect and sequester bacteria, for istance, such as Gram-positive bacteria even at ultralow concentrations using a vancomycin-conjugated FePt magnetic nanoparticles.[67] Using a silica-coated MNPs covered with sugars (glucose and galactose) *E.coli* strains could be detected,[68] while MNPs coated with sugars (mannose, galactose, fucose and sialic acid) were used to localize certain tumor cells. [69]

1.7 Gold Nanoparticles

Colloidal gold nanoparticles (AuNPs) had technological application since ancient times due to their optical properties, in particular for staining glass. Systematic investigations on gold colloids could be traced back to the days of Faraday, though the breakthrough of their use for biological applications took place only in the last decade.[70]

AuNP absorbs and scatters light intensely at its surface plasmon resonance (SPR) wavelength region and such properties make AuNPs as one of the most valuable optical probes for sensing applications. [71] The SPR wavelength of gold nanoparticles can be tuned from the visible to the near IR region by changing the size and shape of the gold nanoparticles. The strong absorption or scattering of AuNPs in the visible light region makes them easily observable by naked eye or detectable by inexpensive instruments. The

possibility of tuning the SPR band of AuNPs (including nanorods, shells, stars, and other shapes) to the near IR region makes them promising materials for in vivo imaging and analysis. The optical properties of AuNPs are further dependent on the surface chemistry and the inter-particle interactions and are governed by their unique localized surface plasmon resonance (LSPR), which is the collective oscillation of the nanostructure's conduction band electrons in resonance with the incident electromagnetic field. [72]

Upon analyte binding, the surface plasmon resonance of the AuNPs changes due to the surface chemistry change, or inter-particle interaction modification. This surface plasmon resonance change of AuNPs can then be detected either by light absorption or light scattering techniques. A typical AuNP contains two structural components: the metal core and the surface coating. The detection methods as mentioned above are mainly based on the property and property changes of the metal core. Since nanoparticles have a large surface area/volume ratio and the surface chemistry can be well controlled, the surface coating layer of AuNPs provides additional opportunity for detection and sensing of analytes (fig. 1.12).

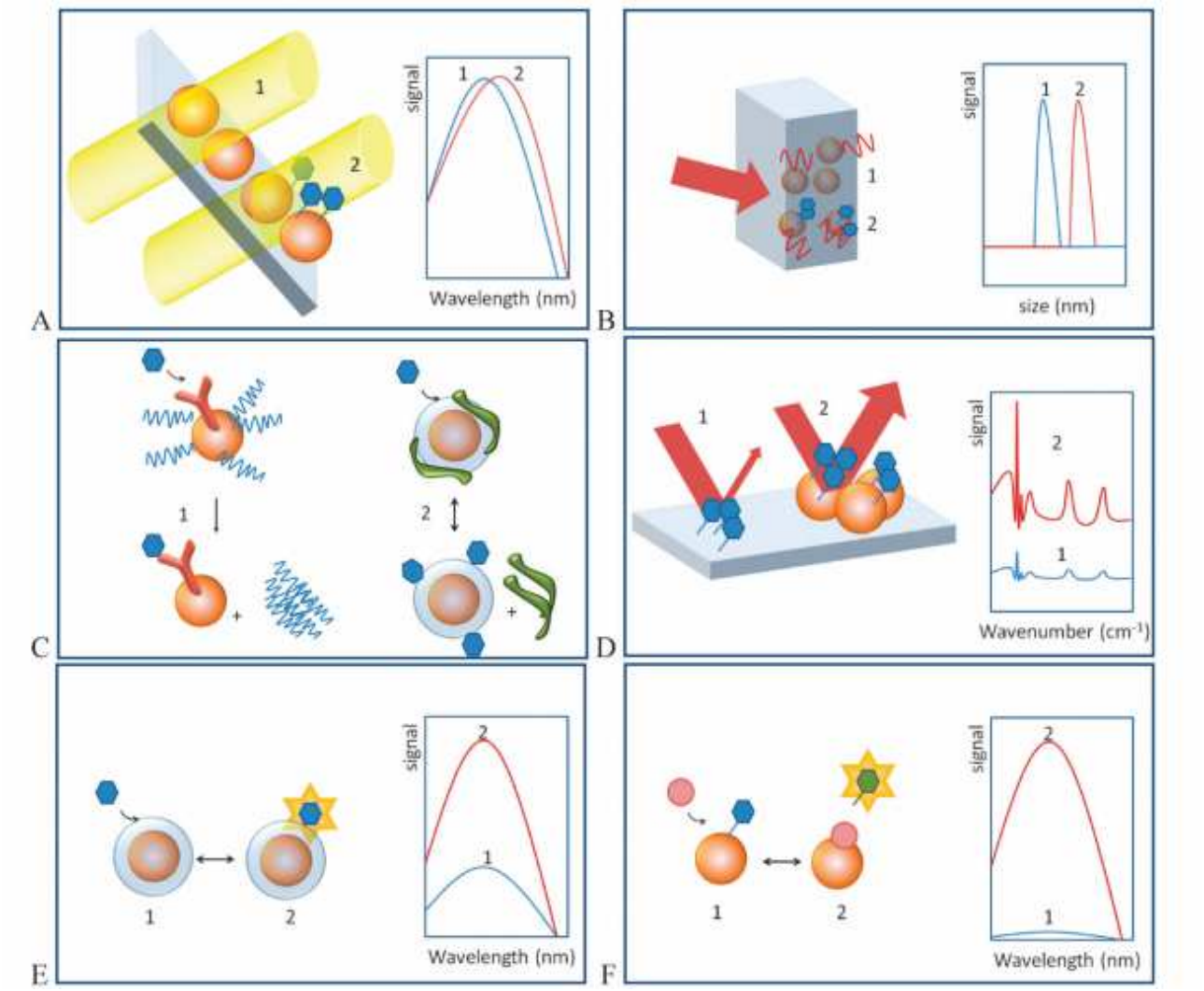

Figure 1.12 Illustration of six detection mechanisms using the optical properties of AuNPs. (A) LSPR concept: (1) Irradiation of the gold nanoparticles gives rise to a collective oscillation of their conduction band electrons resulting in a plasmon absorption in the visible range of the electromagnetic spectrum. (2) This plasmon resonance is sensitive to changes in the local environment, for example the binding of biomolecules. (B) (1) When nanoparticles are irradiated with laser light, they will scatter the light elastically in all directions. By monitoring the change in the scatter pattern the diameter of the solid nanoparticles can be deduced. (2) When biomolecules are attached on the nanoparticle surface the size increase can be monitored. (C) Detection using the surface chemistry and ligands of AuNPs. (1) Signal amplification based on the large number of DNA strands (bar-codes) released from the AuNPs. (2) Surface chemistry-controlled reversible biomolecular binding to AuNPs in a competitive assay. (D) (1) Normal Raman scattering is inherently weak. (2) When biomolecules of interest are bound to nanoparticles, the Raman signal can be enhanced due to the enhanced electromagnetic field which is excited or due to a charge transfer mechanism. When molecules are attached to AuNPs their properties can change. (E) Metal enhanced fluorescence can occur when a fluorophore is placed at a fixed position from the metal nanoparticle surface. (F) When the fluorophore is in short or direct contact with the metal nanoparticle surface quenching will occur. In this case, a competitive assay format is often used for the target analyte detection.[73]

The synthesis of gold nanoparticles with diameters ranging from a few to several hundreds of nanometres is well established in aqueous solution as well as in organic solvents. In typical syntheses, gold salts such as $AuCl_3$ are reduced by the addition of a reducing agent which leads to the nucleation of Au ions to nanoparticles. In addition, a stabilizing agent is also required which is either adsorbed or chemically bound to the surface of the Au nanoparticles. This stabilizing agent (often also called a surfactant) is typically charged, so that the equally charged nanoparticles repel each other so that they are colloidally stable.[74] Similar synthesis routes can also be performed in organic solvents, [75,76] though in this case the reducing agent is different from the stabilizing agent. For particles dispersed in organic solvents, frequently surfactants based on hydrophobic alkane chains are bound to the particle surface in order to provide colloidal stability.

As in the case of MNPs, also for AuNPs a surface modification is possible after synthesis. The stabilizer molecules can be replaced by other stabilizer molecules in a ligand exchange reaction. As thiol moieties bind with high affinity to gold surfaces, most frequently thiol-modified ligands are used which bind to the surface of the Au particles (which are by several groups also called ‘‘monolayer-protected clusters’’) by formation of Au–sulfur bonds.[77] It it also possible to change the particles surface taking advantage of lipophilic interaction between the lipophilic stabilizer of the NPs and the hydrophobic part of an amphiphilic receptor. Ligand exchange in fact allow, for example, the transfer of Au particles from an aqueous to an organic phase (and vice versa) by exchanging hydrophilic surfactants with hydrophobic surfactants (and vice versa).[78]

Many examples of AuNPs covered with biomolecules can be found in literature. Most of the time the approach used is a covalent one, but some cases of use of non-covalent interaction was reported.

The surface of AuNPs could be covered with amines or quaternary ammonium salts, in order to bind DNA thanks to electrostatic interactions, and, due to the surface modification with a photoactive liker, are also able to release the DNA after UV irradiation.[79] The most commonly used biomolecules in derivatizing gold surface of NPs are antibodies. Such molecules can be adsorbed on the surfaces by using formation of covalent bonds or taking advantage of hydrophobic or ionic interactions.[80] Some other examples describe how the gold surfaces could be covered with a dense core of synthetic

oligonucleotides,[81] with oligopeptides[82] or both.[72] Recently, lipids joined other biomolecule in AuNPs funtionalization. Lipids are used to form by-layer on AuNPs, the first layer adsorbed on the surface using a thiolated lipid and the second layer attached to the previous one thanks to hydrophobic effects.[83] There are also some examples of glycosylated AuNPs, where the surface is covalently covered with lactose, in order to study and confirm carbohydrate-carbohydrate interaction in water,[84] or a mixture of saccharides, used for example for preparation of potential anticancer vaccines,[85] or with di- tri- tetra- or more mannose units to intervene against HIV infection. [86]

1.8 Luminescent Platinum(II) Complexes

Fluorescence has become one of the most powerful and extensively used tools in cell biology, physiology and related areas of the biomedical sciences. [87] Widely utilised for the sensitive detection of species in "in vitro" bioassays, often in conjunction with immunological methods, the applications of fluorescence have been greatly extended by coupling it to optical microscopy.[88,89,90] This combination has allowed huge advances to be made in visualising, for example, intracellular structure and function, including those of live cells and tissue sections.[91,92] Most recently, the use of low-energy red and near-infrared light, to which biological tissue is relatively transparent, has led to fluorescence methods being applied even to animal specimens.[93,94]

Three key features of fluorescence render it especially attractive. The first is the exquisite sensitivity that has become possible, thanks to the extraordinarily high efficiency with which light can be detected.[95] Secondly, the wavelength range of visible light is such that spatial resolution of around 1μm is easily achievable with simple optical microscopes, a length-scale that is compatible with the study of many intracellular structures. Finally, the timescale of light emission is fast, typically on the nanosecond to microsecond timescale.

One of the attractions of complexes based on cyclometallating ligands, for example, is the possibility to have facile colour tuning. For instance, in complexes such as $[Ir(ppy)_2(bpy)]^+$ and Pt(dpyb)Cl (fig. 1.13), the HOMO and LUMO are primarily localised on mutually different parts of the molecule.[96,97] The HOMO is based largely on the metal and metallated aryl units, whereas the LUMO is based on the pyridyl rings. This allows their

energy levels to be tuned essentially independently of one another, and complexes emitting across the spectrum are readily possible. This contrasts with many fluorescent organic structures where control over colour is more limited.

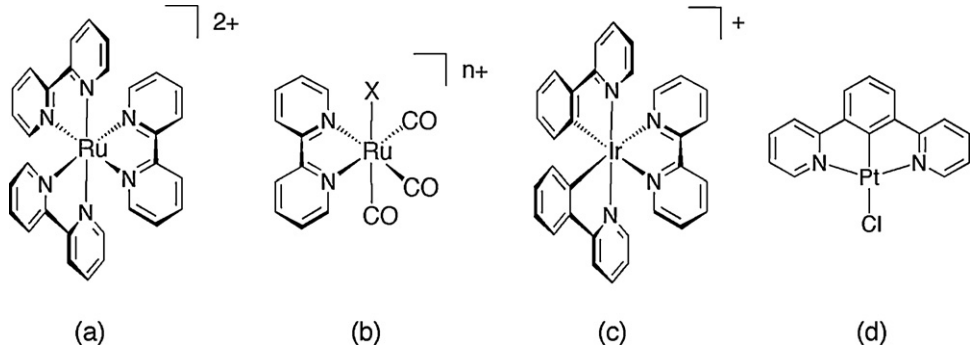

Figure 1.13 Structures of some of the main types of core units used in imaging with metal complexes to date: (a) $[Ru(bpy)_3]^{2+}$; (b) the $Ru(bpy)(CO)_3X$; (c) the cis-$[Ir(ppy)_2(bpy)]^+$ unit common to many iridium-based imaging agents investigated; (d) Pt(dpyb)Cl, an example of a cylometallated platinum(II) complex that has been used for imaging, incorporating a strong-field tridentate ligand.

A second point relates to synthetic issues. Modification of many fluorescent organic structures can be demanding, whereas many metal complex types can be prepared using well-defined strategies, often involving stepwise introduction of different ligands. Purification is also often straightforward via crystallisation or chromatography. One argument sometimes raised against the use of metals such as iridium and platinum is their high cost. However, for an application such as imaging, the amounts of material in question are minimal, and the cost of the metal is often only a relatively minor fraction of the total synthetic costs.

A third point relates to the difference in energy between the absorbing and emitting states. For most organic fluorophores, the state in question is the same (normally the S1 state) and the difference in energy between the lowest energy absorption band and the emitting band (the Stokes' shift) is often small, arising from the reorganisation of solvent molecules that occurs to stabilise the excited state after absorption and prior to emission. For triplet-emitting metal complexes, the emission emanates from a state (the triplet state) different from that which is excited by absorption of light (normally singlet states), and spin correlation effects stabilise the former with respect to the latter. Overlap of absorption and emission is almost never a problem for such complexes. Probably the really key distinction of luminescent metal complexes for bioimaging lies in the longer lifetimes of emission:

lifetimes of triplet-emitting transition metal complexes are typically two to three orders of magnitude longer than those of organic fluorophores.[98] In bioassays and bioimaging, long-lived probes can allow the elimination of background fluorescence from biological molecules on the basis of time.[99,100]

There are also potential disadvantages of using long-lived emitters. One is that the long lifetime allows more time for excited-state quenching processes to occur. For example, the triplet excited states of transition metal complexes may be efficiently deactivated by dissolved molecular oxygen in solution, often leading to the formation of singlet oxygen.[101] The high reactivity of singlet oxygen with organic molecules and biological entities can lead to phototoxicity, a desirable feature in photodynamic therapy, for example,[102] but clearly not for imaging purposes. Nevertheless, research to date suggests that singlet oxygen production is not necessarily problematic in imaging work, possibly because the diffusion rate of oxygen in the cell and its interaction with metal complexes bound to large biomolecules is reduced.

In order to be realistic candidates for imaging in life sciences, luminescent probe molecules should ideally satisfy a number of requirements: high extinction coefficient in the visible range, leading to population of the emissive excited state close to 100% yield; high emission quantum yield; solubility in water; high cell permeability; low cytotoxicity; high chemical stability, i.e. maintaining its chemical integrity in the imaged object; and high photostability, i.e. the compound should not undergo photobleaching when irradiated during use, as happens for many of the commercial labels used currently.

Of course to achieve all the criteria in the list above is clearly unrealistic, but each new probe should be tensioned against at least some of them.[103]

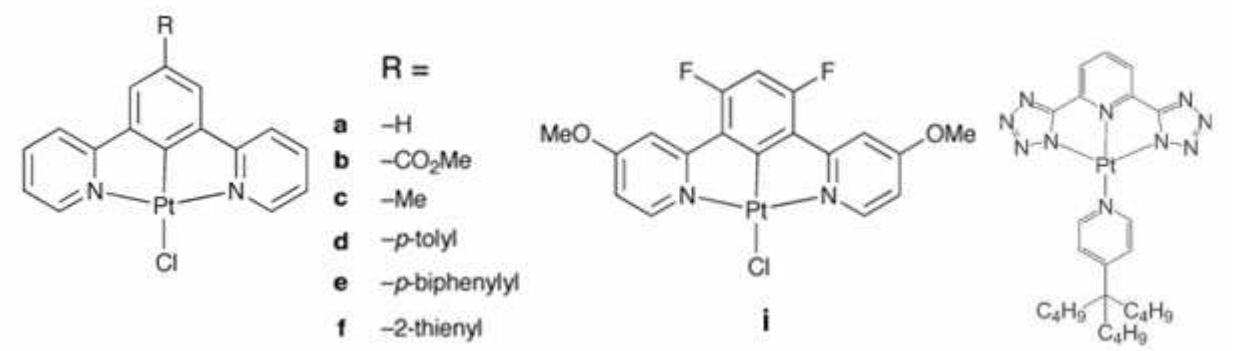

Figure 1.14 Some examples of Pt(II) complexes.[104]

Platinum(II) differs from the other elements – Ru(II), Re(I) and Ir(III), in that it is a d8 metal ion, and hence normally adopts a 4-coordinate square planar geometry as opposed to the distorted octahedral complexes of the d6 metal ions. The presence of strong- field ligands is particularly important in the design of emissive platinum(II) complexes, in order to ensure that metal-centred d–d states – which are highly distorted compared to the ground state and hence potentially deactivating – are displaced to high energy. [105] The most brightly emissive platinum(II) complexes, including those which have been investigated for bioimaging, containg cyclometallating ligands such as 2-phenylpyridines or their tridentate analogues (fig 1.14), as well as strongly-donating acetylide ligands in conjunction with accepting di- or tri-imine ligands like bpy or tpy.[106,107,108] From the point of view of interactions with biological molecules and intrinsic biolocalization within a cell, the square planar geometry might lead one to anticipate quite different behaviour for platinum(II) complexes compared to those of the other elements.[109]

Importantly from the point of view of applications, the emission can be tuned over a very wide spectral range (sky-blue to red), without significantly compromising the luminescence quantum yield, through simple substitution of the central aryl or lateral pyridyl rings (fig. 1.15).[110,111,112]

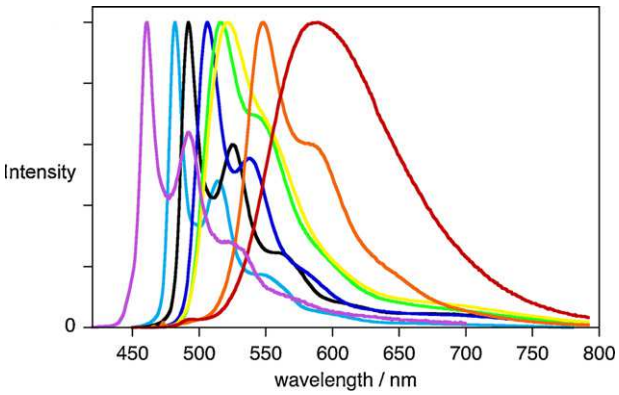

Figure 1.15 Shows how the emission spectra of the Pt(N^C^N) class of complex can be tuned from that of Pt(dpyb)Cl (a, black line), either to longer wavelengths through the introduction of electron-donating alkyl or aryl substituents at the 4-position (c–f), or to shorter wavelengths using an electron-withdrawing substituent ester group at this position (b, light blue line)/electron-donating methoxy substituents in the pyridyl rings (i, purple line).[113]

In these platinum(II) complexes, one often refers to the ancillary ligand to indicate the non-chelating ligand of platinum(II), often a chloride or a pyridine moiety. The use of ancillary ligands often allow to a quite easy modification of the ancillary ligand itself, for example, by simply functionalizing the pyridine moiety in in one of its positions and giving the possibility to enhance or tune the solubility, changing the uptake property and biological activity and the aggregation ability. In fact, as mentioned before, the most important part for emitting property is the tridentate ligand.

Triplet emitters based on platinum(II) can form aggregates or eximers, causing shifts in the emitted wavelengths and affecting the photoluminescence quantum yield (PLQYs) [114]. Is well known that terpyridine ligands and their N^C^N and N^N^C analogues have been coordinated to platinum(II), leading to neutral, mono-, or doubly charged species, some of which display bright luminescence. They can form supramolecular structures, such as nanowires, nanosheets, and polymeric mesophases, with interesting optical and supramolecular properties.[115,116,117,118]

References

[1] T. W. Rademacher, R. B. Parekh, R. A. Dwek *Annu. Rev. Biochem.* **1988**, *57*, 785.
[2] A. Varki *Glycobiology* **1993**, *3*, 97.
[3] Y. C. Lee, R. T. Lee *Acc. Chem. Res.* **1995**, *28*, 321.
[4] H. Lis, N. Sharon *Acc. Chem. Res.* **1998**, *98*, 637.
[5] Adapted from Evolution textbooh, Chapter 24, figure 24.9
http://www.evolution-textbook.org/content/free/figures/ch24.html
[6] H.-J. Gabius *Naturwissenschaften* **2000**, *87*, 108-121.
[7] A. Varki, R. Cummings, J. Esko J, H. Freeze, G. Hart, J. Marth, *Essential of glycobiology*. Cold Spring Hatbor Laboratory Press, New York, **1999**.
[8] H.-J. Gabius, *The Sugar Code. Fundamentals of glycosciences*, Wiley-VCH, Weinheim, **2009**.
[9] E. I. Buzas, B. Gyorgy, M. Pasztoi, I. Jelinek, A. Falus, H.J. Gabius, *Autoimmunity*, **2006**, *39* (8), 691.
[10] R.A. Dwek, *Chem. Rev.*, **1996**, *96* (2), 683.
[11] D.A. Calarese, C.N. Scanlan, M.B. Zwick, S. Deechongkit, Y. Mimura, R. Kunert, P. Zhu, M.R. Wormald, R.L. Stanfield, K.H. Roux, J.W. Kelly, P.M. Rudd, R.A. Dwek, H. Katinger, D.R. Burton, I.A. Wilson, *Science*, **2003**, *300* , 2065.
[12] K.S. Lau, J.W. Dennis, *Glycobiology*, **2008**, *18*, 750.
[13] W.J. Snell, J.M. White, *Cell*, **1996**, *85*, 629.
[14] P.M. Rudd, T. Elliott, P. Cresswll, I.A. Wilson, R.A. Dwek, *Science,* **2001**, *291,* 2370.
[15] H. Lis, N. Sharon, *Chem. Rev.*, **1998**, *98*, 637.
[16] E.E. Simanek, G.J. McGarvey, J.A. Jablonowski, C.H. Wong, *Chem. Rev.*, **1998**, *98*, 833.
[17] H. Lis, N. Sharon, *Acc. Chem. Res.* ***1998***, *98*, 637.
[18] H.J. Gabius, *Eur. J. Biol.* **1997**, *243*, 543.
[19] H.J. Gabius, *Eukaryotic Glycosylation and Lectins: Hardware of the Sugar Code (Glycocode) in Biological Information Transfer*, Eurekah, **2001**.
[20] H. Lis, N. Sharon, *The Lectins: Properties, Functions and Applications in Biology and Medicine*, Eds. Academic Press, Inc. Orlando, **1986**, 293.
[21] R. A. Dwek Chem. Rev. **1996**, 96, 683.

[22] S.H. Barondes, D.N.W. Cooper, M.A. Gitt, H. Leffler, *Journal of Biological Chemistry*, **1994**, *269*, 20807.
[23] R.C. Hugues, *Biochem. Biophys. Acta*, **1999**, *1473*, 172.
[24] H. Leffer, *Results. Probl. Cell. Differ.*, **2001**, *33*, 57.
[25] N.L. Perillo, M.E. Marcus, L.G. Baum, *Mol. Med.*, **1998**, *76*, 402.
[26] G.A. Rabinovich, *Scand. J. Immunol.* **2007**, *66*, 143.
[27] F.T. Liu, D.K. Hsu, *Drug News Perspect*, **2007**, *20*, 455.
[28] N.L. Perillo, K.E. Pace, J.J. Seilhamer, L.G. Baum, *Nature*, **1995**, *378*, 736-739.
[29] R.Y. Yang, D.K. Hsu, F.T. Liu, Proc. *Natl. Acad. Sci. U.S.A.*, **1996**, *93*, 6737.
[30] M. Huflejt, H. Leffler, *Glycoconjugate J.*, **2003**, *20*, 247.
[31] Y. Takenaka, T. Fukumori, A. Raz, A. *Glycoconjugate J.*, **2002**, *19*, 543.
[32] H. Lahm, S. André, A. Hoeflich, H. Kaltner, H.C. Siebert, B. Sordat, C.W. von der Lieth, E.; Wolf, H.J. Gabius, H. J. *Glycoconjugate J.*, **2003**, *20*, 227.
[33] A. Varki, R.D. Cummings, J. D. Esko, *Essentials of Glycobiology. 2nd edition*. **2009**, Eds. Cold Spring Harbor (NY): Cold Spring Harbor Laboratory Press.
[34] H. Leffler, S. Carlsson, M. Hedlund, Y. Qian, F. Poirier, *Glycoconjugate Journal*, **2004**, *19*, 433.
[35] M. Mammen, S.K. Choi, G. M. Whitesides, *Angew. Chem. Int. Ed. Engl.* **1998**, *37*, 2754.
[36] J.J. Lundquist, E. J. Toone, *Chem. Rev.* **2002**, *102*, 555.
[37] Image taken from: L. Baldini, A. Casnati, F. Sansone, R. Ungaro, *Chem. Soc. Rev.*, **2007**, *36*, 254.
[38] J.D. Badjić, A. Nelson, S. Cantrill, B. Turnbull, F. Stoddart, *Acc. Chem. Res.*, **2005**, *38*, 723.
[39] G. Ercolani, *J. Am. Chem. Soc.* **2003**, *125*, 16097.
[40] W. P. Jenks, *Proc. Natl. Acad. Sci. U. S. A.* **1981**, *78*, 4046.
[41] Kitov, P. I; Bundle, D. R. *J. Am. Chem. Soc.* **2003**, *125*, 16271.
[42] J. Rao, J. Lahiri, R.M. Weis, G. M. Whitesides, *Angew. Chem. Int. Ed.*, **2000**, *122*, 2698.
[43] R. Roy, *Top Curr Chem* **1997**, *187*, 241.
[44] C. D. Gutsche, *Calixarenes: An Introduction*, ed. J. F. Stoddart The Royal Society of Chemistry, Cambridge, **2008**, 276.
[45] L. Baldini, F. Sansone, A. Casnati, R. Ungano, *Calixarenes in molecular recognition*, 12, vol. 3, 863.
[46] F. Sansone, A. Casnati, *Chem. Soc. Rev.*, **2013**, *42*, 4623.
[47] A. Dondoni, A. Marra, *Chem. Soc. Rev.*, **2012**, *41*, 573.
[48] A. Dondoni, A. Marra, M.C. Schermann, A. Casnati, F. Sansone, R. Ungaro, *Chem-Eur J.*, **1997**, *3*, 1774.
[49] A. Dondoni, M. Kleban, X. Hu, A. Marra, H.D. Banks, *J. Org. Chem,*, **2002**, *67*, 4722.
[50] H.C. Kolb, M.G. Finn, K.B. Sharpless, Angew. Chem. Int. Ed., **2001**, *40*, 2004.
[51] C.W. Tornøe, C. Christensen, M. Meldal, J. Org. Chem., 2002, 67, 3057.
[52] F. Himo, T. Lovell, R. Hilgraf, V.V. Rostovtsev, L. Noodleman, K.B. Sharpless, V.V. Fokin, *J. Am. Chem. Soc.*, **2005**, *127*, 210.
[53] F. Sansone, E. Chierici, A. Casnati, R. Ungaro, *Org. Biomol. Chem.*, **2003**, *1*, 1802.
[54] S.P. Bew, R.A. Brimage, N. L'Hermite, S.V. Sharma, *Org. Lett.*, **2007**, *9*, 3713.
[55] A. Dondoni, A. Marra, *J. Org. Chem.*, **2006**, *71*, 7546.
[56] S. Andrè, F. Sansone, H. Kaltner, A. Casnati, J. Kopitz, H.J. Gabius, R. Ungaro, *ChemBioChem*, **2008**, *9*, 1649.
[57] M. Colombo, S. Corregal-Romero, M.F. Casula, L. Gutierrez, M.P. Morales, I.B. Bohm, J.T. Heverhagen, D. Prosperi, W.J. Parak, *Chem. Soc. Rev.*, **2012**, *41*, 4306.
[58] D. H. Martin, *Magnetism in solids*, The M.I.T press, Cambridge, Massachussets, **1967**.
[59] D. Jiles, *Introduction to magnetism and magnetic materials*, Chapman & Hall, **1991**.
[60] M. P. Morales, S. Veintemillas-Verdaguer, M. I. Montero, C. J. Serna, A. Roig, L. I. Casas, B. Martinez and F. Sandiumenge, *Chem. Mater.*, **1999**, *11*, 3058.
[61] A. Sandhu, H. Handa and M. Abe, *Nanotechnology*, **2010**, *21*, 442001.
[62] R. E. Rosensweig, *J. Magn. Magn. Mater.*, **2002**, *252*, 370.
[63] R. Massart, IEEE *Trans. Magn.*, **1981**, *17*, 131.
[64] L. Josephson, C.-H. Tung, A. Moore, R. Weissleder, *Bioconjugate Chem.*, **1999**, *10*, 186.
[65] E. Y. Sun, R. Weissleder, L. Josephson, *Small*, **2006**, *2*, 1144.
[66] T. Atanasijevic, M. Shusteff, P. Fam, A. Jasanoff, *Proc. Natl. Acad. Sci. U. S. A.*, **2006**, *103*, 14707.
[67] H. Gu, P. L. Ho, K. W. Tsang, L. Wang, B. Xu, *J. Am. Chem. Soc.*, **2003**, *125*, 15702.
[68] K. El-Boubbou, C. Gruden, X. Huang, *J. Am. Chem. Soc.*, **2007**, *129*, 13392.
[69] K. El-Boubbou, D.C. Zhu, C. Vasileiou, B. Borhan, D. Prosperi, W. Li, X. Huang, *J. Am. Chem. Soc.*, **2010**, *132*, 4490.

[70] T. Jennings, G. Strouse, in *Bio-Applications of Nanoparticles*, Springer Science+Business Media, New York, **2007**, *620*, 34.
[71] J. Yguerabide, E. E. Yguerabide, *Anal. Biochem.*, **1998**, *262*, 137; P. K. Jain, K. S. Lee, I. H. El-Sayed, M. A. El-Sayed, *J. Phys. Chem. B*, **2006**, *110*, 7238; J. J. Storhoff, A. A. Lazarides, R. C. Mucic, C. A. Mirkin, R. L. Letsinger, G. C. Schatz, *J. Am. Chem. Soc.*, **2000**, *122*, 4640; M. Hu, J. Chen, Z. Li, L. Au, G. V. Hartland, X. Li, M. Marquez, Y. Xia, *Chem. Soc. Rev.*, **2006**, *35*, 1084; Y. Sun and Y. Xia, *Analyst*, **2003**, *128*, 686–691; 27 H. Wang, D. Brandl, P. Nordlander, N. J. Halas, *Acc. Chem. Res.*, **2006**, *40*, 53; B. Luk'yanchuk, N. I. Zheludev, S. A. Maier, N. J. Halas, P. Nordlander, H. Giessen, C. T. Chong, *Nat. Mater.*, **2010**, *9*, 707; N. J. Halas, S. Lal, W. Chang, S. Link, P. Nordlander, *Chem. Rev.*, **2011**, *111*, 3913; M. R. Jones, K. D. Osberg, R. J. Macfarlane, M. R. Langille, C. A. Mirkin, *Chem. Rev.*, **2011**, *111*, 3736; B. Sepu´lveda, P. C. Angelome´, L. M. Lechuga, L. M. Liz-Marza´n, *Nano Today*, **2009**, *4*, 244; P. Englebienne, A. Van Hoonacker, M. Verhas, *Spectroscopy*, **2003**, *17*, 255; K. Aslan, J. R. Lakowicz, C. D Geddes, *Curr. Opin. Chem. Biol.*, **2005**, *9*, 538; S. K. Ghosh, T. Pal, *Chem. Rev.*, **2007**, *107*, 4797; K. A. Willets, R. P. Van Duyne, *Annu. Rev. Phys. Chem.*, **2007**, *4*, 267.
[72] H. Jans, Q. Huo, *Chem. Soc. Rev.*, **2012**, *41*, 2849.
[73] Image from ref. 56
[74] R.A. Sperling, P. Rivera Gil, F. Zhang, M. Zanella, W. J. Parak, *Chem. Soc. Rev.*, **2008**, *37*, 1896.
[75] M. Brust, M. Walker, D. Bethell, D. J. Schiffrin, R. Whyman, *J. Chem. Soc. Chem. Commun.*, **1994**, 801.
[76] N. R. Jana and X. Peng, *J. Am. Chem. Soc.*, **2003**, *125*, 14280.
[77] A. C. Templeton, W. P. Wuelfing and R. W. Murray, *Acc. Chem. Res.*, **2000**, *33*, 27.
[78] T. Pellegrino, S. Kudera, T. Liedl, A. M. Javier, L. Manna and W. J. Parak, *Small*, **2005**, *1*, 48.
[79] G. Han, C.C. You, B.J. Kim, R.S. Turingan, N.S. Forbes, C.T. Martin, V.M. Rotello, *Angew. Chem.*, **2006**, *118*, 3237; *Angew. Chem. Int. Ed.*, **2006**, *45*, 3165.
[80] G.T. Hermanson, *Bioconjugate Tecniques*, Academic Press San Diego, CA, **1996**.
[81] C.A. Mirkin, R.L. Letsinger, R.C. Mucic, J.J Storhoff, *Nature*, **1996**, *383*, 607.
[82] P.C. Patel, D.A. Giljohann, D.S. Seferos, , C.A. Mirkin, *Proc. Nat. Acad. Sci. USA*, **2008**, *105*, 17222.
[83] C.S. Thaxton, W.L. Daniel, D.A. Giljohann, A.D. Thomas, C.A. Mirkin, *J. Am. Chem. Soc.*, **2009**, *131*, 1384.
[84] K. El-Boubbou, X. Huang, *Curr. Med. Chem.*, **2011**, *18*, 2060.
[85] A.G. Barrientos, J.M. de la Fuente, T.C. Rojas, A. Fernandez , S. Penadés, *Chem.-Eur. J.*, **2003**, *9*, 1909; R. Ojeda, J.L. de Paz, A.G. Barrientos, M. Martin-Lomas, S. Penadés, *Carbohydr. Res.*, **2007**, *342*, 448.
[86] O. Martinez-Avila, K. Hijazi, M. Marradi, C. Clavel, C. Campion, C. Kelly, S. Penadés, *Chem.-Eur. J.*, **2009**, *15*, 9874.
[87] E.M. Goldys (Ed.), *Fluorescence Applications in Biotechnology and Life Sciences*, Wiley, Hoboken, **2009**.
[88] B. Herman, *Fluorescence Microscopy*, Springer-Verlag, New York, **1998**.
[89] F.W.D. Rost, *Quantitative Fluorescence Microscopy*, Cambridge University Press, Cambridge, **1991**.
[90] X.F. Wang, B. Herman (Eds.), *Fluorescence Imaging Spectroscopy and Microscopy*, Wiley, New York, **1996**.
[91] N. Johnsson, K. Johnsson, *Am. Chem. Soc. Chem. Biol.*, **2007**, *2*, 31.
[92] L. Bachmann, D.M. Zezell, A.D. Ribeiro, L. Gomes, A.S. Ito, *Appl. Spectrosc. Rev.*, **2006**, *41*, 575.
[93] U. Mahmood, C.H. Tung, A. Bogdanov, R. Weissleder, *Radiology*, **1999,** *213*, 866.
[94] A. Becker, C. Hessenius, K. Licha, B. Ebert, U. Sukowski, W. Semmler, B. Wiedenmann, C. Grotzinger, *Nat. Biotechnol.*, **2001**, *19*, 327.
[95] R. Rigler, M. Orrit, T. Basché, *Single Molecule Spectroscopy*, Springer, Berlin, **2001**.
[96] F. De Angelis, S. Fantacci, N. Evans, C. Klein, S.M. Zakeeruddin, J.E. Moser, K. Kalyanasundaram, H.J. Bolink, M. Grätzel, M.K. Nazeeruddin, *Inorg. Chem.*, **2007**, *46*, 5989.
[97] D.L. Rochester, S. Develey, S. Zálisˇ, J.A.G. Williams, *Dalton Trans.*, **2009**, 1728.
[98] J.L. Kropp, M.W. Windsor, *J. Chem. Phys.*, **1965**, *42*, 1599.
[99] T. Lövgren, K. Pettersson in: K. Van Dyke, R. Van Dyke (Eds.), *Luminescence Immunoassay and Molecular Applications*, CRC Press, Boca Raton, **1990**.
[100] A. Beeby, S.W. Botchway, I.M. Clarkson, S. Faulkner, A.W. Parker, D. Parker, J.A.G. Williams, J. *Photochem. Photobiol. B*, **2000**, *57*, 83.
[101] A. Ruggi, F.W.B. van Leeuwen, A.H. Velders, *Coord. Chem. Rev.*, **2011**, *255*, 2542.
[102] D. Phillips, *Pure Appl. Chem.*, **2011**, *83*, 733.
[103] E. Baggaley at al., *Coord. Chem. Rew.*, **2012**, *256*, 1762.
[104] Adapted from ref 76 and 92
[105] F. Barigelletti, D. Sandrini, M. Maestri, V. Balzani, A. von Zelewsky, L. Chassot, P. Jolliet, U. Maeder, *Inorg. Chem.*, **1988**, 27, 3644.
[106] J.A.G. Williams, *Top. Curr. Chem.*, **2007**, *281*, 205.

[107] L. Murphy, J.A.G. Williams, *Top. Organomet. Chem.*, **2010**, *28*, 75.
[108] F.N. Castellano, I.E. Pomestchenko, E. Shikhova, F. Hua, M.L. Muro, N. Rajapakse, *Coord. Chem. Rev.*, **2006**, *150*, 1819.
[109] I. Eryazici, C.N. Moorefield, G.R. Newkome, *Chem. Rev.*, **2008**, *108*, 1834.
[110] S.J. Farley, D.L. Rochester, A.L. Thompson, J.A.K. Howard, J.A.G. Williams, *Inorg. Chem.*, **2005**, *44*, 9690.
[111] S. Develay, O. Blackburn, A.L. Thompson, J.A.G. Williams, *Inorg. Chem.*, **2008**, *47*, 11129.
[112] M. Cocchi, J. Kalinowski, L. Murphy, J.A.G. Williams, V. Fattori, *Org. Electron.*, **2010**, *11*, 388.
[113] Adapted from Refs. 83-85.
[114] S. Develay, J. A. G. Williams, *Dalton Trans.* **2008**, 4562; B. Ma, P. I. Djurovich, M. E. Thompson, *Coord. Chem. Rev.* **2005**, *249*, 1501
[115] R. P.-L. Tang, K. M.-C. Wong, N. Zhu, V. W.-W. Yam, *Dalton Trans.* **2009**, 3911; P. Jarosz, K. Lotito, J. Schneider, D. Kumaresan, R. Schmehl, R. Eisenberg, *Inorg. Chem.* **2009**, *48*, 2420; H. Zhang, B. Zhang, Y. Li, W. Sun, *Inorg. Chem.*, **2009**, *48*, 3617; A. Y.-Y. Tam, K. M.-C. Wong, V. W.-W. Yam, *J. Am. Chem. Soc.*, **2009**, *131*, 6253.
[116] J. A. G. Williams, *Chem. Soc. Rev.* **2009**, *38*, 1783; D. L. Rochester, S. Develay, S. Zalis, J. A. G. Williams, *Dalton Trans.*, **2009**, 1728; J. A. G. Williams, A. Beeby, E. S. Davies, J. A. Weinstein, C. Wilson, *Inorg. Chem.*, **2003**, *42*, 8609; J. Schneider, P. Du, X. Wang, W. W. Brennessel, R. Eisenberg, *Inorg. Chem.*, **2009**, *48*, 1498; P. Shao, Y. Li, A. Azenkeng, M. R. Hoffmann, W. Sun, Inorg. Chem. 2009, 48, 2407; J. Schneider, P. Du, P. Jarosz, T. Lazarides, X. Wang, W. W. Brennessel, R. Eisenberg, *Inorg. Chem.*, **2009**, *48*, 4306.
[117] M.-Y. Yuen, V. A. L. Roy, W. Lu, S. C. F. Kui, G. S. M. Tong, M.-H. So, S. S.-Y. Chui, M. Muccini, J. Q. Ning, S. J. Xu, C.-M. Che, *Angew. Chem.*, **2008**, *120*, 10043; *Angew. Chem. Int. Ed.*, **2008**, *47*, 9895; W. Lu, S. S.-Y. Chui, K.-M. Ng, C.-M. Che, *Angew. Chem.*, **2008**, *120*, 4644; *Angew. Chem. Int. Ed.*, **2008**, *47*, 4568; W. Lu, Y. Chen, V. A. L. Roy, S. S.-Y. Chui, C.-M. Che, *Angew. Chem.*, **2009**, *121*, 7757; *Angew. Chem. Int. Ed.*, **2009**, *48*, 7621; Y. Chen, K. Li, W. Lu, S. S.-Y. Chui, C.-W. Ma, C.-M. Che, *Angew. Chem.*, **2009**, *121*, 10093; *Angew. Chem. Int. Ed.*, **2009**, *48*, 9909.
[118] C.A. Strassert, C-H Chien, M. D. Galvez Lopez, D. Kourkoulos, D. Hertel, K. Meerholz, L. De Cola, *Angew. Chem. Int. Ed.*, **2011**, *50*, 946.

Chapter 2:

Gal-3 inhibition by lactosyl- and galactosylcalix[4]arenes

2.1 Introduction❖

During the last two or three decades we have witnessed remarkable efforts in research and development activity aimed at obtainment of optical sensors for the measurement of chemical and biological species.
Sensors for analytes of biological interest that rely on rapid and portable screening techniques have been of interest to identify harmful toxins for food safety[1,2] or to detect chemical or biological agents that could be used in bioterrorism.[3,4,5] They are also of interest for research purposes in areas of biophysics and pharmaceutical sciences.

Galectin-3 is a member of the lectin family, of which 15 mammalian Galectins have been identified. Galectin-3 is approximately 30 kDa and, like all Galectins, contains a carbohydrate recognition binding domain (CRD) that enables the specific binding of β-galactosides. This protein has been shown to be involved in a series of fundamental biological processes such as cell adhesion, cell activation, cell growth and differentiation and apoptosis. Galectin-3 has been demonstrated to be involved in cancer, inflammation and fibrosis, heart disease, and stroke. Studies have also shown that the expression of Galectin-3 is linked to a variety of processes associated with heart failure, including myofibroblast proliferation, fibrogenesis, tissue repair, inflammation, and ventricular remodeling.[6] Elevated levels of Galectin-3 have been found to be significantly associated with higher risk of death in both acute decompensated heart failure and chronic heart failure populations. The roles of Galectins and Galectin-3, in particular, in cancer have been heavily investigated. Of note, Galectin-3 has been suggested to play important roles in cancer metastasis. Remarkably interesting is the intrafamily selectivity, that is the ability by an inhibitor to block Gal-3, for instance, but not Gal-1. This property seems quite important since Galectin-1 acts as anti-inflammatory agent,[7] while Galectin-3 has a pro-inflammatory activity[8] and, even more interestingly, Galectin-3 can act as competitive inhibitor against Galectin-1 which, on the other side, induces anoikis of tumor cells.[9] Considering the important areas of biology in which Galectins are involved, their inhibition can therefore have useful consequences. The therapeutic potential for Galectin

❖ This part of the work was carried out with the collaboration of the group of Prof. Francesco Peri, Università Bicocca, MI

inhibitors as anti-inflammatory and immunomodulation agents can be envisaged, but their potential in cancer therapeutics is the most obvious. Many of the biological functions of Galectins exploit multivalent binding, and fot this reason multivalent inhibitors that take advantage of this inherent ability can have a significant advantage over monovalent inhibitors. While inhibition and modulation of Galectin activities is an important goal it is also of strategic importance to have cheap and convenient methods for the detection and quantification of Galectins in tissues for biological studies and, in the future, in patient samples for early diagnosis and prognosis. This is because biological data that link the presence of Galectins, and especially Galectin-3, to an increased likelihood of malignacy or metastasis, and in specific cases to a reduced survival likelihood, is accumulating rapidly. [10]

SPR biosensing relies on the principle that any changes on the dielectric sensing surface will cause a shift in the angle of reflectivity, followed by a detector, in order to satisfy the resonance condition. There are different possible configuration that can be used for SPR sensing, but regardless of the configuration, environmental changes in the dielectric medium cause an alteration to the phase, amplitude, polarization or spectral distribution of the incident light, which can be attributed to changes in the propagation constant and, hence, changes in the refractive index are detected in real time. The most common use for SPR sensing is to evaluate protein-ligand, protein-protein, or nucleotide hybridization events. Since it is typically not advantageous to directly deposit biological molecules onto surfaces, especially surfaces of inert metals such as silver or gold, surface functionalization should be used to create a more functionally active environment and reduce non-specific binding on the surface. Protein-carbohydrate interactions can also be monitored by glycan-modified surfaces. Nickel nitrilotriacetic acid (Ni-NTA) derivatized surfaces are also convenient for specific capturing of proteins that have been genetically engineered with an N- or C-terminal polyhistidine tag, a common affinity moiety used during protein expression and purification processes. [11]

On the other hand, our research group has been working for the last few years on the design and synthesis of glycocalixarenes potentially able to interact with lectins of clinical interest, such as the VAA (*Viscum Album Agglutinin*) plant toxin, that acts as potent biohazard, and human Galectins, that act as factor in tumor progression and migration.

An interesting class of glycoclusters, that showed to be very effective and selective in the interaction with human Galectins, is represented by the lactosyl-thioureido-calix[4]arenes represented in figure 2.1[12].

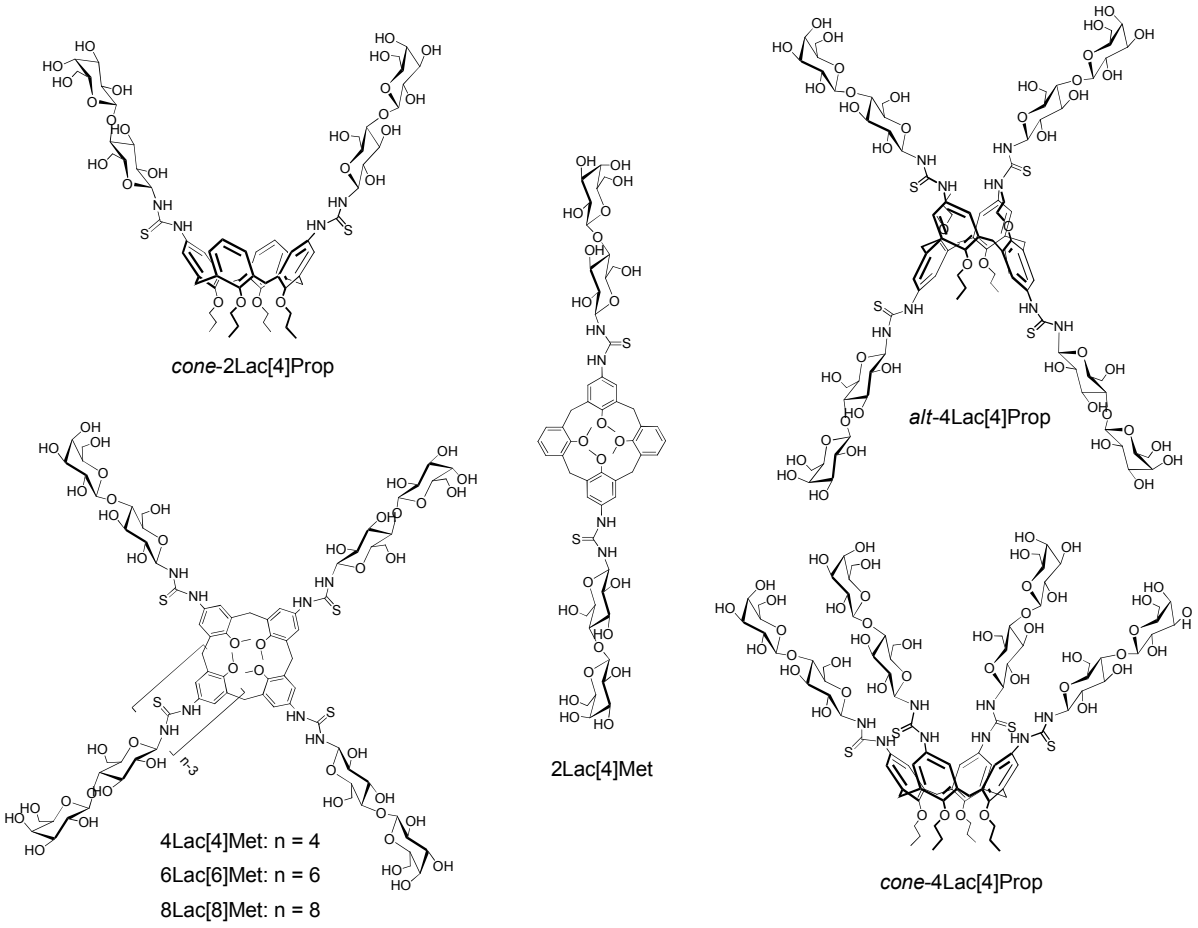

Figure 2.1 Examples of lactosyl-thioureido calix[4]arenes.

Cell-binding inhibition assays demonstrated that these compounds present the capacity to inhibit the adhesion of Galectins to the surface of tumor cells, and therefore they represent good candidates for antiadhesion therapies. For these studies selected human tumor lines were used. Binding of biotinylated Galectins to these cell lines was determined by quantitative fluorescence detection through a Fluorescence Activated Cell Sorter (FACS-Scan) by using streptavidin/R-phycoerythrin as indicator. Interestingly, these glycoclusters present the ability to selectively recognize different types of Galectins. For example the tetralactosylcalix[4]arene in the 1,3-alternate structure (*alt*-4-Lac[4]Prop, fig. 2.1) is a potent inhibitor for Gal-1, while it is the worst inhibitor for Gal-3. On the contrary, the *cone*-tetralactosylcalix[4]arene (*cone*-4Lac[4]Prop, fig. 2.1) is highly effective in the inhibition of Gal-3, but shows very low affinity for Gal-1. Similar experiments were

performed with the corresponding galactosyl-thioureido-calix[n]arenes, but these compounds showed to be less effective than the lacto-clusters. These bioassays pointed out the existence of a strict relationship between the stereochemical disposition of the glycosyl units around the different calixarenes and their inhibitory activity. Therefore, these glycoclusters present the possibility to selectively target the Galectins with an unprecedented *intra*-family selectivity (selectivity for some of the members of this family). This is important because, depending on the pathology, different types of these lectins can be involved.

Aim of this study is to find new compounds able to inhibit Gal-3. For this reason we synthesize a new class of glycocalixarene functionalized both with galactose and lactose units, that are known to be ligands for this type of Galectin. Moreover we decided to use a long spacer between the calixarene scaffold and the sugar moiety, a polyethylenglycol chain, in order to enhance the water solubility of these compounds and to reduce some possible strains due to the interaction.

In order to study the inhibition ability of these new glycocalixarenes compound we use preliminary SPR affinity study with his-tag Gal-3 Ni-NTA chip. Once an effective inhibitor for Gal-3 is found, the perspective of this work is to invert the approach, immobilizing the calixarene inhibitor on the chip. This would ideally allow to devise a sensor for the important analyte Gal-3, hopefully endowed of a high selectivity and sensitivity.

2.2 Results and discussion

For the binding test towards the modified Gal-3 three different glycocalixarenes were chosen (fig 2.2), which differ in conformation or type of the sugar they are functionalized with. Compound **1** and **2** are in cone structure, that means that all the sugars are presented on the same part of the macrocycle. Compound **3** is in 1,3-alternate structure, that means that the sugar are disposed in two different and opposite direction. The spacer between the sugar and the calixarene core is represented by a long polyethylenglycol chain, linked to the multivalent scaffold thanks to a triazole ring. The presence of this long polyethylenglycol chain could possibly enhance solubility in water and biocompatibility. The sugars used for the functionalization are galactose (**1**) and lactose (**2** and **3**) (fig 2.2).

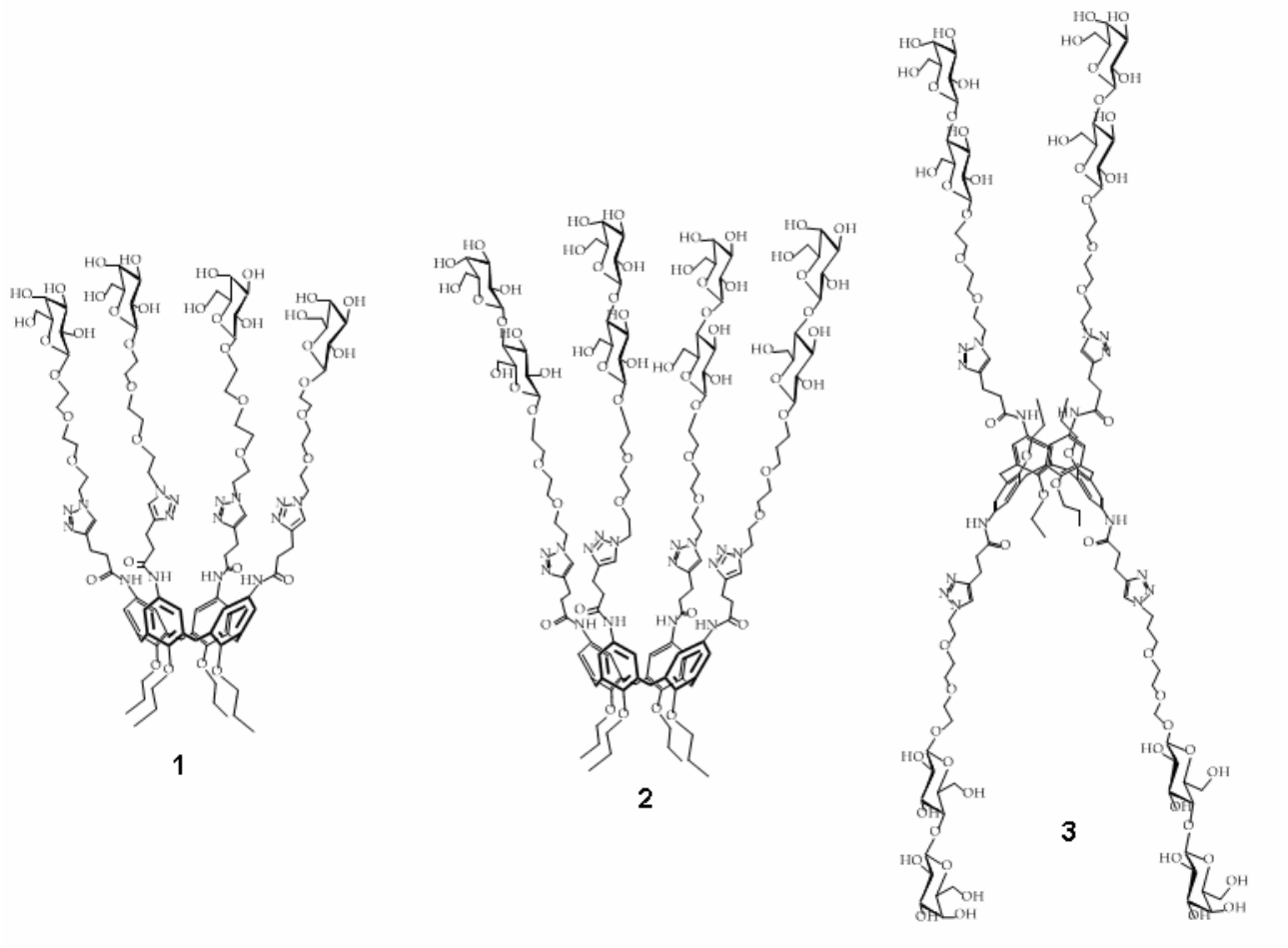

Figure. 2.2 Structure of glycocalixarene **1-3**.

2.2.1 Synthesis of the glycocalixarenes

For the synthesis of these glycocalixarenes a "Click reaction" between an azido glycoside and an alkyne-functionalized calixarene is used, following the protocol of the so-called Copper-catalyzed azido-alkyne cycloaddition reaction (CuAAC) that is characterised by extremely high yields and high regioselectivity on the triazole ring formation, with the 1,4-isomer highly favoured over the 1,5-attach.[13, 14]

Initially, the azido galactoside **6** was synthesized (fig. 2.3). The pentaacetyloxygalactoside **4** was directly reacted with 2-(2-(2-chloroethoxy) ethoxy)ethanol using $BF_3 \cdot Et_2O$ as Lewis acid to promote the glycosylation reaction. To minimize the formation of the α-anomer the temperature was initially kept at 0 °C and then slowly allowed to reach room temperature. A mixture of the two α- and β-anomers was obtained, however, the separation of the two anomers of compound **5** via column chromatography yielded, without particular

difficulties, the pure β-compound **5**. The ^{1}H NMR spectrum proved the success of the glycosylation reaction and of the purification step. Diagnostic is the coupling constant of 8.0 Hz for the signal of H_1 proton at 4.55 ppm, that unambiguously confirmed the presence of the product with the desired β-stereochemistry. Once obtained, compound **5** was reacted with NaN_3 to give the corresponding azido derivative **6** in satisfactory yield (72%).

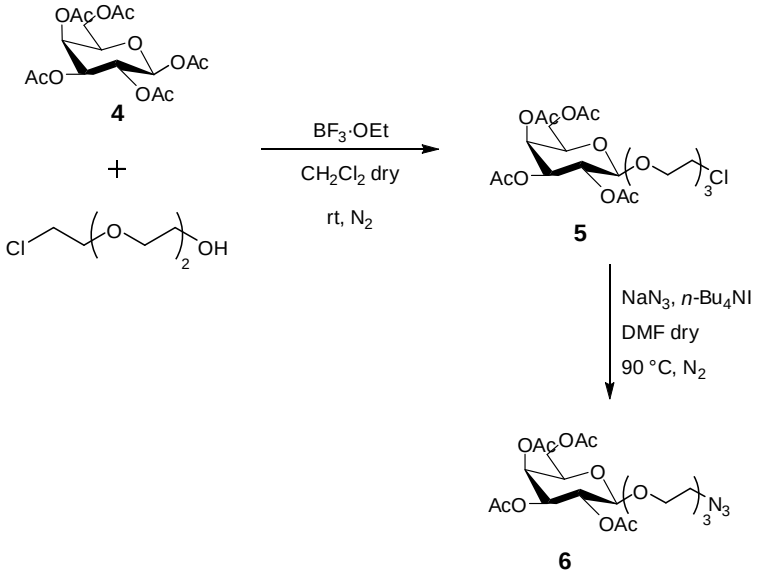

Figure 2.3 Synthesis of the azido galactoside **6.**

Amino-calix[4]arene **10** (fig. 2.4) was synthesized according to literature procedures (fig 2.4).[15] *p-tert*-Butyl-calix[4]arene **7** was alkylated at the lower rim by using propyl iodide in the presence of NaH as base to fix the macrocycle in the cone conformation and obtain compound **8.**[16,17] With the subsequent ipso-nitration reaction compound **9** was formed.[18,19] This reaction led to the desired compound **9** in high yields and with complete substitution of the *tert*-butyl groups with nitro functions, as confirmed by ^{1}H NMR that shows the total disappearance of the *tert*-butyl signals at around 1 ppm. By treating compound **9** with hydrazine and Pd/C (10%), product **10** was obtained.[20] The complete reduction of the nitro groups to amines was easily confirmed by ^{1}H NMR spectroscopy, where a broad signal at 3.1 ppm, corresponding to the amine groups, appears and an high-field shift for the signal of the aromatic protons, compared to that of the nitro derivative **9**, is observed. (fig. 3.7)

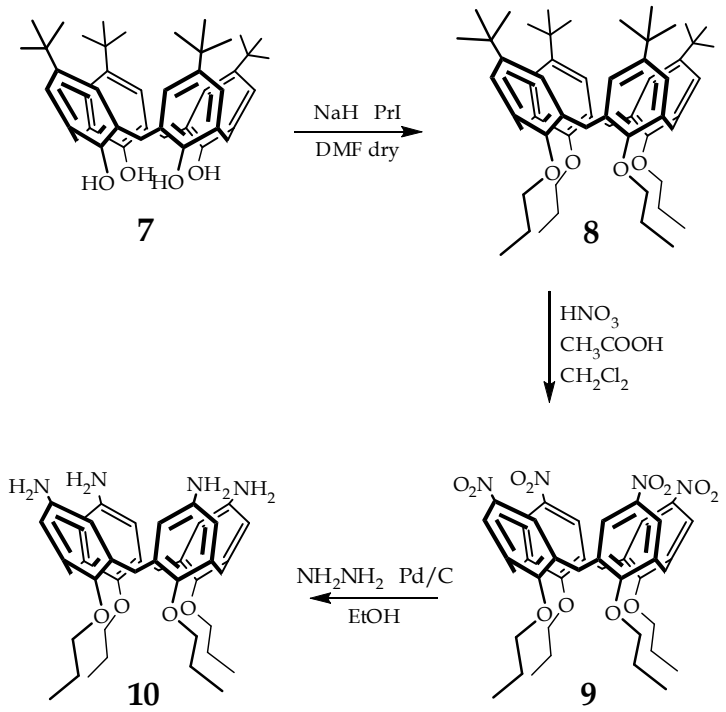

Figure 2.4 Synthesis of tetra-amino calix[4]arene **10**

Coupling reaction between amino-calix[4]arene **10** and 4-pentynoic acid in presence of 1-ethyl-3-(3-dimethylaminopropyl) carbodiimide (EDC) led to compound **11** in 66% yield. Calixarene **11** resulted to be very soluble in methanol, while it showed almost no solubility in CH_2Cl_2.

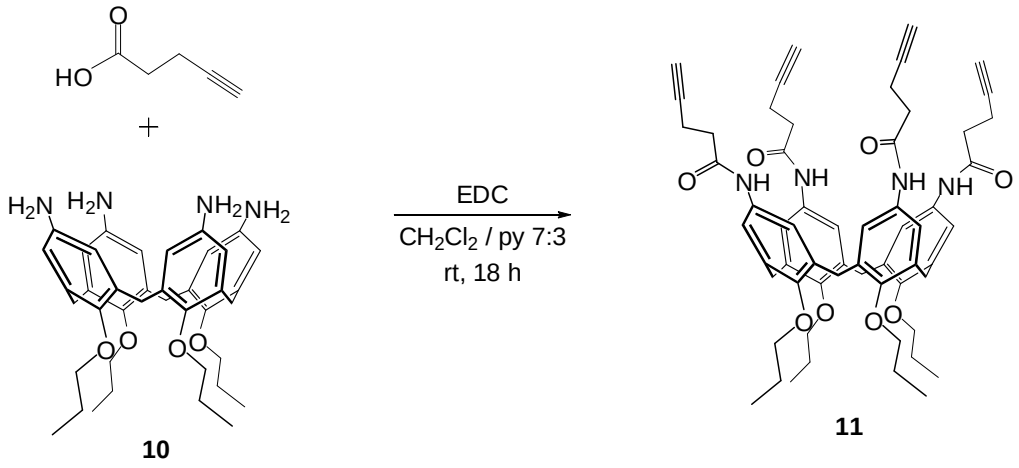

Figure 2.5 Synthesis of the alkyne calixarene **11**

The CuAAC reaction between the tetra-alkyne calix[4]arene **11** and azido-galactoside **6** to give glycocluster **12** (fig. 2.6) was performed in DMF and H_2O. $CuSO_4$ was used as copper source and sodium ascorbate was added as reducing agent. Also thanks to the use of a

microwave-assisted procedures[21] it was possible to efficiently prepare glycocluster **12**, that was obtained in 20 minutes at 150 W and 80 °C in 83% yield. No partially functionalized compounds or other byproducts were detected in the crude mixtures. Purification by column chromatography was necessary just to remove the excess of starting galactoside reagents used in the reactions. The ^{1}H NMR spectrum of galactosyl-calix[4]arene **12** presents a broad signal at 7.75 ppm for the proton of the triazole ring and complete absence at 2.27 ppm of the peak for the alkyne group present at the upper rim of the reagent **11**.

The deprotection from the acetyl groups was performed via transesterification reaction in presence of CH_3ONa in CH_3OH at room temperature according to the standard Zemplen procedure[22] (fig. 2.6). Complete deacetylation was achieved in 1 hour, as confirmed by ^{1}H NMR spectra of the obtained compound **1**, where it is possible to observe the complete absence of the acetyl signals between 2.15 and 1.90 ppm**.**

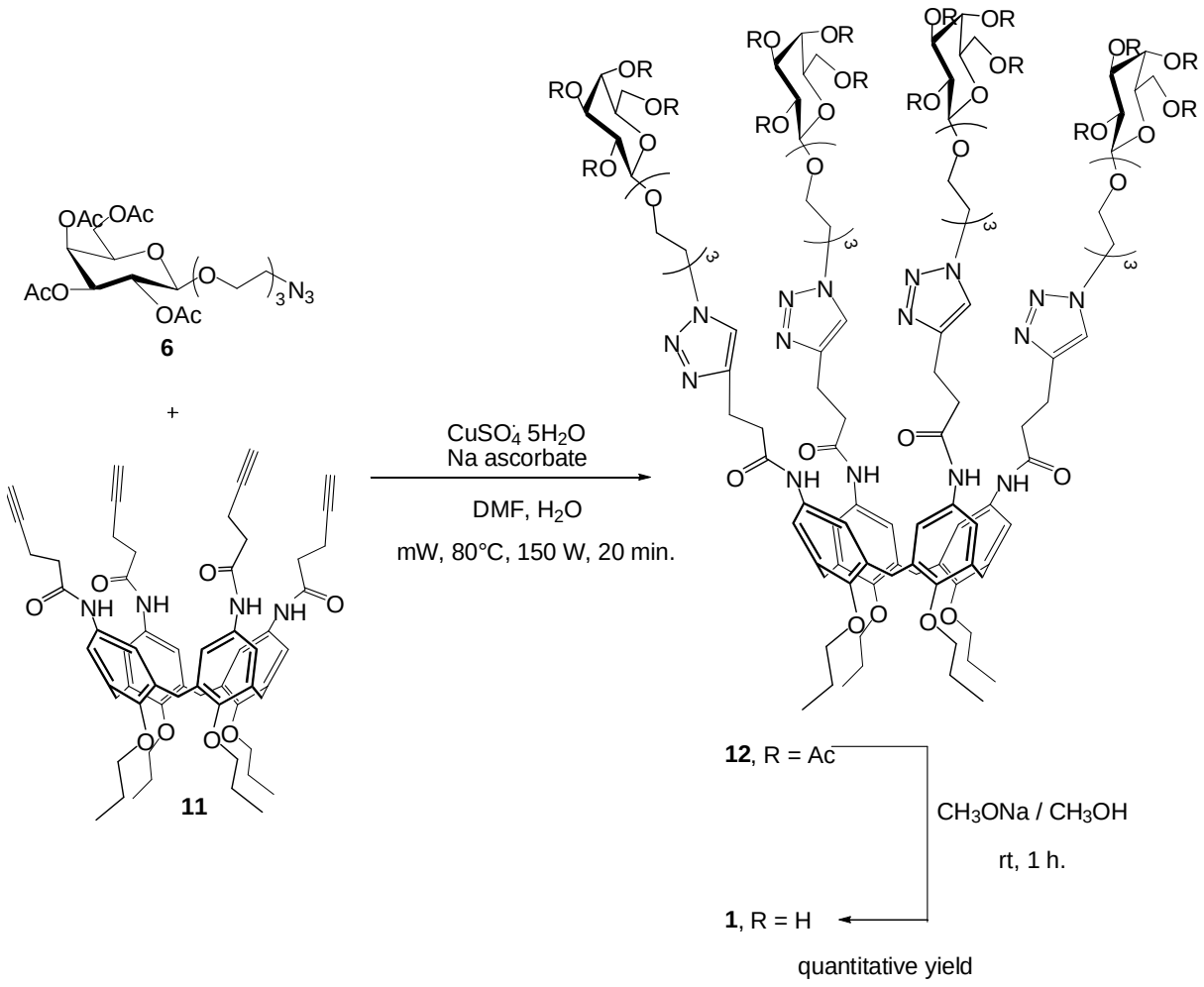

Figure 2.6 Synthesis of the galactosylcalixarene **1**

Cone-compound **2**, similar to compound **1** but functionalized with lactose units, and compound **3**, that presents lactose moieties connected to a 1,3-alternate calixarene core, were obtained using a similar synthetic strategy.

The first step of their synthesis consisted in the preparation of lactoside derivative **15** (fig. 2.7). When octa-*O*-acetyl-lactose **13** was reacted with 2-(2-(2-chloroethoxy)ethoxy)ethanol in presence of $SnCl_4$ and CF_3CO_2Ag, compound **14** was obtained mainly, but not exclusively, as β-anomer. Column chromatography purification could anyway yield to pure β-compound in 74% yield. The subsequent reaction of chlorinated compound **14** with NaN_3 led to the corresponding azido derivative **15** in 60% yield after 24 hours.

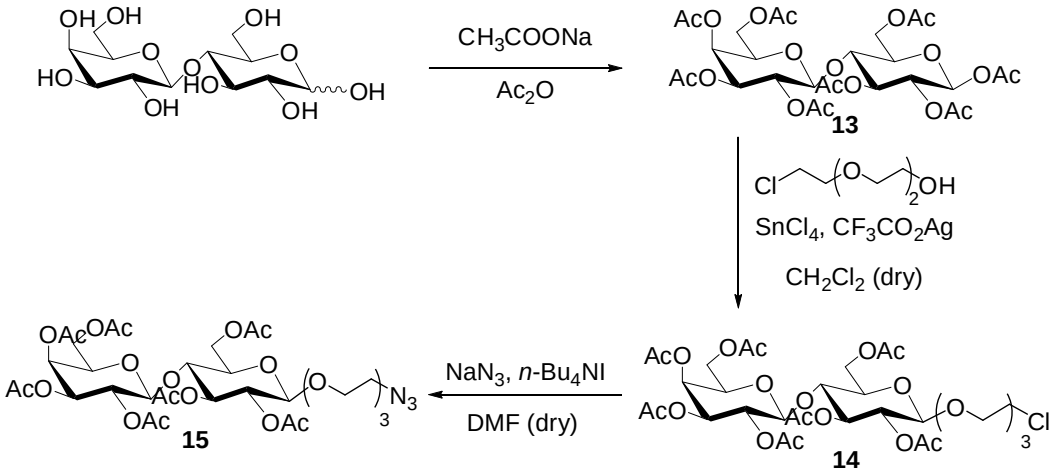

Figure 2.7 Synthesis of the lactoside derivative **15.**

1,3-Alternate-tetra-propargyl-calix[4]arene **20** (*Alt*-tetra-propargyl-calix[4]arene) was obtained from the corresponding 1,3-*alt*-amino-calix[4]arene **19** (fig. 2.8) via reaction with EDC in CH_2Cl_2 and pyridine 7:3 as previously described for compound **11**. Amino-*alt*-calixarene **19** was synthesized following a three steps procedure from *p-tert*-butyl-calix[4]arene **16,** that was alkylated at the lower rim with propyl bromide in presence of Cs_2CO_3 in dry CH_3CN to fix the macrocycle in the 1,3-alternate conformation,[23,24] and yielding compound **17**. Subsequent ipso-nitration allowed the complete substitution of the *p-tert*-butyl groups with nitro groups, yielding tetranitro derivative **18**[24], that was then treated with hydrazine and Pd/C (10%) to obtain the tetraamino-product **19**[25].

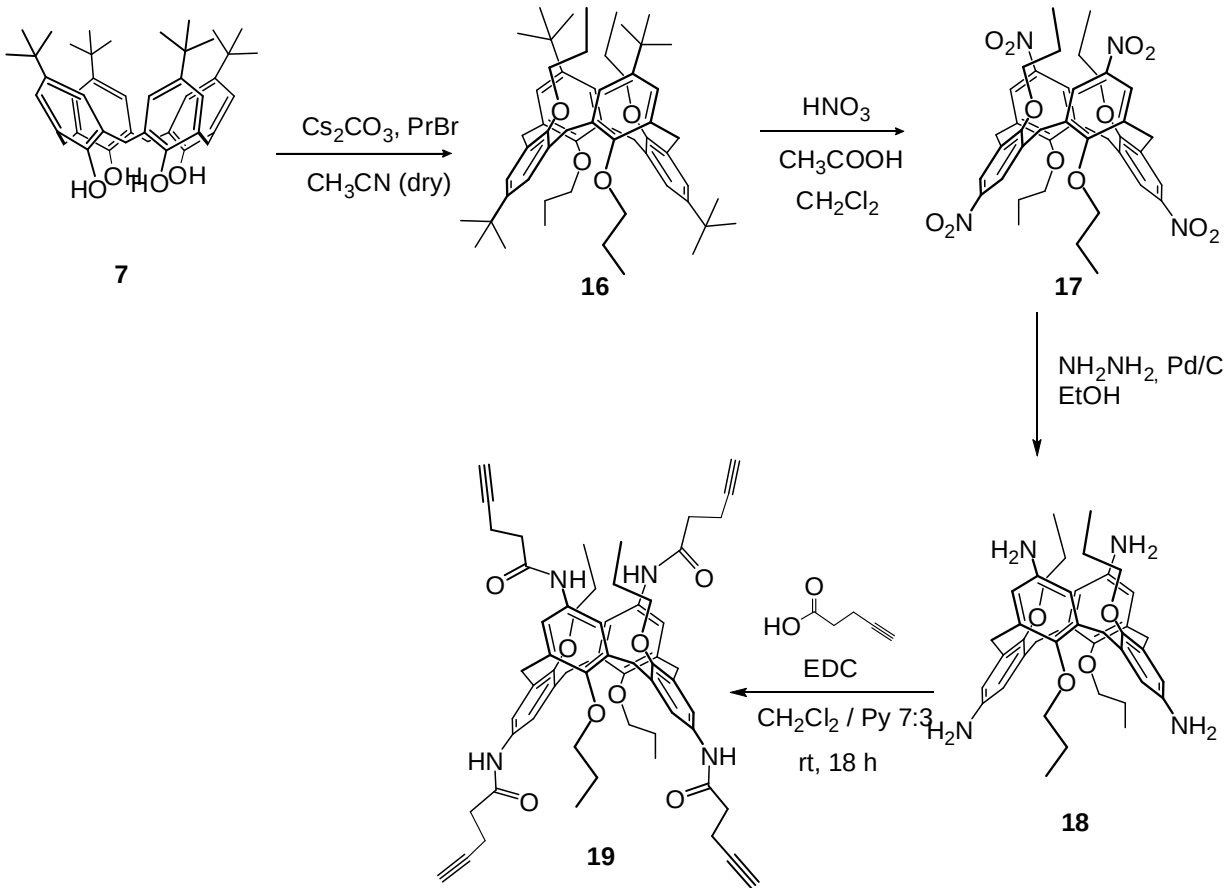

Figure 2.8 Synthesis of the 1,3-*alt*-tetra-propargyl-calix[4]arene **19.**

Azido-lactoside **15** was then reacted with the *cone*- and 1,3-alternate-tetra-alkyne-calix[4]arenes (compound **11** and **19**, respectively), via CuAAC "click" reaction, as previously described for the analogous galacto-clusters, to give respectively *cone*-calix[4]arene **20** (fig. 2.9) and *alt*-calix[4]arene **21** (fig. 2.10) in 45-50% yields. Microwave irradiation (150 W, 80 °C) allowed to obtain complete tetra-functionalization in only 40 minutes reaction. Subsequent deacetylation with Zemplen method led to target compounds **2** and **3.**

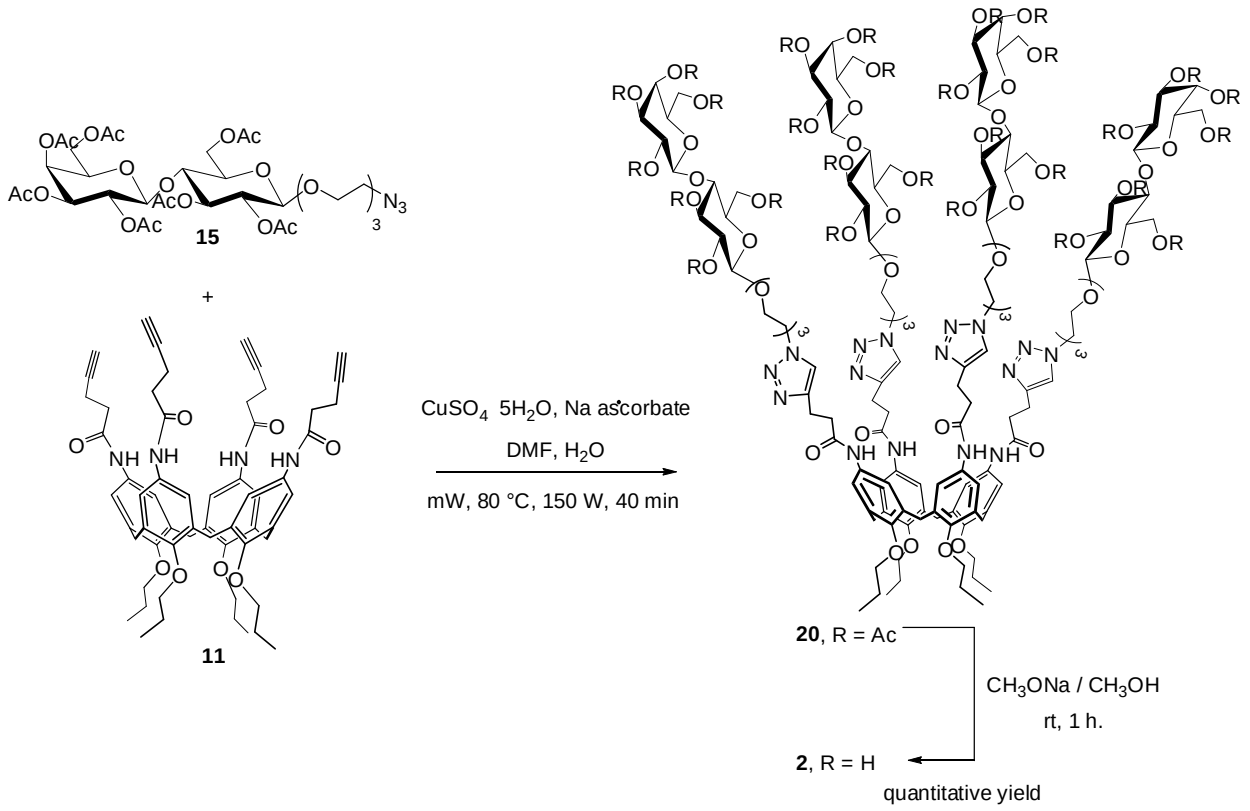

Figure 2.9 Synthesis of the *cone*-lactosylcalix[4]arene **2.**

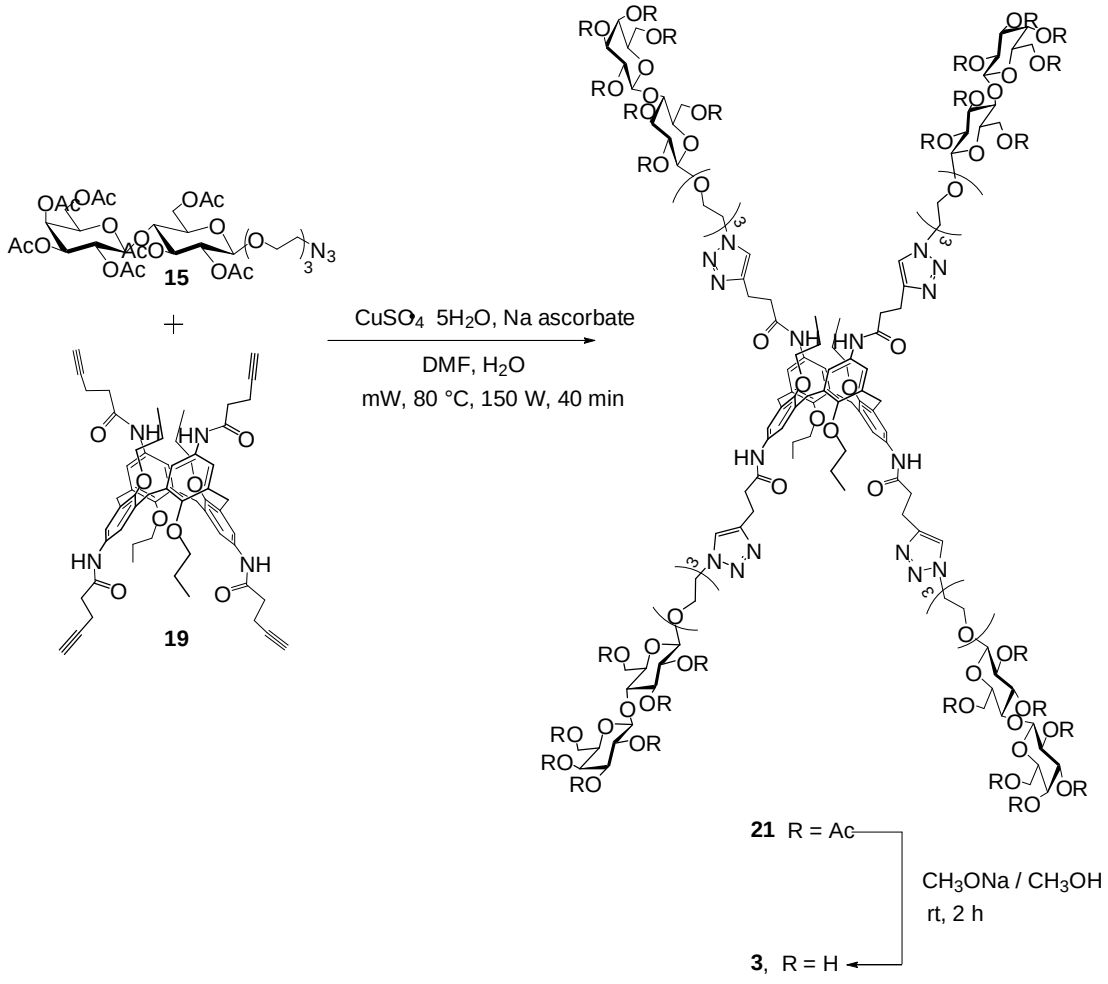

Figure 2.10 Synthesis of the 1,3-*alt*-lactosylcalix[4]arene **3.**

2.2.2 Expression and purification of Gal-3

His-tag Gal-3 (that is Gal-3 with hystidine tail) was expressed in *E. coli* BL121 using classical methodology of expression heterologous proteins. It was decided to express and use Gal-3 in his complete form, and non only its Carbohydrate Recognition Domain (CRD), that is the domain responsible for the galactoside binding, as many other group did before.

After induction with IPTG (Isopropil-β-D-1-tiogalattopiranoside), cells had been lysed and the proteins had been purified via affinity chromatography using IMAC (Immobilized Metal Ion Affinity Chromatography) columns that contains chelated Nickel on the surface, able to interact with the hystidines tails on Gal-3. Purified proteins, at this point, were eluted using an excess of imidazole (150 mM). Purification step was confirmed using electrophoresis in denaturant condition (fig 2.11). The identity of the proteins was confirmed thanks to a digestion on trypsin gel and MS/MS analysis (ESI-MS, Q-trap, Applied Biosystem). Molecular weight was confirmed by electrophoresis gel (fig. 2.11, left) and the secondary structure thanks to circular dichroism spectra (fig. 2.11, right).

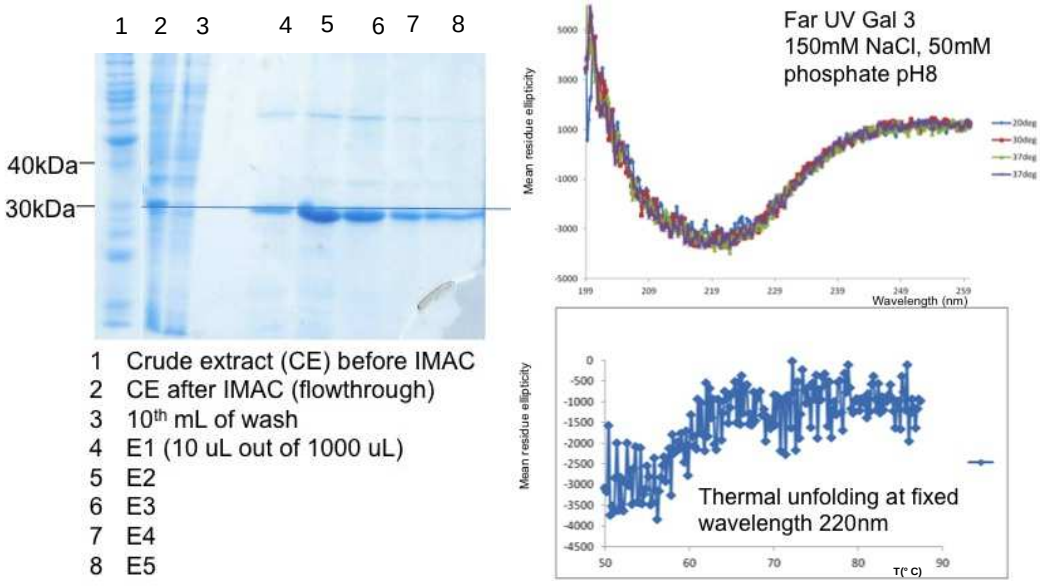

Figure 2.11: On the left: elctrophoresis gel of Gal-3, columns 1 e 2 are the crude extract, fractions 4-7 are different eluetes of IMAC column with the band of pure Gal-3 protein (approximate molecular weight 30 kD). On the right: circular dichrosim spectra and thermical unfolding of purified Gal-3.

This expressed Gal-3 had a hystidine tail that was used to immobilize in a directed way protein on the chip surface for SPR measurements. At this point one of the critical point of the synthesis of his-tag Gal-3 came up: how to determine the activity and functionality of the expressed and purified Gal-3. In fact there are no standard tests to evaluate the ability of Gal-3 to interact with its natural ligands, the only proof that expressed Gal-3 was in native conformation was obtained through circular dichroism spectrometric measurements.

Then protein Gal-3, in its complete form, was immobilized on Ni-NTA chips thanks to interaction with N-terminal hystidine tails (His-tag).

2.2.2 SPR analysis

For a preliminary evaluation of the interaction between the new calixarene **1**, **2**, **3** and immobilized his-tag Gal-3 the sensograms of fig 2.12 were recorded fluxing, over the chip, 1mM solution of calixarene in 10mM HEPES, 150mM NaCl, 50uM EDTA, 0.005% (v/v) Tween 20 at pH 7.4. The Ni-NTA (nitrilotriacetic) chip consists of carboxymethylated dextran with covalently immobilized NTA. The NTA molecule chelates metal ions such as Ni^{2+}, creating coordination sites that bind to polyhistidine tags. Thereafter the analyte of interest is passed over the surface and the binding of the ligand to the his-tag Gal-3 functionalized chip can be detected (figure 2.12).

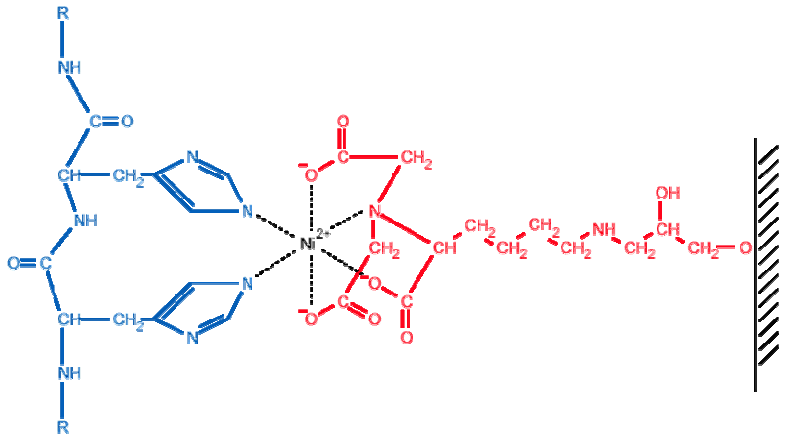

Figure 2.12 Interaction between hys-tag Gal-3 and the Ni-NTA chip.

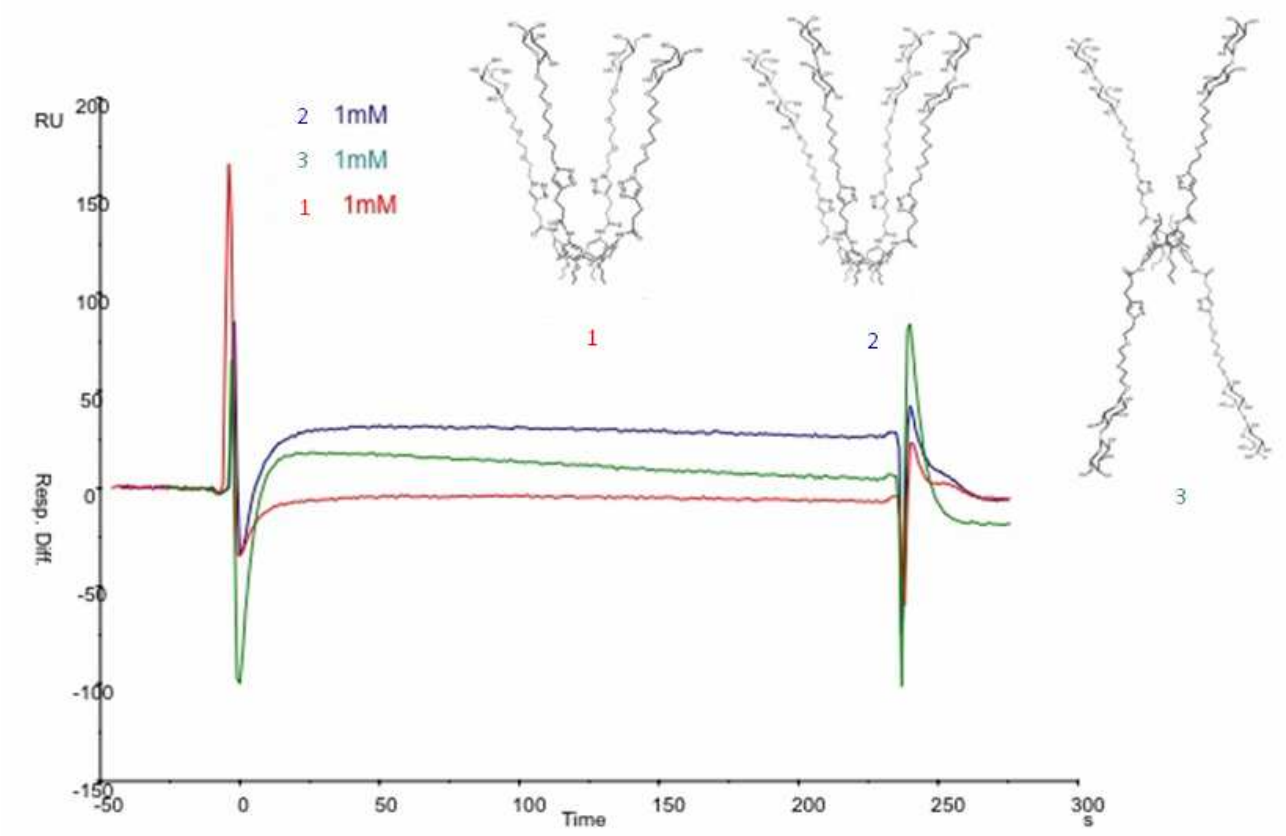

Figure 2.13 Sensorgramms obtained with SPR in binding experiment between Gal-3 immobilized on chip and glycocalixarenes.

Although the increases of resonance units in the sensogramms (fig 2.13) due to the binding with the protein are rather low, the three replicates (fig 2.14) that were obtained always show the same identical trend and order of affinity between ligands and protein. Compound **2** in the cone structure and functionalized with lactose units seems to be the best ligand for gal-3, while glycocalix **3**, in 1,3-alternate structure and also functionalized with lactose is less efficient in binding the lectin. Calixarene **1**, in the cone structure and with galactose units, seems not to interact at all.

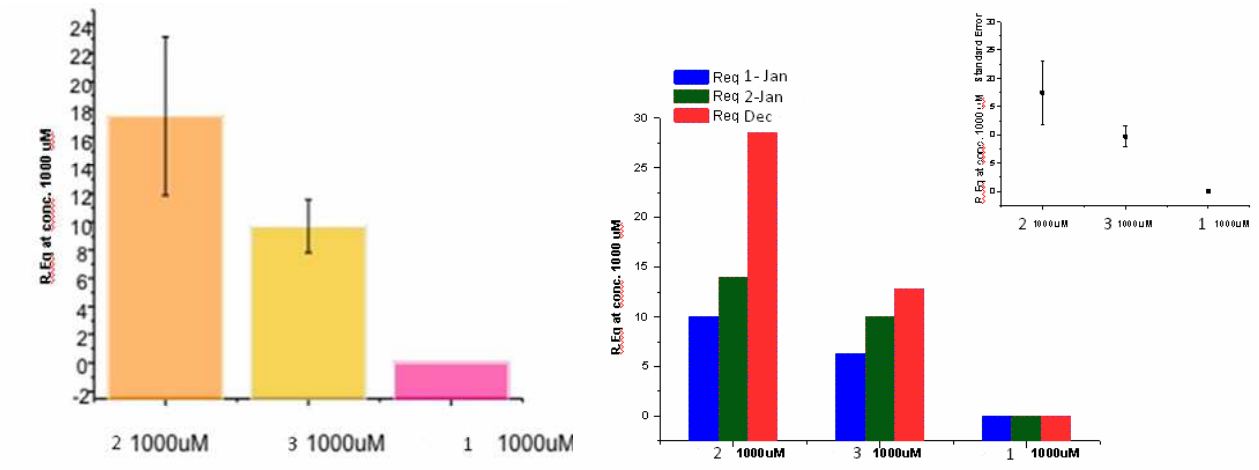

Figure 2.13 Relative affinity of glicocalixarene 1, 2, 5 (conc. 1 mM) towards Gal-3 expressed in term of increase of resonance unit (RU).

From these preliminary experiment it seems quite clear that the disaccharide ligand, lactose, makes the calixarenes better ligands for Gal-3 compared with the monosaccharide galactose; this is clearly consistent with the literature data, that in general confirm that monovalent Lactose is a better ligand for Gal-3 than monovalent galactose. Quite interestingly, also in these conditions the lactosylcalixarene fixed in the cone structure appears to bind better gal-3 than the isomer in the 1,3-alternate structure, confirming the data obtained in a series of inhibition experiments of the same lectin in surface-immobilised asialofetuin and on cells with the lactosylthioureidocalixarenes of figure 2.1.[12] Finally, suspecting that the glycocalixarenes **1-3** might aggregate in aqueous solution due to their amphiphilic structure resulting from polar residues (the sugars) and a lipophilic part (the calixarene core), we carried out some Dynamic Light Scattering (DLS) measurements using 1mM solutions of compounds in buffer 10mM HEPES, 150mM NaCl, 50uM EDTA, 0.005% (v/v) Tween 20 at pH 7.4 (Tab 2.1).

Compound	Micelles size (nm)
1	309
2	386
3	267

Table 2.1. Hydrodynamic radii of the glycocalix aggregates.

The hydrodynamic radii of the glycocalix aggregates show that these compounds indeed self-assemble in water solution to form large aggregates and nearly independently from their structure (cone or 1,3-alternate) or from the carbohydrate. However, 1,3-alternate derivative **3**, having a bolamphiphile structure is the one forming the smallest aggregates, 30% smaller than its cone isomer **2**. This latter compound, having lactose units that are more hydrophilic than galactose one, having a more amphiphilic structure than galactosylcalixarene **1** and hence form larger aggregates.

2.3 Conclusions

Three glycocalixarenes **1-3**, having long linkers between the glycosyl units and the macrocyclic scaffold were studied in the binding to his-tag Gal-3 using SPR. From these studies it was possible to notice that the obtained intensity of the signals due to interaction between the glycocalixarenes **1-3** and the Gal-3 are quite weak and near to the limit of detection of SPR in the used configuration. In fact, the low molecular weights of the glycocalixarenes, usually around 2.5 kDa, only slightly exceed the lower limit of detection of the used instrument (BIACORE). In spite of the weak intensity of the signals obtained, an affinity order for the interaction of ligands **1-3** with the immobilized Gal-3 was obtained. A preference for the lactosyl clusters over the galactose functionalized ones (**2** > **3** >> **1**) and a higher efficiency in the binding of Gal-3 shown by the cone derivative compared to its isomeric 1,3-alternate counterpart (**2** > **3**) were observed. This also confirms with a different technique what is already known in literature[12] that lactosyl-calixarene are more efficient than galactose-calixarene in Gal-3 binding, and that cone isomers are better ligands than the 1,3 alternate ones.

DLS studies also pointed out a slightly different sizes of the aggregates formed by these amphiphiles in water and that might also, in part, influence the affinity studies.

A possible and future development of these studies could consider the possibility to revert the approach and to anchor lower-rim modified lactosyl derivatives of **2** onto the chip, thus allowing to obtain a way to sense and quantify important markers of tumors such as galectins in biological fluids.

2.4 Experimental part

General Information. All moisture sensitive reactions were carried out under nitrogen atmosphere, using previously oven-dried glassware. All dry solvents were prepared according to standard procedures, distilled before use and stored over 3Å or 4Å molecular sieves. Most of the solvents and reagents were obtained from commercial sources and used without further purification. Analytical TLC was performed using prepared plates of silica gel (Merck 60 F-254 on aluminum) and then, according to the functional groups present on the molecules, revealed with UV light or using staining reagents: $FeCl_3$ (1% in H_2O/CH_3OH 1:1), H_2SO_4 (5% in EtOH), ninhydrin (5% in EtOH), basic solution of $KMnO_4$ (0.75% in H_2O). Merck silica gel 60 (70-230 mesh) was used for flash chromatography and for preparative TLC plates. ^1H NMR and ^{13}C NMR spectra were recorded on Bruker AV300 and Bruker AV400 spectrometers (observation of ^1H nucleus at 300 MHz and 400 MHz respectively, and of ^{13}C nucleus at 75 MHz and 100 MHz respectively). All chemical shifts are reported in part per million (ppm) using the residual peak of the deuterated solvent, whose values are referred to tetramethylsilane (TMS, $\delta_{TMS} = 0$), as internal standard. All ^{13}CNMR spectra were performed with proton decoupling. Electrospray ionization (ESI) mass analyses were performed with a Waters spectrometer. Gas chromatography mass analyses (GC-MS, electronic impact 70 eV) were recorded on a HP 6890 Series GC System apparatus, equipped with capillary column DB5 and quadrupolar mass selector HP 5973 Mass Selective Detector. Microwave reactions were performed using a CEM Discovery System reactor.

General procedure to obtain peracetylated carbohydrates (compounds 4 and 13)

Sodium acetate (7 eq) was suspended in acetic anhydride (25 eq) and heated to 130 °C. At this temperature D-galactose (1 eq) was added batchwise. The mixture was stirred at 130 °C and checked via TLC (eluent: AcOEt/hexane 1:1). When the reaction was completed, it was poured into a flask containing ice and water (5 times the volume of acetic anhydride). The mixture was then stirred at room temperature overnight. The solid formed was recovered by filtration on Buchner funnel and then purified via trituration in EtOH.

1,2,3,4,6-Penta-*O*-acetyl-β-D-galactopyranoside 4

Sodium acetate (32.0 g, 0.39 mol), acetic anhydride (134 mL, 1.38 mol), D-galactose (10.0 g, 55.5 mmol) Reaction time: 2 hours. Product **4** was obtained as white solid in 40% yield. **^{1}H NMR** (300 MHz, $CDCl_3$): δ (ppm) 5.69 (d, 1H, J = 8.2 Hz, H1), 5.42 (dd, 1H, J = 0.9 Hz, J = 3.4, H4), 5.33 (dd, 1H, J = 8.2 Hz, J = 10.4 Hz, H2), 5.07 (dd, 1H, J = 3.4 Hz, J = 10.4 Hz, H3), 4.17-4.11 (m, 2H, H6a, H6b), 4.09-4.00 (m, 1H, H5), 2.16, 2.12, 2.04, 1.99 (5s, 15H, Ac). The product shows the same physical and spectroscopic properties reported in the literature[26].

2,3,4,6-Tetra-*O*-acetyl-β-D-galactopyranosyl-(1→4)-2,3,6-tri-*O*-acetyl-β-D-glucopyranoside 13

Sodium acetate (16.1 g, 0.20 mol), acetic anhydride (68 mL, 0.70 mol), D-lactose (10.0 g, 28.0 mmol) Reaction time: 18 hours. Product **13** was obtained as white solid in 61% yield. **^{1}H NMR** (300 MHz, $CDCl_3$): δ(ppm) 5.67 (d, 1H, J = 8.4 Hz, H1), 5.34 (d, 1H, J = 3.3 Hz, H4'), 5.24 (t, 1H, J = 9.2 Hz, H3), 5.15-4.98 (m, 2H, H2, H2'), 4.93 (dd, 1H, J = 3.3 Hz, J = 10.4 Hz, H3'), 4.51-4.39 (m, 2H, H1', H6a), 4.17-4.01 (m, 3H, H6b, H6'a, H6'b), 3.90-3.78 (m, 2H, H4, H5'), 3.77-3.70 (m, 1H, H5), 2.18, 2.11, 2.08 (3s, 9H, Ac), 2.07-1.99 (m, 12H, Ac), 1.95 (s, 3H, Ac). The product shows the same physical and spectroscopic properties reported in the literature.[27]

2-(2-(2-Chloroethoxy)ethoxy)ethoxy-2,3,4,6-tetra-*O*-acetyl-β-D-galactopyranoside 5

Penta-*O*-acetyl-β-galactose **4** (0.50 g, 1.28 mmol) and 2-(2-(2-chloroethoxy)ethoxy)ethanol (0.28 mL, 1.92 mmol) were dissolved in dry CH_2Cl_2 (5 mL). The mixture was cooled to 0 °C with an ice-water bath and $BF_3 \cdot Et_2O$ (0.80 mL, 6.48 mmol) was added dropwise. The mixture, kept under N_2, was allowed to slowly reach room temperature and it was stirred for 24 h. The reaction was checked via TLC (eluent: AcOEt/petroleum ether 1:1) and once finished it was quenched by adding $NaHCO_3$ saturated aqueous solution (20 mL). The aqueous phase was extracted with CH_2Cl_2 (3 x 20 mL). The combined organic phases were washed with water (20 mL), dried over anhydrous Na_2SO_4, filtered and the solvent removed under reduced pressure. The residue was purified by flash chromatography (eluent: AcOEt/petroleum ether 1:1). Product **5** was obtained pure as a yellow oil. Yield: 30%. **^{1}H NMR** (300 MHz, $CDCl_3$): δ (ppm) 5.36 (dd, 1H, J = 1.0 Hz, J = 3.3 Hz, H4), 5.19 (dd, 1H, J = 8.0 Hz, J = 10.5 Hz, H2), 5.01 (dd, 1H, J = 3.3 Hz, J = 10.5 Hz, H3), 4.55 (d, 1H, J

= 8.0 Hz, H1), 4.17-4.07 (m, 2H, H6a H6b), 3.98-3.87 (m, 2H, H_5, β-OCH_a), 3.77-3.59 (m, 11H, β-OCH_b, CH_2 ethylene glycol chain), 2.13, 2.04, 2.03, 1.96 (4s, 12H, Ac). **ESI-MS:** m/z 521.7 [$(M+Na)^+$]. The product shows the same physical and spectroscopic properties reported in the literature. [28]

2-(2-(2-Azidoethoxy)ethoxy)ethoxy-2,3,4,6-tetra-*O*-acetyl-β-D-galactopyranoside 6

NaN_3 (0.23 g, 3.60 mmol) and tetrabutyl ammonium iodide (0.53 g, 1.44 mmol) were added to a solution of galactoside derivative **5** (0.36 g, 0.72 mmol) in dry DMF (5 mL). The mixture was stirred at 90 °C for 48 hours under nitrogen atmosphere. ESI-MS analyses were performed to monitor the reaction. The solvent was subsequently removed *in vacuo* and the residue redissolved in AcOEt (30 mL). The organic phase was washed with water (2 x 30 mL), dried over anhydrous Na_2SO_4, filtered and the solvent removed under reduced pressure. Purification via column chromatography (eluent: AcOEt/petroleum ether 1:1) gave pure product **6** as a light yellow oil. Yield: 72%. **^{1}H NMR** (300 MHz, $CDCl_3$): δ (ppm) 5.37 (dd, 1H, J = 1.2 Hz, J = 4.0 Hz, H4), 5.19 (dd, 1H, J = 8.1 Hz, J = 10.5 Hz, H2), 5.00 (dd, 1H, J = 4.0 Hz, J = 10.5 Hz, H3), 4.56 (d, 1H, J = 8.1 Hz, H1), 4.19-4.08 (m, 2H, H6a, H6b), 3.98-3.87 (m, 2H, β-OCH_a, H5), 3.81-3.71 (m, 1H, β-OCH_b), 3.70-3.59 (m, 8H, CH_2 ethylene glycol chain), 3.87 (t, 2H, J = 5.1 Hz, CH_2N_3), 2.14, 2.05, 2.04, 1.97 (4s, 12H, Ac). **ESI-MS:** m/z 528.2 $(M+Na)^+$. The product shows the same physical and spectroscopic properties reported in the literature.[29]

***Cone*-5,11,17,23-tetrakis[penta-4-ynoyl-amido]-25,26,27,28-tetrapropoxy-calix[4]arene 11**

4-Pentynoic acid (0.18 g, 1.84 mmol) and EDC (0.35 mg, 1.84 mmol) were dissolved in 14 mL CH_2Cl_2 and 6 mL pyridine. The solution was stirred for 30 min at room temperature and then amino-calix[4]arene **10**[15] (0.20 g, 0.31 mmol) were added. The mixture turned immediately red. The reaction was stirred at room temperature for 18 hours and it was monitored via TLC (eluent: CH_2Cl_2/CH_3OH 9:1). The mixture was then diluted with CH_2Cl_2 (20 mL) and washed with 1M HCl (2 x 20 mL) and water (20 mL). The combined aqueous phases were extracted with CH_2Cl_2 (30 mL). The organic layers were collected together and evaporated to dryness. The residue was purified via column chromatography (eluent: CH_2Cl_2/CH_3OH 97:3) to give product **11** as a white solid. Yield: 66%. **^{1}H NMR** (300 MHz, CD_3OD): δ (ppm) 6.88 (s, 8H, Ar), 4.46 (d, 4H, J = 13.2 Hz,

$ArCH_2Ar$), 3.85 (t, 8H, J = 7.5 Hz, $OC\underline{H}_2CH_2CH_3$), 3.11 (d, 4H, J = 13.2 Hz, $ArCH_2Ar$), 2.49–2.46 (m, 16H, $COC\underline{H}_2CH_2$, $COCH_2C\underline{H}_2$), 2.27 (bs, 4H, C≡CH), 2.00–1.93 (m, 8H, $OCH_2C\underline{H}_2CH_3$), 1.03 (t, 12H, J = 7.2 Hz, $OCH_2CH_2C\underline{H}_3$). The product shows the same physical and spectroscopic properties reported in the literature.[30]

2-(2-(2-Chloroethoxy)ethoxy)ethoxy-2,3,4,6-tetra-*O*-acetyl-β-D-galactopyranosyl-(1→4)-2,3,6-tri-*O*-acetyl-β-D-glucopyranoside 14

Octa-*O*-acetyl-lactose **13** (2.03 g, 3.00 mmol) and 2-(2-(2-chloroethoxy)ethoxy) ethanol (0.65 mL, 4.50 mmol) were dissolved in 10 mL dry CH_2Cl_2. CF_3COOAg (0.99 g, 4.50 mmol) and a 1M solution of $SnCl_4$ (0.91 mL, 9.00 mmol) in dry CH_2Cl_2 was added dropwise under argon atmosphere. The reaction was stirred at room temperature under Ar for 3 hours. The reaction was monitored via TLC (AcOEt/petroleum ether 7:3). $NaHCO_3$ saturated aqueous solution (30 mL) was subsequently added for quenching. The precipitate was filtered off through a Celite pad. The organic phase was collected and the aqueous phase was extracted with CH_2Cl_2 (4 x 30 mL). The combined organic phases were washed with water and brine till neutral pH, dried over anhydrous Na_2SO_4, filtered and the solvent removed under reduced pressure. The residue was purified by flash chromatography (elution gradient: AcOEt/hexane 65:35 →7:3). Product **14** was obtained pure as a yellow oil. Yield: 74%. **^{1}H NMR** (300 MHz, $CDCl_3$): δ(ppm) 5.32 (d, 1H, J = 3.3 Hz, H4'), 5.17 (t, 1H, J = 9.3 Hz, H3), 5.08 (dd, 1H, J = 7.9 Hz, J2 = 10.4 Hz, H2'), 4.93 (dd, 1H, J = 3.3 Hz, J = 10.4 Hz, H3'), 4.87 (dd, 1H, J = 7.8 Hz, J = 9.3 Hz, H2), 4.55 (d, 1H, J = 7.8 Hz, H1), 4.51-4.38 (m, 2H, H1', H6a), 4.20-4.00 (m, 3H, H6b, H6'a, H6'b), 3.93-3.79 (m, 2H, H5', β-OCHa), 3.78-3.68 (m, 4H, H4, β-OCHb, CH_2 ethylene glycol chain), 3.67-3.53 (m, 9H, H5, $3CH_2$ ethylen glycol chain, CH_2Cl), 2.13, 2.12, 2.10, 2.09, 2.04, 2.02, 1.94 (7s, 21H, $COCH_3$). The product shows the same physical and spectroscopic characteristics reported in literature.[31]

2-(2-(2-Azidoethoxy)ethoxy)ethoxy-2,3,4,6-tetra-*O*-acetyl-β-D-galactopyranosyl-(1→4)-2,3,6-tri-*O*-acetyl-β-D-glucopyranoside 15

NaN_3 (0.15 g, 2.35 mmol) and tetrabutyl ammonium iodide (0.35 g, 0.94 mmol) were added to a solution of lactoside derivative **14** (0.37 g, 0.47 mmol) in dry DMF (10 mL). The mixture was stirred at 90 °C for 24 hours under nitrogen atmosphere. ESI-MS analyses were performed to monitor the reaction. The solvent was subsequently removed *in vacuo*

and the residue redissolved in AcOEt (40 mL). The organic phase was washed with water (2 x 30 mL), dried over anhydrous Na_2SO_4, filtered and the solvent removed under reduced pressure. Purification via column chromatography (elution gradient: AcOEt/toluene 65:35 → 7:3) gave pure product **15** as a light yellow oil. Yield: 60%. **^{1}H NMR** (300 MHz, $CDCl_3$): δ (ppm) 5.25 (d, 1H, J = 3.3 Hz, H4'), 5.10 (t, 1H, J = 9.3Hz, H3), 5.01 (dd, 1H, J = 7.9 Hz, J = 10.4 Hz, H2'), 4.87 (dd, 1H, J = 10.4 Hz, J = 3.3 Hz, H3'), 4.87 (dd, 1H, J = 7.9 Hz, J = 9.3 Hz, H2), 4.49 (d, 1H, J = 7.9 Hz, H1), 4.44-4.36 (m, 2H, H1', H6a), 4.09-3.94 (m, 3H, H6b, H6'a, H6'b), 3.88-3.76 (m, 2H, H5', β-OCHa), 3.71 (t, 1H, J = 9.3 Hz, H4), 3.67-3.47 (m, 10H, H5, β-OCHb, CH_2 ethylene glycol chain), 3.31 (t, 2H, J = 5.0 Hz, CH_2N_3), 2.06 (s, 3H, $COCH_3$), 2.03 (s, 3H, $COCH_3$), 2.00-1.92 (m, 12H, $COCH_3$), 1.88 (s, 3H, $COCH_3$). The product shows the same physical and spectroscopic properties reported in the literature.[31]

***Alt*-5,11,17,23-tetrakis[penta-4-ynoyl-amido]-25,26,27,28-tetrapropoxy-calix[4]arene 19**

4-Pentynoic acid (90.0 mg, 0.92 mmol) and EDC (176.4 mg, 0.92 mmol) were dissolved in 7 mL CH_2Cl_2 and 3 mL pyridine. The solution was stirred for 30 min at room temperature and then *alt*-tetra-amino calix[4]arene **18**[15] (98.1 mg, 0.15 mmol) was added. The mixture turned immediately red. The reaction was stirred at room temperature for 18 hours and it was monitored via TLC (eluent: CH_2Cl_2/CH_3OH 9:1). The mixture was then diluted with CH_2Cl_2 (10 mL) and washed with 1M HCl (2 x 10 mL) and water (2 x 10 mL). The combined aqueous phases were extracted with CH_2Cl_2 (30 mL). The organic layers were collected together and evaporated to dryness. The residue was purified via column chromatography (eluent: CH_2Cl_2/CH_3OH 97:3) to give product **19** as a white solid. Yield: 65%. **^{1}H NMR** (300 MHz, CD_3OD/$CDCl_3$ 9:1): δ (ppm) 7.31 (s, 8H, Ar), 3.73 (s, 8H, $ArCH_2Ar$), 3.24 (t, 8H, J = 7.4 Hz, $OC\underline{H}_2CH_2CH_3$), 2.57-2.45 (m, 16H, $COC\underline{H}_2CH_2$, $COCH_2C\underline{H}_2$), 2.18-2.14 (m, 4H, C≡CH), 1.34-1.23 (m, 8H, $OCH_2C\underline{H}_2CH_3$), 0.67 (t, 12H, J = 7.4 Hz, $OCH_2CH_2C\underline{H}_3$). The product shows the same physical and spectroscopic properties reported in the literature.[32]

General procedure for "click" reactions (compounds 12, 20, 21)

Calix[4]arene derivative (1 eq) and β-galactoside derivative (6 eq) were dissolved in 2.5 mL of DMF in a microwave tube. $CuSO_4$ $5H_2O$ (0.3 or 0.6 eq), sodium ascorbate (0.6 or 1.2

eq) and 0.5 mL H_2O were then added. The mixture was heated at 80 °C by microwave irradiation (150 W) for a reaction time between 20 and 40 minutes. When the reaction was completed (checked via TLC and ESI-MS), it was quenched by addition of water (15 mL) and extracted with AcOEt (5 x 15 mL). The combined organic layers were dried over anhydrous Na_2SO_4, filtered and the solvent removed under reduced pressure. The crude was purified by flash chromatography to afford pure the peracetylated glycosyl calix[4]arene.

***Cone*-peracetylated-galactosyl-calix[4]arene 12**

Cone-tetra-alkyne calix[4]arene **11** (38.9 mg, 0.04 mmol), azido galactoside **6** (121.3 mg, 0.24 mmol), $CuSO_4 \cdot 5H_2O$ (3.0 mg 12.0 μmol), sodium ascorbate (4.7 mg, 24.0 μmol). Reaction time: 20 min. TLC (eluent: CH_2Cl_2/CH_3OH 95:5). Flash chromatography (elution gradient: CH_2Cl_2/CH_3OH 95:5 → 93:7). Product **12** was obtained as a light yellow solid. Yield: 83%. **^{1}H NMR** (400 MHz, $CD_3OD/CDCl_3$ 4:1): δ(ppm) 7.75 (bs, 4H, C<u>H</u> triazole), 6.83 (s, 8H, Ar), 5.35 (s, 4H, H4), 5.09-5.07 (m, 8H, H2, H3), 4.64 (d, 4H, J = 6.8 Hz, H1), 4.52 (bs, 8H, NC<u>H</u>$_2$CH$_2$), 4.41 (d, 4H, J = 13.2 Hz, ArC<u>H</u>$_2$Ar), 4.12-4.10 (m, 8H, H6a, H6b), 4.05-4.02 (m, 4H, H5), 3.93-3.90 (m, 4H, β-OCHa), 3.84-3.79 (m, 16H, NCH$_2$C<u>H</u>$_2$, OC<u>H</u>$_2$CH$_2$CH$_3$), 3.70-3.67 (m, 4H, β-OCHb), 3.58-3.53 (m, 24H, ethylene glycol chain), 3.09 (d, 4H, J = 13.2 Hz, ArC<u>H</u>$_2$Ar), 3.02 (bs, 8H, COCH$_2$C<u>H</u>$_2$triazole), 2.62 (bs, 8H, COC<u>H</u>$_2$CH$_2$triazole), 2.10, 2.01, 1.99 (3s, 36H, COCH$_3$), 1.93 (s, 20H, COCH$_3$, OCH$_2$C<u>H</u>$_2$CH$_3$), 0.98 (t, 12H, J = 7.2 Hz, OCH$_2$CH$_2$C<u>H</u>$_3$). The product shows the same physical and spectroscopic properties reported in the literature.[25]

***Cone*-peracetylated-lactosyl-calix[4]arene 20**

Cone-tetra-alkyne calix[4]arene **11** (23.5 mg, 24.1 μmol), azido lactoside **15** (119.8 mg, 0.15 mmol), $CuSO_4 \cdot 5H_2O$ (3.6 mg 14.5 μmol), sodium ascorbate (5.7 mg, 28.9 μmol). Reaction time: 40 min. TLC (eluent: CH_2Cl_2/CH_3OH 95:5). Flash chromatography (elution gradient: CH_2Cl_2/CH_3OH 97:3 → 94:6). Product **20** was obtained as a yellow oil. Yield: 46%. **^{1}H NMR** (300 MHz, CD_3OD): δ (ppm) 7.78 (bs, 4H, CH triazole), 6.89 (bs, 4H, Ar), 6.87 (bs, 4H, Ar), 5.33 (d, 4H, J = 3.3 Hz, H4'), 5.16 (t, 4H, J = 9.2 Hz, H3), 5.10 (dd, 4H, J = 3.3 Hz, J = 10.4 Hz, H3'), 4.99 (dd, 4H, J = 7.8 Hz, J = 10.4 Hz, H2'), 4.82 (dd, 4H, J = 7.8 Hz, J = 9.2 Hz, H2), 4.73-4.63 (m, 8H, H1, H1'), 4.62-4.40 (m, 16H, H6a, ArC<u>H</u>$_2$Ar, NCH$_2$), 4.21-4.06 (m,

16H, H5', H6b, H6'a, H6'b), 3.94-3.78 (m, 24H, H4, β-OCHa, $NCH_2C\underline{H}_2$, $OC\underline{H}_2CH_2CH_3$), 3.77-3.61 (m, 8H, H5, β-OCHb), 3.60-3.43 (m, 24H, CH_2 ethylene glycol chain), 3.12 (d, 4H, J = 13.0 Hz, $ArC\underline{H}_2Ar$), 3.01 (t, 8H, J = 6.8 Hz, $COCH_2C\underline{H}_2$triazole), 2.63 (t, 8H, J = 6.8 Hz, $COC\underline{H}_2CH_2$triazole), 2.14, 2.11 (2s, 24H, $COCH_3$), 2.06-1.87 (m, 68H, $COCH_3$, $OCH_2C\underline{H}_2CH_3$), 1.02 (t, 12H, J = 7.4, $OCH_2CH_2C\underline{H}_3$). The product shows the same physical and spectroscopic properties reported in the literature.[27]

***Alt*-peracetylated-lactosyl-calix[4]arene 21**

Alt-tetra-alkyne calix[4]arene **19** (11.9 mg, 12.2 μmol), azido lactoside **15** (58.1 mg, 73.2 μmol), $CuSO_4 \cdot 5H_2O$ (1.8 mg 7.3 μmol), sodium ascorbate (2.9 mg, 14.6 μmol). Reaction time: 40 min. TLC (eluent: CH_2Cl_2/CH_3OH 95:5). Flash chromatography (elution gradient: CH_2Cl_2/CH_3OH 97:3 → 94:6). Product **21** was obtained as a yellow oil. Yield: 46%. **^{1}H NMR** (300 MHz, CD_3OD): δ (ppm) 7.80 (bs, 4H, CH triazole), 7.33 (bs, 4H, Ar), 7.32 (bs, 4H, Ar), 5.33 (d, 4H, J = 3.3 Hz, H4'), 5.16 (t, 4H, J = 9.2 Hz, H3), 5.10 (dd, 4H, J = 3.3 Hz, J = 10.4 Hz, H3'), 4.99 (dd, 4H, J = 7.8 Hz, J = 10.4 Hz, H2'), 4.82 (dd, 4H, J = 7.8 Hz, J2-3= 9.2 Hz, H2), 4.73-4.63 (m, 8H, H1, H1'), 4.58-4.43 (m, 12H, H6a, NCH_2), 4.19-4.05 (m, 16H, H5', H6b, H6'a, H6'b), 3.94-3.80 (m, 16H, H4, β-OCHa, $NCH_2C\underline{H}_2$), 3.79-3.63 (m, 16H, H5, β-OCHb, $ArC\underline{H}_2Ar$), 3.60-3.43 (m, 24H, $3CH_2$ ethylene glycol chain), 3.22 (t, 8H, J = 6.9 Hz, $OC\underline{H}_2CH_2CH_3$), 3.05 (t, 8H, J = 7.2 Hz, $COCH_2C\underline{H}_2$triazole), 2.71 (t, 8H, J = 7.2 Hz, $COC\underline{H}_2CH_2$triazole), 2.11, 2.08, 2.03, 2.02, 2.01, 1.99, 1.91 (7s, 84H, $COCH_3$), 1.38-1.18 (m, 8H, $OCH_2C\underline{H}_2CH_3$), 0.64 (t, 12H, J = 7.4 Hz, $OCH_2CH_2C\underline{H}_3$). The product shows the same physical and spectroscopic properties reported in the literature.[32]

General procedure for deacetylation reactions (compounds 1, 2, 3)

Peracetylated glyco-clusters were dissolved in MeOH and drops of a freshly prepared methanol solution of MeONa were added till pH 8-9. The mixture was stirred at room temperature for 1 or 2 hours. The progress of the reaction was monitored via TLC and/or ESI-MS. When a precipitate was observed, H_2O was added to help complete solubilisation. Amberlite resin IR 120/H^+ was subsequently added for quenching and gently stirred for 30 min till neutral pH. The resin was then filtered off and the solvent removed under vacuum to give pure product.

***Cone*-galactosyl-calix[4]arene 1**

Cone-peracetylated-galactosyl-calix[4]arene **9** (30.0 mg, 10.0 μmol) in 4 mL MeOH. Reaction time: 1 hour. TLC (eluent: butanol/acetone/H_2O 35:35:15). Product **1** was obtained as a white solid. Yield: quantitative. **^{1}H NMR** (300 MHz, CD_3OD): δ (ppm) 7.81 (s, 4H, CH triazole), 6.92 (s, 8H, Ar), 4.52 (t, 8H, J = 4.8 Hz, NCH_2), 4.45 (d, 4H, J = 13.2 Hz, $ArCH_2Ar$), 4.25 (d, 4H, J = 7.2 Hz, H1), 4.00-3.91 (m, 4H, β-OCHa), 3.90-3.78 (m, 20H, H4, $OCH_2CH_2CH_3$, NCH_2CH_2), 3.77-3.71 (m, 8H, H6a, H6b), 3.70-3.61 (m, 4H, β-OCHb), 3.60-3.44 (m, 36H, H2, H3, H5, CH_2 ethylene glycol chain), 3.11 (d, 4H, J = 13.2 Hz, $ArCH_2Ar$), 3.01 (t, 8H, J = 7.4 Hz, $COCH_2CH_2$triazole), 2.64 (t, 8H, J =7.4 Hz, $COCH_2CH_2$triazole), 2.03-1.87 (m, 8H, $OCH_2CH_2CH_3$), 1.01 (t, 12H, J = 7.4 Hz, $OCH_2CH_2CH_3$). The product shows the same physical and spectroscopic properties reported in the literature.[30]

***Cone*-lactosyl-calix[4]arene 2**

Cone-peracetylated-lactosyl-calix[4]arene **18** (46.0 mg, 11.1 μmol) in 10 mL MeOH. Reaction time: 2 hours. Product **2** was obtained as a white solid. Yield: 73%. **^{1}H NMR** (300 MHz, CD_3OD): δ (ppm) 7.82 (s, 4H, CH triazole), 6.93 (bs, 4H, Ar), 6.91 (bs, 4H, Ar), 4.54 (t, 8H, J = 4.5 Hz, NCH_2), 4.45 (d, 4H, J = 13.0 Hz, $ArCH_2Ar$), 4.40-4.29 (m, 8H, H1, H1'), 4.00-3.64 (m, 44H, H4', H6a, H6b, H6'a, H6'b, β-OCH_2, NCH_2CH_2, $OCH_2CH_2CH_3$), 3.63-3.39 (m, 48H, H2', H3', H5', H3, H4, H5, 3CH_2 ethylene glycol chain), 3.26 (t, 4H, J = 8.3 Hz, H2), 3.13 (d, 4H, J = 13.0, $ArCH_2Ar$), 3.02 (t, 8H, J = 7.2 Hz, $COCH_2CH_2$triazole), 2.65 (t, 8H, J = 7.2 Hz, $COCH_2CH_2$triazole), 2.08-1.85 (m, 8H, $OCH_2CH_2CH_3$), 1.02 (t, 12H, J = 7.4 Hz, $OCH_2CH_2CH_3$). The product shows the same physical and spectroscopic properties reported in the literature.[32]

A*lt*-lactosyl-calix[4]arene 3

Alt-peracetylated-lactosyl-calix[4]arene **19** (23.0 mg, 5.5 μmol) in 5 mL MeOH. Reaction time: 2 hours. Product **3** was obtained as a white solid. Yield: 71%. **^{1}H NMR** (400 MHz, CD_3OD): δ (ppm) 8.07 (bs, 4H, CH triazole), 7.35 (bs, 8H, Ar), 4.64 (t, 8H, J = 4.7 Hz, NCH_2), 4.37 (d, 4H, J = 7.7 Hz, H1'), 4.35 (d, 4H, J = 8.0 Hz, H1), 4.04-3.95 (m, 4H, β-OCHa), 3.94-3.68 (m, 40H, H4', H6a, H6b, H6'a, H6'b, NCH_2CH_2, β-OCHb, $ArCH_2Ar$), 3.67-3.39 (m, 48H, 3CH_2 ethylene glycol chain, H2', H3', H5', H3, H4, H5), 3.31-3,21 (m, 12H, H_2, $OCH_2CH_2CH_3$), 3.13 (t, 8H, J = 7.1 Hz, $COCH_2CH_2$triazole), 2.79 (t, 8H, J = 7.1 Hz,

$COCH_2CH_2$triazole), 1.38-1.19 (m, 8H, $OCH_2CH_2CH_3$), 0.67 (t, 12H, J = 7.4, $OCH_2CH_2CH_3$). The product shows the same physical and spectroscopic properties reported in the literature.[32]

References

[1] D. R. Shankaran.; K.V. Gobi, N. Miura, *Sens. Actuator. B*, **2007**, *121*, 158.
[2] J.R. Son, G. Kim, A. Kothapalli, M.T. Morgan; D. Ess, *J. Phys. Conf. Ser.*, **2007**, *61*, 1086.
[3] S.D. Soelberg, T. Chinowsky, G. Geiss, C.B. Spinelli, R. Stevens, S. Near, P. Kauffman, S. Yee, C.E. Furlong, *J. Ind. Microbiol. Biotechnol*., **2005**, *32*, 669.
[4] P. Miroslav, S. Petr, K. Michal, *Def. Sci. J*., **2007**, *57*, 185.
[5] D. Bhatta, E. Stadden, E. Hashem, I.J.G. Sparrow, G.D. Emmerson, *Sens. Actuator. B*, **2010**, *149*, 233.
[6] J.Dumic, S.Dabelic, M.Flögel, *Biochimica et Biophysica Acta*, **2006**, *1760*, 616.
[7] G.A. Rabinovich, *Scand. J. Immunol.* **2007**, *66*, 143.
[8] F.T. Liu, D.K. Hsu, *Drug News Perspect*, **2007**, *20*, 455.
[9] a) S. Andre´, H. Sanchez-Ruderisch, H. Nakagawa, M. Buchholz, J. Kopitz, P. Forberich, W. Kemmner, C. Bock, K. Deguchi, K.M. Detjen, B. Wiedenmann, M. von Knebel Doeberitz, T.M. Gress, S.-I. Nishimura, S. Rosewicz, H.-J. Gabius, *FEBS J*., **2007**, *274*, 3233; b) H. Sanchez-Ruderisch, C. Fischer, K.M. Detjen, M. Welzel, A. Wimmel, J.C. Manning, S. Andre´, H.-J. Gabius, *FEBS J*., **2010**, *277*, 3552.
[10] R.J. Pieters, *ChemBioChem*, **2006**, *7*, 721.
[11] H.N. Daghestani, B.W. Day, *Sensors,***2010**, *10*, 9630.
[12] S. Andrè, F. Sansone, H. Kaltner, A. Casnati, J. Kopitz, H.J. Gabius, R. Ungaro, *ChemBioChem*, **2008**, *9*, 1649.
[13] S.P. Bew, R.A. Brimage, N. L'Hermite, S.V. Sharma, *Org. Lett*., **2007**, *9*, 3713.
[14] A. Dondoni, A. Marra, *J. Org. Chem*., **2006**, *71*, 7546.
[15] F. Sansone, E. Chierici, A. Casnati, R. Ungaro, *Org. Biomol. Chem*., **2003**, *1*, 1802.
[16] L.C. Groenen, B.H. Ruël, A. Casnati, P. Timmerman, W. Verboom, S. Harkema, A. Pochini, R. Ungaro, D.N. Reinhoudt, *Tetrahedron Lett*., **1991**, *32*, 2675.
[17] E. Kelderman, L. Der Haeg, G.J.T. Heesink, W. Verboom, J.F.J. Engbersen, *Angew. Chem*., **1992**, *104*, 1107. *Angew Chem. Int. Ed. Engl*., **1992**, *39*, 1075.
[18] M. Dudič, A. Colombo, F. Sansone, A. Casnati, G. Donofrio, R. Ungano, *Tetrahedron*, **2004**, *60*, 11613.
[19] W. Verboom, A. Durie, R.J.M. Egberink, Z. Asfari, D.N. Reinhoudt, *J. Org. Chem*., **1992**, *57*, 1313.
[20] F. Sansone, E. Chierici, A. Casnati, R. Ungaro, *Org. Biomol. Chem*., **2003**, *1*, 1802.
[21] J.A.F. Joosten, N.T.H. Tholen, F. Ait El Maate, A.J. Brouwer, G.W. van Esse, D.T.S. Rijkers, R.M. Liskamp, R.J. Pieters, *Eur. J. Org. Chem*., **2005**, 3182.
[22] G. Zemplen, E. Pascu, *Ber. Dtsch. Chem. Ges*., **1929**, *62*, 1613.
[23] K. Iwamoto, K. Araki, S. Shinkai, *J. Org. Chem*., **1991**, *56,* 4955.
[24] F. Sansone, M. Dudič, G. Donofrio, C. Rivetti, L. Baldini, A. Casnati, S. Cellai, R. Ungaro, *J. Am. Chem. Soc.* **2006**, *128,* 14528.
[25] G. Mislin, E. Graf, M.W. Hosseini, *Tetrahedron Lett*., **1996**, *37,* 4503.
[26] Z. Liu, H.S. Byun, R. Bittman, *Org. Lett*., **2010**, *12*, 2974.
[27] R. Šardzík, G.T. Noble, M.J. Weissenborn, A. Martin, S.J. Webb, S.L. Flitsch, *Beilstein J. Org. Chem.* **2010,** *6,* 699.
[28] A. Sasaki, N. Murahashi, H. Yamada, A. Morikawa, *Biol. Pharm. Bull*., **1994**, *17*, 680.
[29] C. Bouillon, A. Mayer, S. Vidal, A. Jochum, Y. Chevolot, J.P. Colarec, J. P. Praly, J. J. Vasseur, F. Morvant, *J. Org. Chem*., **2006**, *71*, 4700.
[30] P. Fezzardi, Master Thesis, **2010,** Università degli Studi di Parma.
[31] H. Kato, H. Uzawa, T. Nagatsuka, S. Kondo, K. Sato, I. Ohsawa, M. Kanamori-Kataoka, Y. Takei, S. Ota, M. Furuno, H. Dohi, Y. Nishida, Y. Seto, *Carbohydrate Research*, **2011**, 346, 1820.
[32] S. Bernardi, PhD Thesis, **2011**, Università degli Studi di Parma.

Chapter 3:

Noncovalent Functionalization of Gold Nanoparticles with Glycocalixarenes

3.1 Introduction

Gold nanoparticles (AuNPs) are some of the most extensively studied nanomaterials. Because they have many unique optical, chemical, electrical, and catalytic properties, AuNPs have attracted enormous attention for biological and chemical sensing applications. [1] Although AuNPs have been used for both chemical and biological detection and analysis, most of the efforts have been devoted to biological applications. In terms of chemical detection, the main interest is more focused on applications in environmental protection and homeland security, for example, for the detection of toxic metal ions and explosive chemicals. For biological and biomedical applications, the type of target analytes spans a wide range of entities from proteins, DNAs, small biomolecules, to microorganisms including bacteria and viruses. The use of AuNPs for cancer-related detection and analysis is as an extremely active area of research of the last few years.[1] A significant number of studies are indeed aimed to sense and target cancer biomarkers and cells. [2,3,4] As one of the most challenging medical problems, cancer causes economic burdens to society that outweighs the effect of all other human disease. Innovative technologies are needed to bring breakthrough advances to the field. It is expected that the development of nanoparticle-based technologies to improve cancer diagnosis and treatment will continue to remain a hot topic in the future.

As we already discussed in the previous chapter, glycocalixarene are proved to possess good ability to interact with lectins of clinical interest, such as the VAA (*Viscum Album Agglutinin*) plant toxin, that acts as potent biohazard, and human galectins, that act as factor in tumor progression.[5]

In the literature, it is possible to find a large number of publication discussing functionalization of gold nanoparticles with calixarene for many different aims, such as templating agent for the formation of the particles,[6,7] complexation of small molecule[8] or ions[9]. In all the cases, the calixarene scaffold are attached to the surface in a covalent way using the most common sulfur-gold bond[10,11] or nitrogen-gold bond[12], but only a few cases report a non-covalent approach[13,14] and there are no examples of glycocalixarenes attached on AuNPs.

Our aim in this project was to found a fast and convenient strategy to obtain new water soluble AuNPs functionalized with glycocalixarene scaffolds and therefore exposing a carbohydrate coating on the surface of the NP similar to that present on the surface of cells and called *glycocalyx*.

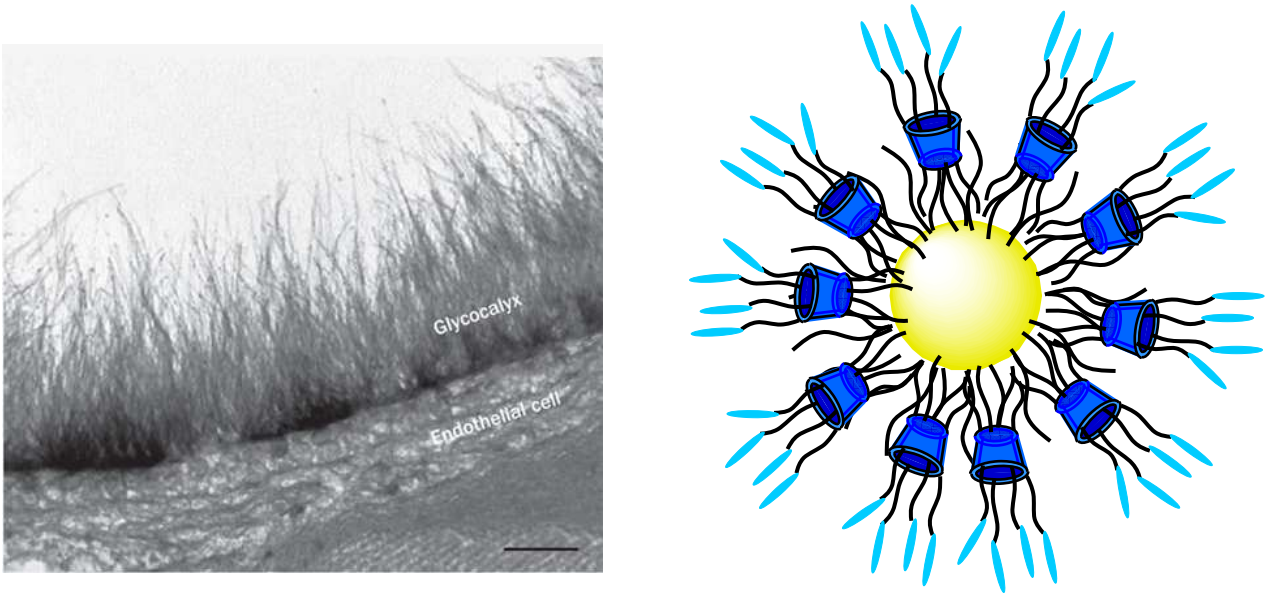

Figure 3.1 Representation of the *glycocalyx*[15] and schematic representation of AuNPs functionalized with glycocalixarenes. Light blue ellipsoids represent the carbohydrate units.

This special arrangement of carbohydrates could possibly be able to efficiently and selectively recognize cells exposing on the outer surface membrane the lectins specific for those carbohydrates present on the glycocalixarene-functionalized AuNPs. This study should therefore produce the proof-of-principle that calixarenes functionalized with proper carbohydrates can be used to adorn nanoparticles and that these structures are potentially able to specifically target tumor or unhealthy cells thus suggesting new nanomaterials with diagnostic and therapeutic perspectives. In fact, glycocalixarenes functionalized with lactose or N-Acetyl-lactose are known to specifically inhibit the adhesion of Galectins to the surface of cancer cells.[16] Morover, exploiting AuNPs properties and, thanks to the ability of calixarenes to complex small drugs in their hydrophobic cavity, this approach could also allow to develop new materials as targeted drug delivery systems.

In contrast with what can be found in the literature, where the use of nitrogen or sulfur containing calixarene to be grafted on AuNPs is generally needed, we decided here to

explore an easier and more convenient approach to functionalize NPs. The presence of the sugar units on the calixarene scaffolds, in fact, prompted us to keep the structures of glycocalixarenes and their syntheses as simple as possible, thus avoiding all those demanding synthetic modifications required to add thiol or amine groups at the lower rim of the macrocycles. This novel approach that we are proposing, simply requires the noncovalent adhesion of amphiphilic glycocalixarenes on AuNPs covered with dodecanthiol chains exploiting hydrophobic effects that reach their maximum importance in water solution where such glycocalix functionalised AuNPs are designed to work.

3.1 Results and discussion

In this chapter the unprecedented functionalization of AuNPs with glycocalixarenes is presented and discussed. The synthesis of the glycocalixarenes used on AuNPs is also described together with that of two phenylthioureido-glycosides (so-called monomers) used as monovalent acyclic equivalents of the calixarene glycoclusters. Even if the sugar structure varies, some important features are kept constant in the design of these glycocluster molecules (fig. 3.2) with respect to the previously studied lactosyl-thioureido calix[n]arenes.[5] The calixarene scaffold always constitutes the cyclic platform where the sugar moieties are covalently anchored and the calixarene structures reported in this chapter have always a ring size of 4 phenolic units, are blocked in the cone conformation and bear propyl chains at the lower rim. Instead, for the monovalent counterparts, the monomers, the phenolic oxygen atom is functionalized with propyl or even with hexyl group, in order to increase lipophilicity and to favor the affinity with the AuNPs. The thiourea unit was chosen as proper spacer to connect the carbohydrate unit to the calixarene backbone, since it can be easily obtained *via* a "click" reaction of aminocalixarenes with the proper glycosyl-isothiocyanates in very high yields and practically absence of by-products. Moreover this kind of conjugation does not involve bond formation at the anomeric carbon atoms of the glycosides and thus prevents any stereochemistry problems during the glycoconjugation reaction. In addition, the hydrogen atoms of the two urea NH groups allow further potential hydrogen bonding that could increase the binding with the lectins or help the inclusion of drug molecules[17,18]. The sugar

moieties are usually linked to the thiourea groups through β anomeric bonds except that in the case of the mannose glycocalixarene (**14**) where an α bond is present. In fact, in the case of mannose, the synthesis of β glycosides or derivatives is extremely difficult and takes place in very low yields due to the presence of the OH group in axial-2-position of the piranose ring.

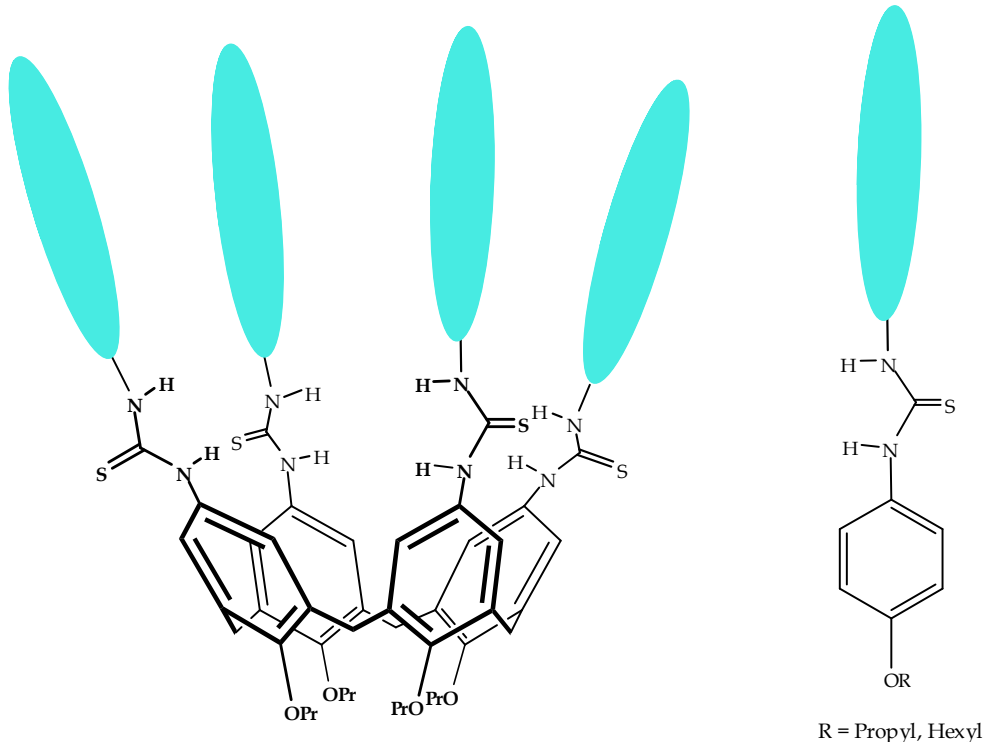

Figure 3.2 Schematic representation of glycosyl-thioureido calixarenes and their monovalent acyclic counterparts called monomers. Light blue ellipsoids represent the carbohydrate units.

In order to easily identify these compounds, whose IUPAC nomenclature results to be rather long and complicated, in the thesis the code *conf*-mScalix[n]arene is used. For each compound are indicated: the conformation *conf* of the calixarene, the number m and the type of saccharide S and the size [n] of the macrocycle.

For the functionalization of the AuNPs we did not used the classical covalent approach used by Arduini and Secchi[2,3,10] that exploits the functionalization of the lower rim of calixarene with long aliphatic chains ending with a thiol group, necessary to form the very strong and stable sulfur-gold bonds. In our case, this kind of approach is synthetically rather demanding because of the complexity of the synthesis of a calixarene functionalized at the upper rim with a carbohydrate and at the lower rim with a primary chain. Therefore

we decided to use a completely different and new approach, characterised by the noncovalent binding, *via* hydrophobic effects, between glycocalixarene and AuNPs. In fact, glycocalixares are amphiphilic molecules: the upper rim, characterized by the presence of the several hydroxyl groups of the sugars, represents the polar part while the aromatic core of the calixarene and the aliphatic chains on the lower rim represent the apolar counterpart. Taking advantage of the amphiphilic characteristic of these glycocalixarenes it seemed feasible to anchor them on particles covered with a liphophilic alkyl layers thanks to strong hydrophobic effects between the apolar scaffold of the calixarene and the apolar surface of the AuNPs. This functionalization strategywill also direct the carbohydrate moieties towards the exterior of the AuNP making them water soluble and potentially available to interact with biological macromolecular structures.

3.2.1 Syntesis of the new *cone*-glycocalixarenes

In the perspective of specifically targeting different cells, we decided to synthesize a new cone-4Man-calix[4]arene and to re-synthesize the already studied *cone*-4Gal-[5] and *cone*-4GlcNAc-calix[4]arene[19]. For the synthesis of the two already known compounds the synthetic strategy[5], found in literature shown in figure 3.3, was used.

The thiourea unit was used as proper spacer to connect the carbohydrate units to the calixarene backbone since it can be easily obtained *via* a "click" reaction of aminocalixarenes with the proper glycosyl-isothiocyanates in very high yields and pratically absence of by-products.[20]

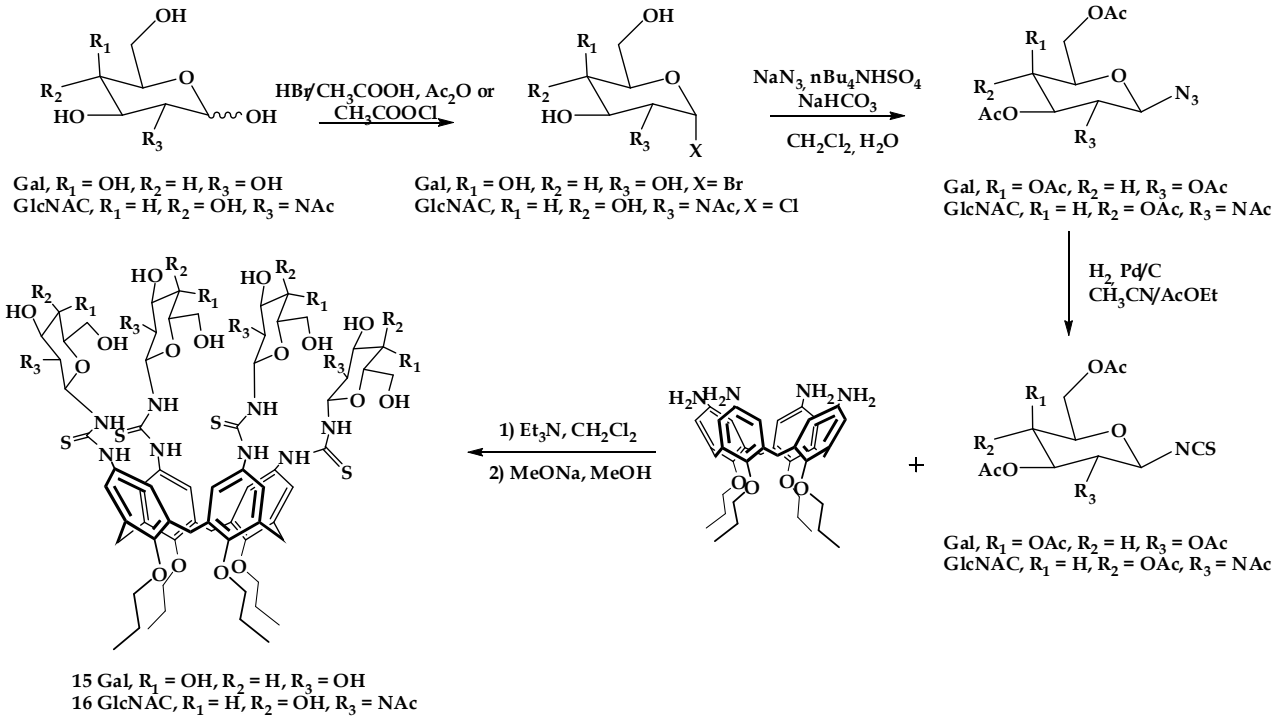

Figure 3.3 Reaction schemes for the synthesis of Gal and GlcNAc functionalized *cone*-calix[4]arene

To synthesize compound **9** (fig 3.4) we used the same approach as illustrated in scheme 3.2. This molecule is blocked in the cone conformation and functionalized at the upper rim with four units of Mannose (fig 3.4). Differently from the previous case, the mannose glycocalixarene (**9**) an α bond is present. In fact, in the case of mannose, the synthesis of glycosyl-β-isothiocyanate or other β-glycoside derivatives is extremely difficult and takes place only in very low yields due to the presence of the axial OH group in 2-position of the piranose ring. [21]

Mannose is well-known to be a biologically relevant saccharide that is found to be recognized from Mannose-binding lectin (MBL), also called mannose-binding protein(MBP), a lectin that is instrumental in innate immunity.[22]

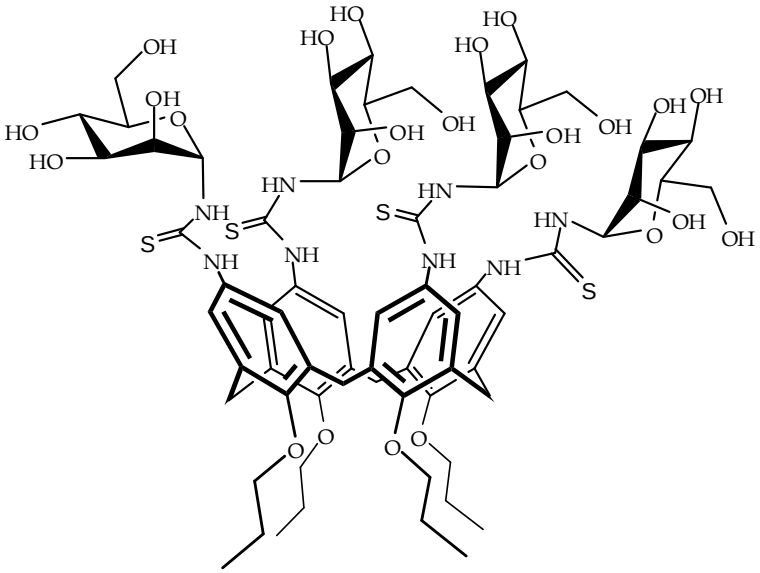

Figure 3.4 C*one*- 4man-calix[4]arene **9.**

Tetraamine-tetrapropyl-calix[4]arene **4**[20] and peracetylated Man-α-isothiocyanate **3** were prepared and conjugated thanks to the isothiocyanate-amine "click" reaction. The synthesis of compound **3** started with the reaction of commercially available mannose **1** with hydrobromic acid and acetic acid in acetic anhydride, to give the peracetylated compound **2**. In one step it was possible to achieve simultaneously the acetylation of the hydroxyl groups of the carbohydrate and the introduction of a bromine atom in anomeric α position.[23] This reaction leads exclusively to the α isomer, as confirmed by the ^{1}H NMR spectrum, where it is possible to observe the presence of a doublet signal at 6.28 ppm with a coupling constant of 1.4 Hz, diagnostic for the α anomer. Once compound **2** was isolated by using potassium isothiocyanate and tetrabutylammonium hydrogen sulfate in acetonitrile the mannopyranoyl-α-isothiocyanate **3** is obtained (fig 3.5) in just one step[24].

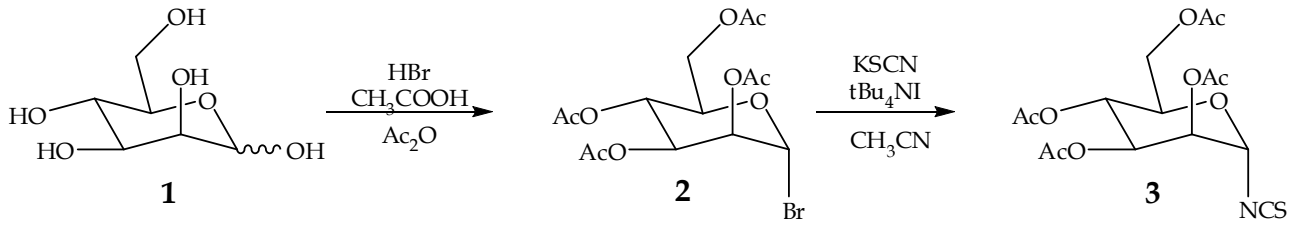

Figure 3.5 Synthetic pathway to mannopyranosyl-α-isothiocyanate **3.**

Mannose derivative **3** was then conjugated to the calix[4]arene core **4** through the formation of a thiourea group (fig. 3.6). This "click" reaction gave compound **5** in high

yield (65%), and the purification was necessary only to remove the excess of mannosyl isothiocyanate used. NMR analyses confirmed the success of the reaction.

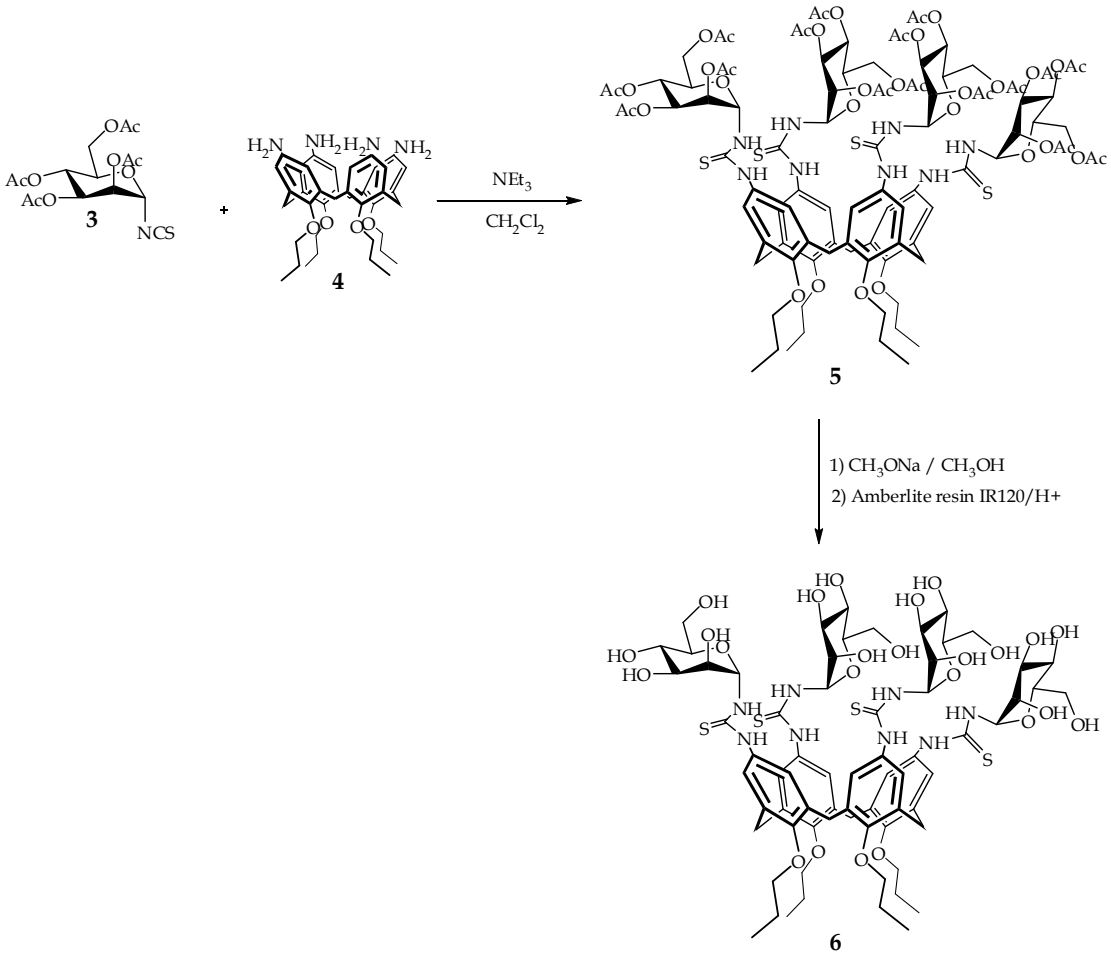

Figure 3.6 Synthesis of the glycosylcalixarene **6.**

The ^{1}H NMR spectrum (300 MHz, MeOD, fig. 3.7) of compound **5** shows the presence of the thiourea NH protons at 6.75, and of two doublets at 4.47 and 3.24 ppm attributed to the axial and equatorial protons of the calixarene methylene bridge, respectively. From these data we could conclude that the calixarene, in the cone structure, had a C_4 symmetrical substitution at the upper rim with four identical saccharide units. The anomeric protons, resonating at 6.06 ppm, confirmed that the sugar maintained, as expected, its α-configuration at C_1 during the "click" reaction.

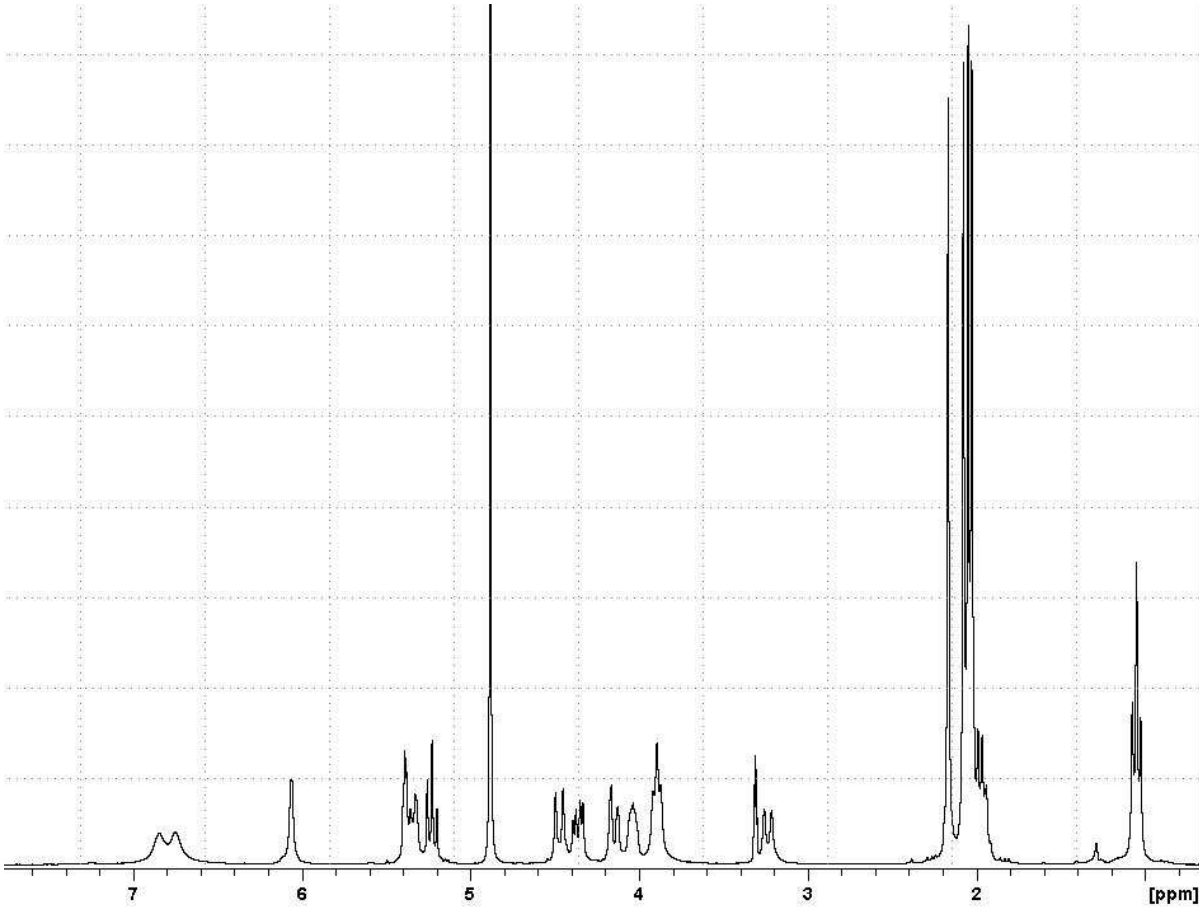

Figure 3.9 ^{1}H-NMR spectrum (300 MHz, CD_3OD) of the acetylated glycocluster compound **5.**

The subsequent deprotection of the peracetylated Man-calix[4]arene **5** was carried out at room temperature by adding a freshly prepared sodium methoxide solution in methanol according to the standard Zemplén procedure[25]. Complete removal of the acetyl groups could be achieved in 3 hours as determined by ESI-MS analyses: the peak at m/z 1560.3 corresponding to the $[M+Na]^+$ species unambiguously confirmed that the desired compound **6** was obtained. Product **6** was completely characterized with NMR techniques. ^{1}H NMR spectrum of **6** (fig. 3.10) shows the disappearance of the methyl singlets of the acetyl groups between 2.10-1.60 ppm and the presence of different conformation for this compound.

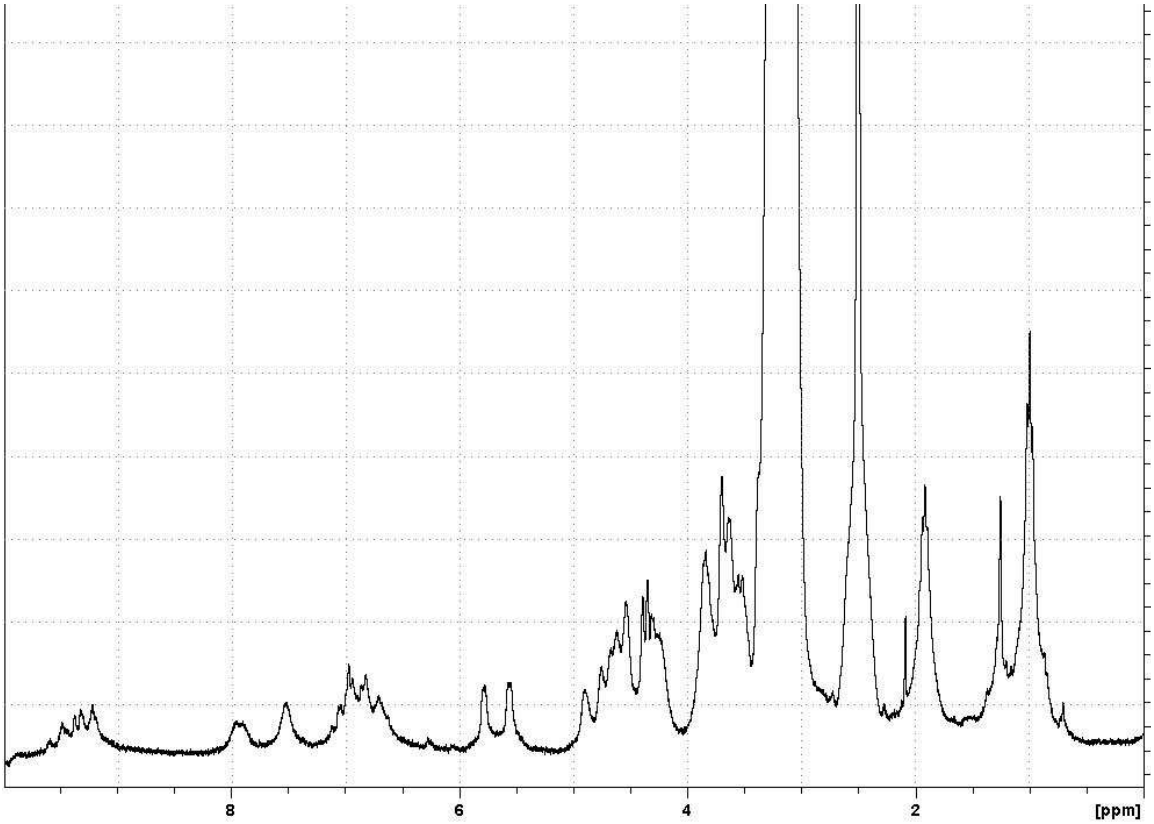

Figure 3.10 ^{1}H-NMR spectrum (300 MHz, DMSO-d_6, 70 °C) of the acetylated glycocluster compound **6.**

From the NMR spectra we observed the presence of different signals for the proton of the ureidic NH protons close to the sugars, for the H1 of the sugar moieties and also for the aromatic protons. Such behaviour is quite common in ureido glycosides although was not frequently observed previously in glycosylcalixarenes. This seems to be due to the fact that thiourea linkers have different possible configurations (*ZZ, ZE, EZ or EE*)[20] that are in equilibrium between each other and are possibly stabilized by intramolecular hydrogen bonding. These equilibria usually influence the ^{1}H-NMR spectra only in non polar solvent and at room temperature; in this case of compound **6**, however, high temperatures and changes to more polar solvents (T = 70° C, DMSO-d_6) seem not to significantly change the ^{1}H-NMR profiles. It is feasible, therefore, that this anomalous splitting of protons might originate from the particular stereochemistry of α-mannosylthioreido groups which present both the 1,2 bulky substituents (the OH group and, expecially, the thioureidocalixarene) in axial positions on both C1 and C2 and that might affect the pyranosyl conformation (*vide infra* for a comparison with the conformation of monomers **12** and **14**). This hypothesis is confirmed from a COSY experiment where it is possible to

see a correlation between the aromatic peaks and the H1 signals of the different configurations that, in turn, correlate with only one H2.

Another confirmation to the hypothesis of the presence of different conformations for compound **6**, and thus indicating that the compound is pure, comes from the ESI-MS analysis where the main peak present is that of the sodiated molecular ion at *m/z* 1560.4.

3.2.2 Synthesis of the monomers

In order to compare the behaviour of the glycocalixarene structure with those of acyclic monovalent systems, we also decided to synthesize two different and simpler glycosides, constituted by a single aromatic nuclei bearing only one saccharide unit and thus resembling the monomeric homologue of the compound **6**. The first one is a propyl ether derivative (**12**) exactly as glycocalix **6**, while the second one (**14**) bears a longer lipophilic hexyl chain, to increase the liphophilic character of the amphiphile system. This should help the adhesion of the monomer onto the AuNPs and the stability of the resulting water soluble particles.

The synthesis of the two monomers was carried out in a way similar to that of the calixarene (fig. 3.11). We started from the commercially available *para*-nitrophenol that was alkylated on the hydroxyl group using propyl iodide or hexyl bromide and K_2CO_3 in refluxing acetonitrile. This reaction lead to the desired products (**7** and **9**) without any further purification and in quantitative yields. The nitro groups were subsequently reduced to amino groups using hydrazine and Pd/C (10%) in ethanol. Also in these cases no purification step was needed and the yield was very high (90-95%). The complete reduction is confirmed by ^{1}H-NMR spectra that show the appearance of the broad singlet of the NH_2 between 3.40 and 3.50 ppm and the shift and the superimposition of the aromatic proton signals at higher field.

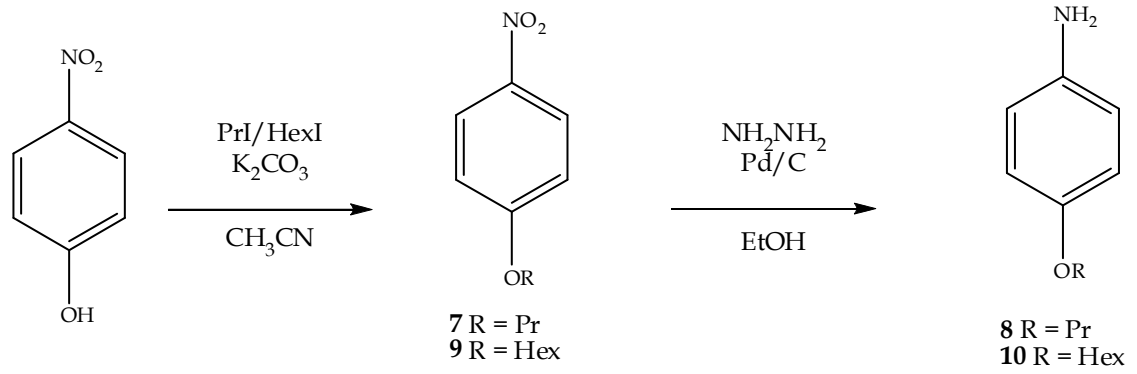

Figure 3.11 Synthesis of the amino intermediates **8** and **10** of the monomeric analogues **12** and **14**.

The conjugation of α-mannosyl isothiocyanate was carried out similarly to that on the calixarene scaffold (fig. 3.12), using a click reaction to link the phenolic ring to the sugar moiety and thus obtaining a thiourea spacer. Also in this case the reaction gave the mannosyl conjugates (**11** or **13**) without significant by-products and only a simple purification step was necessary to remove the excess of mannosyl isothiocyanate. The presence of the desired products was confirmed from the signals of the thiourea NH over 8.5 ppm in ^{1}H-NMR spectra.

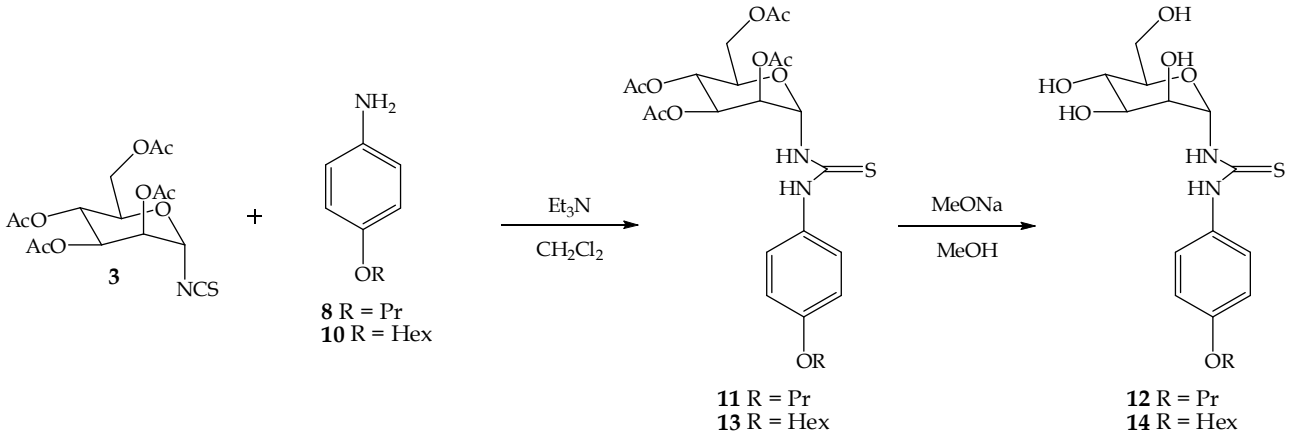

Figure 3.12 Synthesis of monomeric analogues **12** and **14** of mannosylcalixarene **6**.

The subsequent step was the deprotection of the peracetylated compounds (**11** and **13**) to give products **12** and **14**. The methanolysis of the acetate groups was carried out at room temperature by adding a freshly prepared sodium methoxide solution in methanol to compound **11** or **13**[22]. Complete removal of the acetyl groups could be achieved in 3 hours and was followed *via* ESI-MS analyses.

As in the case of compound **6**, the ^{1}H-NMR spectra of monomers show splitting of some of the signals. In these cases, due to the simplicity of the structure, it is more simple to evidence the presence of two different sets of signals, that do not interconvert one into the other even in polar solvent or at high temperature. These two sets of signals are more evident in the protected compounds (**11** or **13**), where two different signals for NH protons, H1, H3 and H6 are clearly evident (figure 3.13). Also in this case COSY experiment and ESI-MS spectra helped to confirm the hypothesis that in any case we are in presence of the single desired compounds **11** and **13**. Contrary to what observed in calixarene **9**, however, the ^{1} HNMR spectra of the deprotected compounds **12** and **14** (fig 3.14) have only a simple set of signals that is indicative of a system with only a single species present.

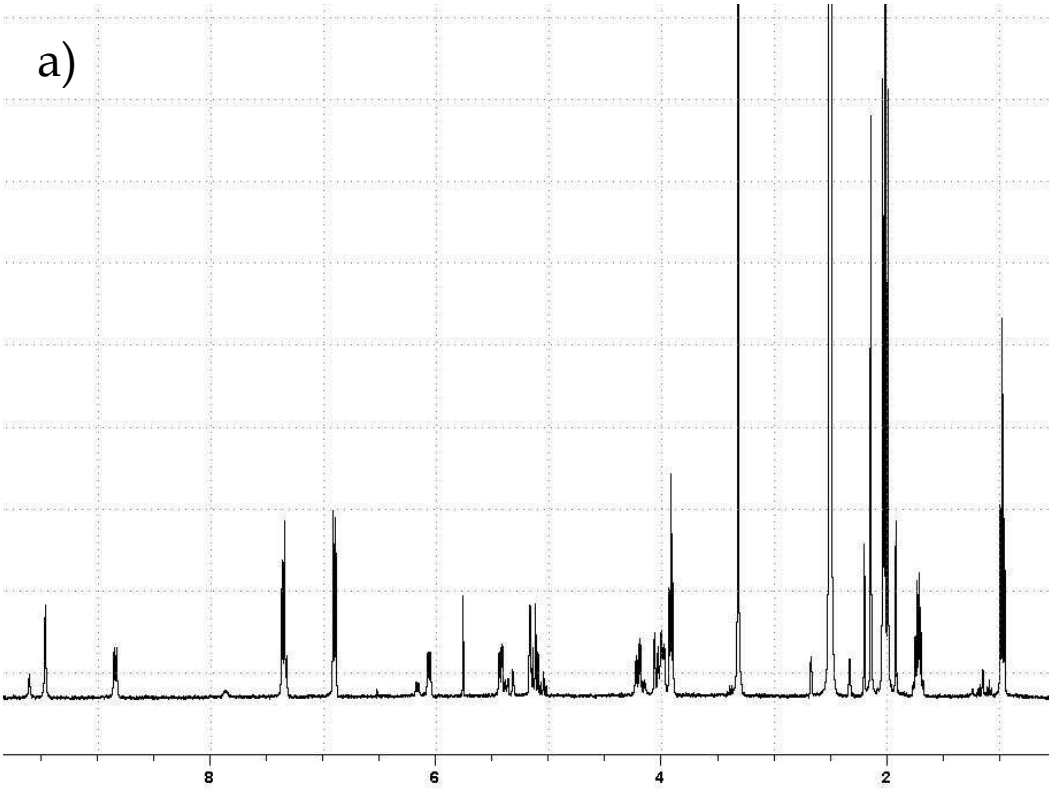

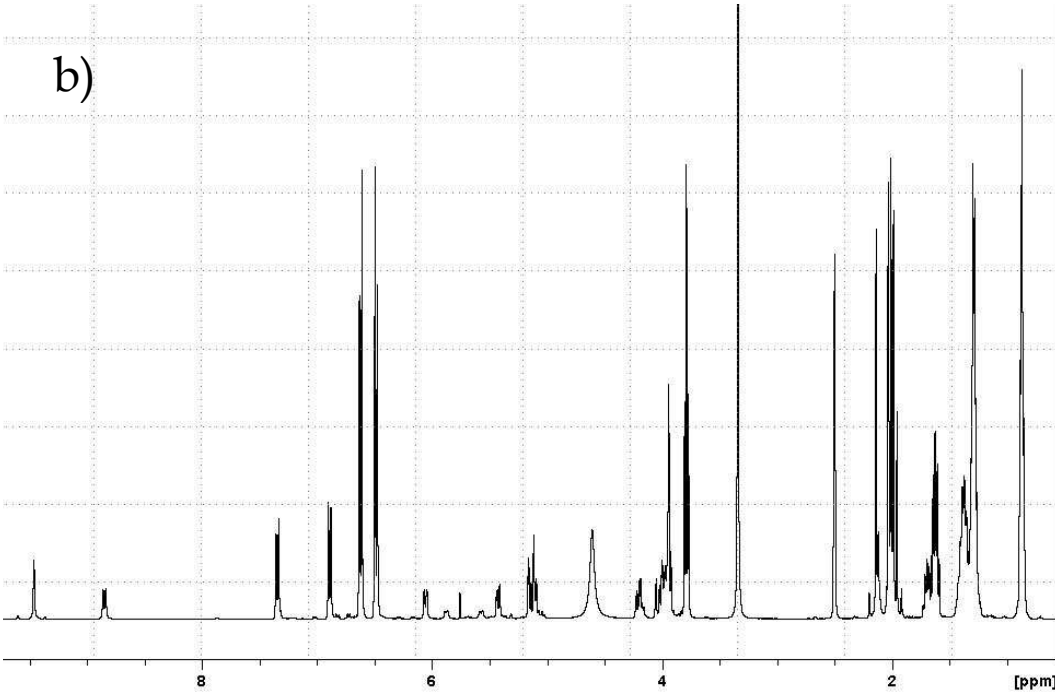

Figure 3.13 ^{1}H-NMR (400MHz, DMSO-d_6) spectra: a) CD_3OD, **13**; b) CD_3OD/D_2O = 9/1, **17**.

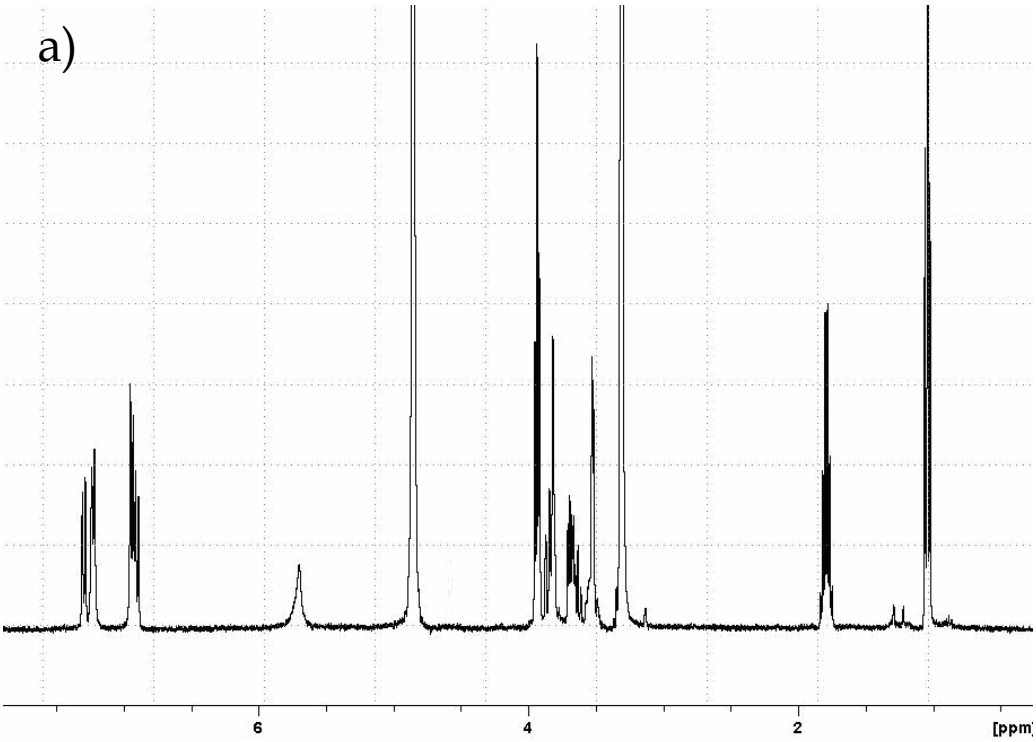

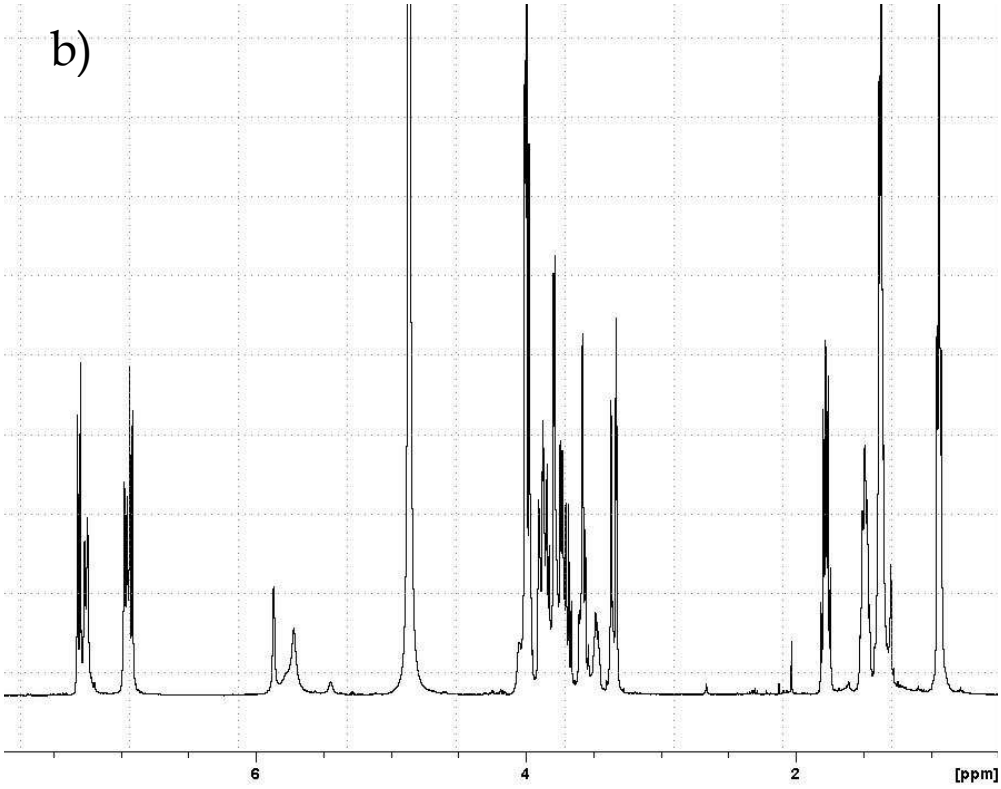

Figure 3.14 ^{1}H-NMR (400MHz) spectra: a) CD_3OD, **14**; b) CD_3OD/D_2O = 9/1, **18**.

3.2.3 Synthesis and functionalization of gold nanoparticles§

Colloidal solutions of metals have been known for a long time and a large variety of preparative techniques is now available. Depending on the preparative conditions, the particles have a tendency to agglomerate slowly, eventually lose their disperse character and flocculate. The removal of the solvent generally leads to the complete loss of the ability to reform a colloidal solution. Preparation of colloidal metals in a two-phase system was introduced by Faraday[26], who reduced an aqueous gold salt with phosphorus in carbon disulfide and obtained a ruby red coloured aqueous solution of dispersed gold particles. Combining this two-phase approach with more recent techniques a new synthetic strategy comes up. [27,288]

The strategy followed consisted in growing the metallic clusters with the simultaneous attachment of self-assembled thiol monolayers on the growing nuclei. In order to allow the surface reaction to take place during metal nucleation and growth, the particles were

§ This part of the work is carried out with the collaboration of the group of Prof. Davide Prosperi, Università Bicocca, MI

grown in a two-phase system. Two-phase redox reactions can be carried out by an appropriate choice of redox reagents present in the two phases. In the present case, $AuCl_4^-$ was transferred from the aqueous solution to toluene using tetraoctylammonium bromide as the phase-transfer reagent and reduced with aqueous sodium borohydride, followed by functionalization with dodecanethiol ($C_{12}H_{25}SH$) (Brust – Schiffrin Method).[28] These types of AuNPs are "soluble" and stable only in organic non polar solvents (fig 3.15). This fact limits consistently the applicability of these materials for most of biological applications, where the most important characteristic is water-solubility.

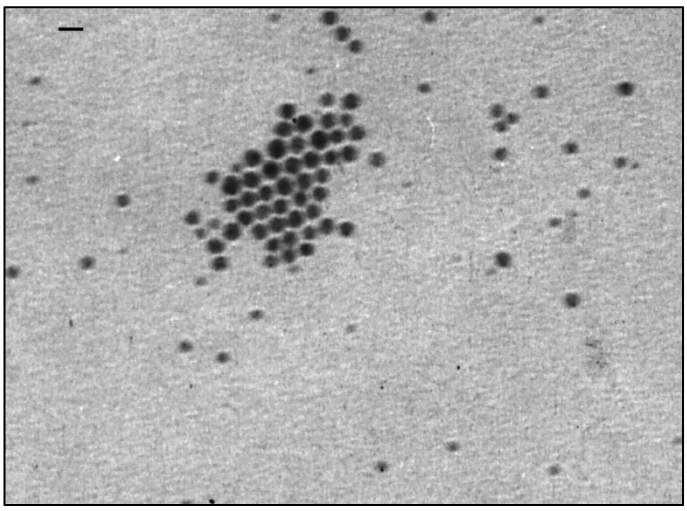

Figure 3.15 TEM image of AuNPs

So in order to obtain new nanoparticles that can be used for bio-recognition, bio-imaging and targeted drug delivery it is necessary to have water-soluble AuNPs. To achieve this purpose there are, in literature, many methodologies describing functionalization of AuNPs, but almost all of them are based on a covalent modification of the Au surface of nanoparticles mainly with thiols and thioesters.

In our case, we decided to explore a new methodology and to functionalize AuNPs using non-covalent interactions, specifically hydrophobic effects between the lipophilic part of glycocalixarene and the long alkyl chains on NPs surface. Following such strategy, we planned therefore to exploit the lipophilic properties of the dodecanthiol outer layer of AuNPs to possibly fix glycocalixarenes on the nanoparticles. This should ensure the exposure of the glycosyl units on the outer NP layers making them water soluble and potentially efficient multivalent ligands for the interaction with proteins (lectins) that are

present on cellular surface or over-expressed in tumor cells. For this purpose we decided to limit this studies to the sugar moieties of mannose and galactose on calixarenes **6** and **15**, respectively (fig. 3.16).

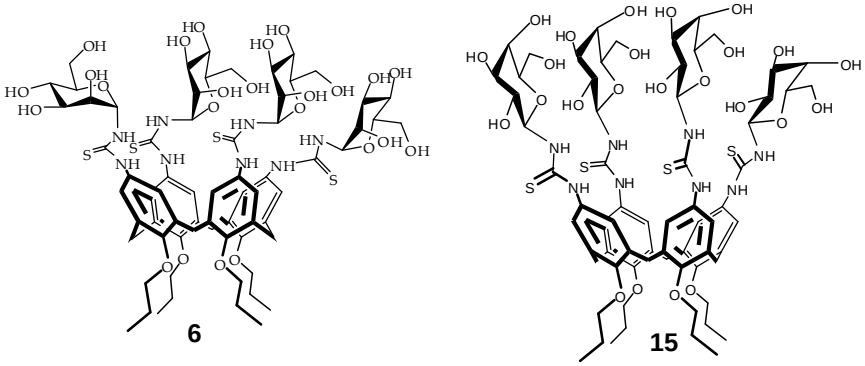

Figure 3.16 Glycocalixarene used for AuNPs funtionalization.

In order to compare the real role of the calixarene scaffold in both stabilizing AuNPs and in the interaction efficiency/selectivity with appropriate cell lines we decided also to try to functionalize AuNPs with monovalent compounds (monomers) **12** and **14** that represent the monovalent acyclic analogs of the mannose calix[4]arene **6** used (fig. 3.17).

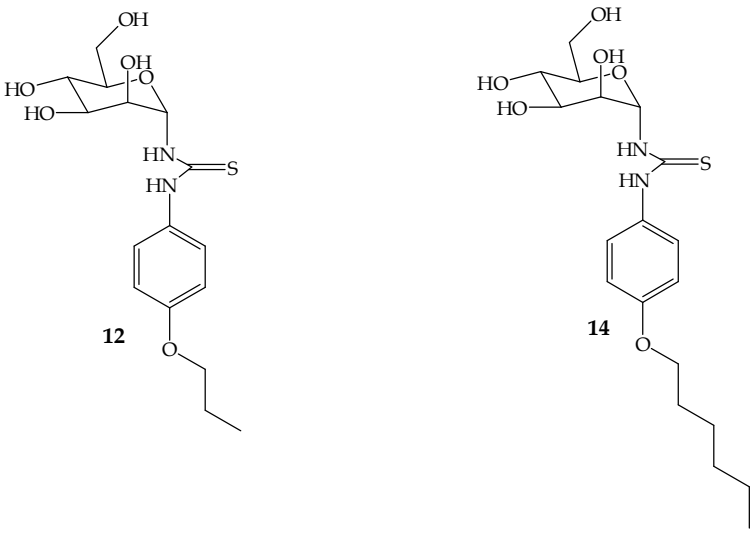

Figure 3.17 Monovalent compounds.

All the glycosyl-functionalized AuNPs were prepared using the same procedure: the glycocalixarene or monomer dissolved in methanol is added to a suspension of AuNPs in chloroform. The mixture was allowed to interact for a few minutes, afterwards the

solvents were evaporated giving a red-colored thin film of nanoparticles. At this point sodium borate buffer (SBB: pH 12) was added and sonicated for a few minutes resulting in stable water soluble nanoparticles. As prepared NPs were washed by repeated centrifugation and re-dispersion in SBB. The final concentration of the AuNPs was calculated from the UV-VIS spectrum using extinction coefficient of 3.07×10^{7} $M^{-1}cm^{-1}$. All the particles covered with calixarene result to be stable in water for a long time (1 month at least).

A quite different behaviour was found for the two monovalent compounds, monomers **12** and **14**, using very similar procedure. Only for **14**, in fact, it was possible to obtain stable water-soluble particles. In this latter case a 4-fold excess of monomer was used compared to the cases of calixarene **6** and **15** in order to roughly keep the same ratio between sugar moieties and AuNPs. In case of monomer **12,** on the other hand, it was impossible to dissolve the particles in water in none of the concentrations tried, probably because the lipophilic tail of the monomer (propyl chain) was too short to give rise to a stable interaction with the aliphatic NP surface.

Au@Glycoside	AuNPs (mol)	Glyconjugate (mol)	Sugar/AuNPs Molar ratio
Au@6	4.41×10^{-9}	6.26×10^{-6}	5680/1
Au@15	1.93×10^{-9}	6.00×10^{-6}	6216/1
Au@14	4.03×10^{-9}	24×10^{-6}	5955/1

Table 3.1 Mole and molar ratios of gold NPs and glycosylated compounds used in each of the functionalization steps.

All stable particles were characterized using UV-Vis, DLS and Z-potential. In the UV-Vis spectra it was possible to identify the absorbance band of the calixarene compounds (220-300 nm) and the plasmonic band of gold at around 520 nm. The band of gold is much less intense than expected and this might be attributed to the high concentration of calixarene bonded on the NP surface, that gives rise to a very high UV-Vis absorbance between 220 and 300 nm (fig. 3.18).

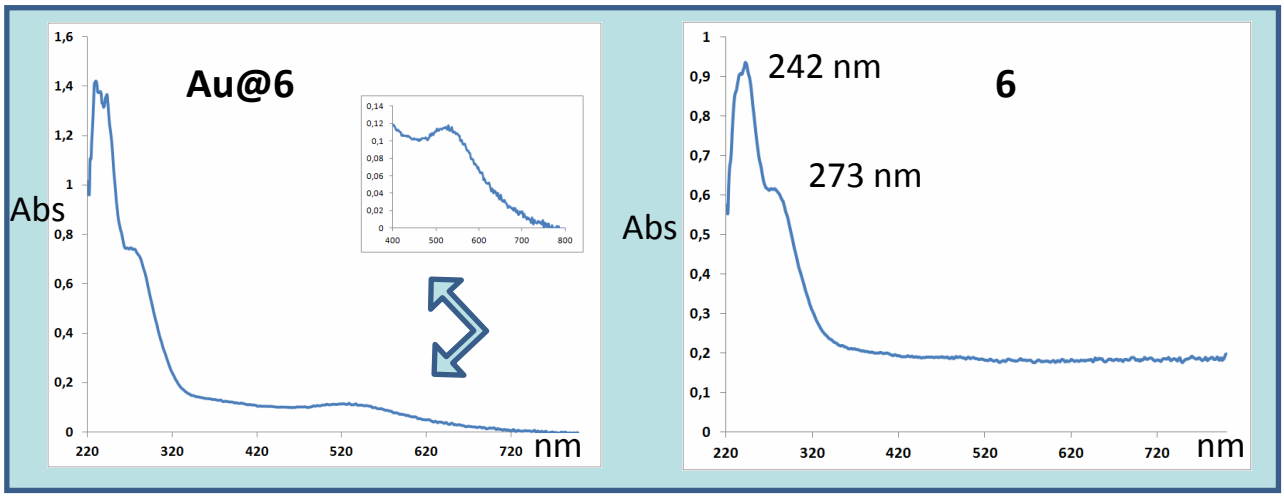

Figure 3.18 Examples of UV-Vis spectra.

From the DLS measurements and the polydispersion index (PDI) it is also possible to understand that the particles are well monodispersed. The Z-potential values measured are quite negative (lower than -30) and this is a further confirmation of the stability of the functionalized AuNPs (table 3.2).

Au@Glycoside	DLS (nm)	Z-potential (mV)	UV-vis (nm)
Au@6	47.2 (PDI 0.268)	-41.31±1.79	522
Au@15	53.2 (PDI 0.228)	-40.59±2.71	522
Au@14	59.4 (PDI 0.223)	-37.65±1.94	527

Table 3.2 DLS and Z-potential of the studied NPs.

3.2.4 Preliminary uptake studies of glycosiylated Au nanoparticles**

In a preliminary experiment, the glycosylated AuNPs (50 nM) were incubated for 2 h at 37°C with HeLa cells that are known to have specific receptors for mannose and galactose.[29] Cells were subsequently washed five times with PBS in order to remove the excess of unbound gold nanoparticles. Cells were also manually counted, for each sample, using a hemacytometer. In order to quantify the amount of gold present in the cells, 5 mL of aqua regia was added and the mixture was left for 72 h, leading to the complete dissolution of

** This part of the work is carried out with the collaboration of the group of Prof. Davide Prosperi, Università Bicocca, MI

all the organic material. The samples were diluted with water to a final volume of 16 mL and the amount of gold was determined by ICP-AES (table 3.3).

Sample code	NPs concentration, nM	Number of NP per cell
Au@6	50 nM	13.5 x10^6
Au@15	50 nM	36.8x10^6
Au@14	50 nM	2.0 x10^6

Table 3.3 Determination of gold contents in HeLa cells.

The data obtained indicate a clear dependence of the AuNP uptake from the type of glycoside present on the outer NP layer. Quite interestingly, the AuNPs fuctionalized with glycocalixarenes are much better uptaken than **Au@14** even if, also in this case, one should assume that the layer covering the NP is characterized by a multivalent presentation of carbohydrates. The presentation of mannoside units on a nultivalent scaffold such as calixarene **6** ensure a nearly 7 times higher uptake of **Au@6** NP from the cells than in the case of the monovalent functionalized NPs **Au@14**. Moreover, galactoside functionalized **Au@15** are bound by cells nearly three- and twenty-times better than mannoside functionalized NP **Au@6** and **Au@14**, respectively. Therefore, even if preliminary, these data show a glycoside-dependent uptake of NPs by HeLa cells and, even more interestingly, that the presentation of the glycosides on a calixarene scaffold does give a significant advantage in terms of efficiency of binding of AuNPS to the cells.

3.3 Conclusion

Water-soluble gold nanoparticles functionalized with glycocalixarenes and with a phenylglycoside, taken as monomeric counterpart of these macrocycles, were obtained using a new non-covalent approach, that takes advantage of hydrophobic effects between the surface of the NPs and the lipophilic part of the glycosylated compounds. These new AuNPs were studied using UV-Vis spectroscopy and DLS evidencing a high stability in aqueous solutions even for long times. This methods represents therefore a novel and easy way to fuctionalize AuNPs with calixarene coatings and ensuring a fairly good solubility in aqueous solutions of these important materials for nanotechnology applications in

water. Preliminary studies of interaction of these glycosylated AuNPs with HeLa cells were carried out, and the amount of AuNP per cell was evaluated using ICS-AES technique. From these data it is possible to evidence a clearly different uptake of the three different AuNPs by the cells. Both the type of sugar present and the multivalent presentation of sugars on the NP seems to influence the uptake. Mannoside functionalised NPs (**Au@14** and **Au@6**) are uptaken to a lower extent than galactoside functionalised **Au@15** NPs. Quite interestingly, the presentation of the glycosides on calixarene scaffolds gives significant advantages in terms of efficiency of binding of AuNPS to the cells.

3.4 Experimental Part

General Information. All moisture sensitive reactions were carried out under nitrogen atmosphere, using previously oven-dried glassware. Dry solvents were prepared according to standard procedures, distilled before use and stored over 3 or 4 Å molecular sieves. Most of the solvents and reagents were obtained from commercial sources and used without further purification. Analytical TLC were performed using prepared plates of silica gel (Merck 60 F-254 on aluminum) and then, according to the functional groups present on the molecules, revealed with UV light or using staining reagents: H_2SO_4 (5% in EtOH), basic solution of $KMnO_4$ (0.75% in H_2O). Merck silica gel 60 (70-230 mesh) was used for flash chromatography and for preparative TLC plates. ^{1}H NMR and ^{13}C spectra were recorded on Bruker AV300 and Bruker AV400 spectrometers (observation of ^{1}H nucleus at 300 MHz and 400 MHz respectively, and of ^{13}C nucleus at 75 MHz and 100 MHz respectively). All chemical shifts are reported in part per million (ppm) using the residual peak of the deuterated solvent, whose values are referred to tetramethylsilane (TMS, $\delta_{TMS} = 0$), as internal standard. All ^{13}C NMR spectra were performed with proton decoupling. Electrospray ionization (ESI) mass analyses were performed with a Waters spectrometer. Melting points were determined on an Electrothermal apparatus in closed capillaries. Microwave reactions were performed using a CEM Discovery System reactor.
Compounds **15** and **16** was synthesized according to literature procedure, respectively ref. 20 and 19.

Nomenclature of calix[4]arene compounds.

In this thesis the simplified nomenclature proposed by Gutsche is used to name the calix[4]arene compounds. The positions on the macrocycle are numbered as indicated in the following figure. The hydroxyl substituent defines the ipso position: subsequently the ortho, meta and para positions on the aromatic rings are identified without ambiguity.

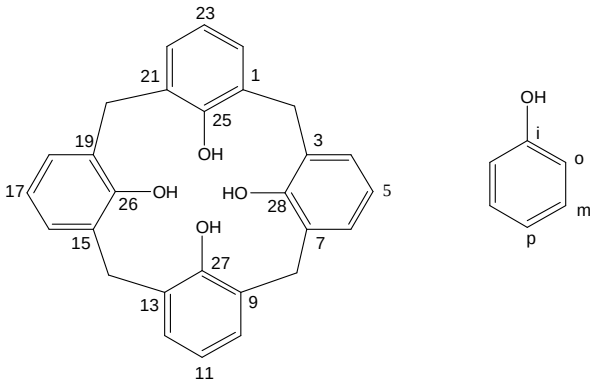

2,3,4,6-Tetra-*O*-acetyl-α-D-mannopyranosyl bromide 2

In a round bottom flask D-mannose (1.0 g, 5.6 mmol) was dissolved in acetic anhydride (5 mL, 55 mmol) and then 3mL of hydrogen bromide until the sugar is completely dissolved, the other 3 mL (6 mL, 144 mmol). The mixture was stirred at room temperature for 8 h and checked via TLC (eluent: AcOEt/hexane 4:6). When completed, the solvent was removed under reduced pressure to give a brownish syrup, that was dissolved in toluene (three times) and then in Et_2O (one time) and the solvent always removed. The crude syrup is purified via flash column chromatography (eluent hexane/AcOEt 6:4) to give the product ad a yellowish syrup with 51% yield**.** ^{1}H-NMR (300 MHz, $CDCl_3$): δ(ppm) 6.23 (d, J = 1.4 Hz,1H, H1), 5.63 (dd, J = 3.3, 10.2Hz, 1H, H3), 5.36 (dd, J = 1.4, 3.3 Hz, H2), 5.29 (t, J = 9.9 Hz, H4), 4.26 (dd, J = 4.8, 12.3 Hz, 1H, H6), 4.17 – 4.12 (m, 1H, H5), 4.06 (dd, J = 2.1, 12.3 Hz, 1H, H6'), 2.10, 2.03, 2.00, 1.93 (4s, 12H, CH_3). The product shows the same physical-chemical properties reported in the literature. [8]

2,3,4,6-Tetra-*O*-acetyl-α-D-mannopyranosyl isothiocyanate 3

In a round bottom flask under nitrogen KSCN (0.150 g, 1.57 mmol), tBu_4NI (0.285 g, 0.77 mmol) were dissolved in CH_3CN (10 mL) and stirred for 3h with 4Å molecular sieves. Then the sugar **2** (0.318 g, 0.77 mmol) dissolved in CH_3CN (3 mL) is added dropwise. The

reaction is refluxed for 24h and monitored with TLC (eluent hexane/AcOEt 6:4). The solution is cooled to room temperature and filtered. The solvent is removed by rotary evaporation and the crude is purified by flash column chromatography (eluent hexane/AcOEt 6:4). The product is obtained as a yellowish oil in a 63% yield. **^{1}H-NMR** (300 MHz, $CDCl_3$): δ(ppm) 5.52 (d, J = 1.8 Hz, 1H, H1), 5.31 – 5.20 (m, 3H, H3, H2, H4), 4.24 (dd, J = 5.1, 12.5 Hz, 1H, H6), 4.12 – 4.04 (m, 2H, H5, H6'), 2.12, 2.05, 2.01, 1.96 (4s, 12H, CH_3). The product shows the same physical-chemical properties reported in the literature. [9]

***Cone*-5,11,17,23-tetrakis[2,3,4,6-tetra-*O*-acetyl-α-D-mannopyranosyl-thioureido]-25,26,27, 28-tetrapropoxycalix[4]arene 5**

Isothiocyanate derivative **3** (50 mg, 0.08 mmol) was added to a solution of amino-calix[4]arene **4**[20] (149 mg, 0.38 mmol) in 5 mL of dry CH_2Cl_2. Et_3N (42 µL, 0.30 mmol) was also added and then the mixture was stirred at room temperature over night under N_2 atmosphere. The reaction progression was checked via TLC (eluent: AcOEt/hexane/CH_3OH 5:5:1). The solvent was then removed under vacuum and the residue purified via column chromatography (eluent: AcOEt/hexane/CH_3OH 5:5:1) to give product **5** as a light yellow solid. Yield: 65%. **^{1}H NMR** (300 MHz, CD_3OD): δ (ppm) 6.85 (bs, 8H, ArH), 6.75 (bs, 8H, NH), 6.06 (bs, 4H, H1), 5.39 – 5.32 (m, 8H, H2, H3), 5.23 (t, J = 8.7 Hz, 4H, H4), 4.47 (d, J = 13.2 Hz, 4H, ArCH_2Ar), 4.36 (dd, J = 5.4, 12.2 Hz, 4H, H6), 4.16 – 4.13 (m, 4H, H6'), 4.09 – 3.95 (m, 4H, H5), 3.89 (t, J = 7.3 Hz, 8H, O$CH_2CH_2CH_3$), 3.24 (d, J = 13.2 Hz, 4H, ArCH_2Ar) 2.17, 2.08, 2.05, 2.02 (4s, 48H, COCH_3), 1.96 (q, J = 7.3 Hz, 8H, $OCH_2CH_2CH_3$), 1.05 (t, J = 7.3 Hz, 12H, $OCH_2CH_2CH_3$). **^{13}C NMR** (75 MHz, CD_3OD): 182.6 (CS), 171.9, 171.2, 170.2, 170.0 (CO), 154.7 (Ar), 135.4 (Ar), 133.2 (Ar), 124.6 (Ar), 79.7 (C4), 76.7 (OCH_2), 70.4 (C5), 69.1 (C2), 68.9 (C3), 66.5 (C4), 62.0 (C6), 30.3 ($ArCH_2Ar$), 23.1 (OCH_2CH_2), 19.4, 19.2, 19.1 ($COCH_3$), 9.4 (CH_2CH_3)**. ESI-MS:** m/z 1128.2 $(M+2Na)^{2+}$.

***Cone*-5,11,17,23-tetrakis[α-D-mannopyranosyl-thioureido]-25,26,27,28-tetrapropoxy calix[4]arene 6**

In a round bottom flask compound **5** (102 mg, 0.046 mmol) was dissolved in MeOD. Some drops of a solution 1M of MeONa were added until pH 9. The reaction was stirred for 3h at room temperature and was monitored with TLC (eluent AcOEt/MeOH/H_2O 5:2:1).

Amberlite resin IR 120/H^+ was subsequently added for quenching. After neutralization, the resin was filtered off and the solvent removed from the filtrate under vacuum to give pure product in a quantitative yield. **^{1}H NMR** (300 MHz, DMSO-d_6): δ (ppm) 9.46 – 9.16 (m, 8H, NH), 7.03 – 6.63 (m, 8H, Ar), 5.79 – 5.55 (m, 4H, H1), 4.86 – 4.50 (m, 12H), 4.37 (d, J = 12.9 Hz, 4H, $ArCH_2Ar$), 4.27 – 4.19 (m, 4H), 3.84 (t, J = 6.6 Hz, 8H, $OCH_2CH_2CH_3$), 3.70 – 3.38 (m, 8H), under solvent peak (4H, $ArCH_2Ar$), 1.92 (q, J = 6.6 Hz, 8H, $OCH_2CH_2CH_3$), 0.99 (t, J = 6.6 Hz, 12H, $OCH_2CH_2CH_3$). **^{13}C NMR** (400 MHz, DMSO-d_6): δ (ppm) 181.1 (CS), 153.6 (Ar), 134.8 (Ar), 129.3 (Ar), 123.9 (Ar), 81.8, 79.1, 77.1, 74.8, 70.3, 66.9, 61.4, 30.7 ($ArCH_2Ar$), 23.2 (OCH_2CH_2), 10.6 (CH_3)**.. ESI-MS:** m/z 1560.4 $(M+Na)^+$.

1-Nitro-4-propoxybenzene 7

In a round bottom flask under N_2 4-nitrophenol (300 mg, 2.2 mmol) and K_2CO_3 (600 mg, 4.3 mmol) were dissolved in 30 mL CH_3CN dry. Then iodopropane (420 µL, 4.3 mmol) was added and the reaction is vigorously stirred and refluxed for 24h. The reaction was checked with TLC (eluent: hexane/AcOEt 1:1). The hot solution is filtered and the solvent is removed under reduced pressure. The compound is dissolved in CH_2Cl_2 and filtered again. The solvent is evaporated giving the pure compound as a yellow oil in a 97% yield. **^{1}H NMR** (400 MHz, $CDCl_3$): δ (ppm) 8.18 (d, J = 7.2 Hz, 2H, Ar), 6.93 (d, J= 7.2 Hz, 2H, Ar), 4.00 (t, J = 6.4 Hz, 2H, $OCH_2CH_2CH_3$), 1.84 (q, J = 6.4 Hz, 2H, $OCH_2CH_2CH_3$), 1.05 (t, J = 6.4 Hz, 3H, $OCH_2CH_2CH_3$). The product shows the same physical-chemical properties reported in the literature.[30]

1-Amino-4-propoxybenzene 8

In a round bottom flask compound **7** (375 mg, 2.06 mmol) was dissolved in 15 mL EtOH and hydrazine hydrate (2 mL, 41 mmol) was added together with a catalytic amount of Pd/C. The reaction was stirred and refluxed for 24h. The solution was filtered and the solvent was removed under reduced pressure the pure product as a colorless oil in a 99% yield. **^{1}H NMR** (300 MHz, $CDCl_3$): δ (ppm) 6.76 (d, J = 9.0 Hz, 2H, Ar), 6.62 (d, J= 9.0 Hz, 2H, Ar), 3.85 (t, J = 7.0 Hz, 2H, $OCH_2CH_2CH_3$), 3.42 (bs, 2H, NH_2), 1.78 (q, J = 7.0 Hz, 2H, $OCH_2CH_2CH_3$), 1.04 (t, J = 7.0 Hz, 3H, $OCH_2CH_2CH_3$). The product shows the same physical-chemical properties reported in the literature.[12]

1-Hexyloxy-4 nitrobenzene 9

In a round bottom flask under nitrogen 4-nitrophenol (300 mg, 2.2 mmol) and K_2CO_3 (600 mg, 4.3 mmol) were dissolved in 30mL CH_3CN dry. Then iodohexane (640µL, 4.3 mmol) was added and the reaction was vigorously stirred and refluxed for 24h. The reaction was checked with TLC (eluent: hexane/AcOEt 1:1). The hot solution was filtered and the solvent was removed under reduced pressure. The compound was dissolved in CH_2Cl_2 and filtered again. The solvent was evaporated giving the pure compound as a yellow oil in a 98% yield. **^{1}H NMR** (300 MHz, $CDCl_3$): δ (ppm) 8.09 (d, J = 9.3 Hz, 2H, Ar), 6.87 (d, J= 9.3 Hz, 2H, Ar), 3.97 (t, J = 6.3 Hz, 2H, OC*H*$_2$), 3.49 (bs, 2H, NH_2), 1.73 (q, J = 6.3 Hz, 2H, OCH_2CH_2), 1.43 – 1.25 (m, 6H, CH_2), 0.85 (t, J = 6.3 Hz, CH_3). The product shows the same physical-chemical properties reported in the literature.[31]

1-Hexyloxy-4 aminobenzene 10

In a round bottom flask compound **9** (506 mg, 2.3 mmol) was dissolved in 30 mL EtOH and hydrazine hydrate (2.2 mL, 45 mmol) was added together with a catalytic amount of Pd/C. The reaction was stirred and refluxed for 24h. The solution was filtered and the solvent was removed under reduced pressure the pure product as a in a 86% yield. **^{1}H NMR** (300 MHz, $CDCl_3$): δ (ppm) 6.69 – 6.61 (m, 4H, Ar), 3.80 (t, J = 6.6 Hz, 2H, OCH_2), 1.65 (q, J = 6.6 Hz, 2H, OCH_2CH_2), 1.37 – 1.17 (m, 6H, CH_2), 0.81 (t, J = 6.6 Hz, 3H, CH_3). The product shows the same physical-chemical properties reported in the literature.[13]

4-(2,3,4,6-Tetra-O-acetyl-α-D-mannopyranosyl-thioureido)-1-propoxybenzene 11

Isothiocyanate derivative **3** (580 mg, 1.0 mmol) was added to a solution of **8** (150 mg, 1.5 mmol) in 20 mL of dry CH_2Cl_2. Et_3N (200 µL, 1.5 mmol) was also added and then the mixture was stirred at room temperature over night under N_2 atmosphere. The reaction was checked via TLC (eluent: AcOEt/hexane 4:6). The solvent was then removed under vacuum and the residue purified via column chromatography (eluent: AcOEt/hexane) to give product **11** as a light yellow solid. Yield: 93%. **^{1}H NMR** (400 MHz, DMSO-d_6): δ (ppm) 9.59 (s, 0.3H, NH), 9.45 (s, 0.7H, NH), 8.83 (d, J = 8.8Hz, 1H, NH), 7.34 (d, J = 8.8 Hz, 2H, ArH), 6.99 (d, J = 8.8 Hz, 2H, ArH), 6.15 (d, J = 6.8 Hz, 0.3H, H1), 6.05 (d, J = 6.8 Hz, 0.7H, H1), 5.42 (dd, J = 3.6, 9.4 Hz, 1H, H3), 5.17 - 5.04 (m, 2H, H2, H4), 4.20 (dd, J = 5.2, 12.2 Hz, 1H, H6), 4.06 – 3.97 (m, 2H, H6', H5), 3.91 (t, J = 7.0 Hz, 2H, $OCH_2CH_2CH_3$), 2.14,

2.03, 2.01, 1.98 (4s, 12H, OCH_3), 1.71 (q, J = 7.0 Hz, 2H, $OCH_2CH_2CH_2CH_3$), 0.97 (t, J = 7.0 Hz, 3H, $OCH_2CH_2CH_2CH_3$). **^{13}C NMR** (100 MHz, CD_3OD): δ (ppm) 182.9 (CS), 171.0, 170.1, 170.0, 169.9 (CO), 157.5, 157.4 (Ar), 126.4 (Ar), 126.3 (*Ar*H), 114.2 (*Ar*H), 79.4 (C1), 69.4 (C2), 69.9 ($OCH_2CH_2CH_3$), 68.8 (C3), 66.6 (C4), 62.0 (C5), 61.9 (C6), 22.2 ($OCH_2CH_2CH_3$), 19.2 ($COCH_3$), 9.4 ($OCH_2CH_2CH_3$). **ESI-MS:** m/z 563.1 $(M+Na)^+$, 1103.3 $([M-M]+Na)^+$.

4-α-D-mannopyranosyl-thioureido-1-propoxybenzene 12

In a round bottom flask compound **11** (458 mg, 0.85 mmol) was dissolved in MeOD. Some drops of a solution 1M of MeONa were added until pH 9. The reaction was stirred for 3h at room temperature and was monitored with TLC (eluent AcOEt/MeOH/H_2O 5:2:1). Amberlite resin IR 120/H^+ was subsequently added for quenching. After neutralization, the resin was filtered off and the solvent removed from the filtrate under vacuum to give pure product in a quantitative yield. **^{1}H NMR** (400 MHz, CD_3OD): δ (ppm) 7.29 (d, J = 8.8 Hz, 1H, ArH), 7.23 (d, J = 8.8 Hz, 1H, ArH), 6.94 (d, J = 8.8 Hz, 1H, ArH), 6.90 (d, J = 8.8 Hz, 1H, ArH), 5.69 (bs, 1H, H1), 3.93 (t, J = 6.8 Hz, 2H, $OCH_2CH_2CH_3$), 3.87 – 3.81 (m, 2H, H6, H2), 3.70 – 3.61 (m, 2H, H6'), 3.52 – 3.49 (m, 2H, H5, H3), under solventi peak (H4), 1.79 (q, J = 6.8 Hz, $OCH_2CH_2CH_3$), 1.04 (t, J = 6.8 Hz, $OCH_2CH_2CH_3$). **^{13}C NMR** (100 MHz, CD_3OD): δ (ppm) 181.1 (CS), 156.8, 157.2 (Ar), 126.6 (*Ar*H), 114.9 (*Ar*H), 82.0 (C1), 78.3 (C4), 74.3 (C3), 70.7 (C2), 69.4 ($OCH_2CH_2CH_3$), 66.7 (C5), 61.5 (C6), 22.2 ($OCH_2CH_2CH_3$), 9.4 ($OCH_2CH_2CH_3$). **ESI-MS:** m/z 395.1 $(M+Na)^+$, 767.4 $([M-M]+Na)^+$.

4-(2,3,4,6-Tetra-O-acetyl-α-D-mannopyranosyl-thioureido)-1-hexyloxybenzene 13

Isothiocyanate derivative **3** (450 mg, 1.1 mmol) was added to a solution of **10** (150 mg, 0.77 mmol) in 15 mL of dry CH_2Cl_2. Et_3N (160 μL, 1.1 mmol) was also added and then the mixture was stirred at room temperature over night under nitrogen atmosphere. Reaction checked via TLC (eluent: AcOEt/hexane 3:7). The solvent was then removed under vacuum and the residue purified via column chromatography (eluent: AcOEt/hexane) to give product **13** as a light yellow solid. Yield: 90%. **^{1}H NMR** (300 MHz, DMSO-d_6): δ (ppm) 10.40 (d, J = 9 Hz, 0.3H, NH), 9.44 (s, 1H, NH), 8.83 (d, J = 9 Hz, 0.7H, NH), 7.32 (d, J = 9 Hz, 2H, ArH), 6.87 (d, J = 9 Hz, 2H, ArH), 6.03 (d, J = 6.9 Hz, 0.7H, H1), 5.85 (d, J = 6.9 Hz, 0.3H, H1), 5.40 (dd, J = 3.6, 9.3 Hz, 1H, H3), 5.15 – 5.07 (m, 2H, H2, H4), 4.22 – 4.16 (m, 1H, H6), 4.03 – 3.90 (m, 4H, H6', H5, OCH_2CH_2), 2.02, 1.99, 1.98, 1.97 (4s, 12H, OCH_3), 1.67

(m, 2H, OCH_2CH_2), 1.38 – 1.29 (m, 6H, CH_2), 0.95 – 0.80 (m, 3H, CH_3). **^{13}C NMR** (100 MHz, DMSO-d_6): δ (ppm) 182.1 (C=S), 170.5, 170.4, 169.9, 169.8 (C=O), 156.5 (Ar), 132.1 (Ar), 126.0 (*Ar*H), 114.6 (*Ar*H), 79.6 (C1), 69.6 (C3), 68.8 (C2), 68.0 (OCH_2), 66.6 (C4), 62.5 (C6), 62.3 (C5), 31.4, 29.1, 25.6, 22.5 (CH_2), 14.4 (CH_3). **ESI-MS:** m/z 605.3 $(M+Na)^+$, 1187.7 ([M-M]+Na)$^+$.

4-α-D-Mannopyranosyl-thioureido-1-hexyloxybenzene 14

In a round bottom flask compound **13** (140 mg, 0.24 mmol) was dissolved in MeOH. Some drops of a solution 1M of MeONa were added until pH 9. The reaction was stirred for 3h at room temperature and was monitored with TLC (eluent AcOEt/MeOH/H_2O 5:2:1). Amberlite resin IR 120/H^+ was subsequently added for quenching. After neutralization, the resin was filtered off and the solvent removed from the filtrate under vacuum to give pure product in a quantitative yield. **^{1}H NMR** (400 MHz, CD_3OD): δ (ppm) 7.26 (m, 2H, ArH), 6.91 (m, 2H, ArH), 5.86 (bs, 0.3H, H1), 5.69 (bs, 0.7H, H1), 3.97 (t, J = 6.2 Hz, 2H, OCH_2CH_2), 3.87 – 3.61 (m, 3H, H2, H6, H6'), 3.53 – 3.45 (m, 2H, H3, H5), under solvent peak (H4), 1.77 (q, J = 6.2 Hz, 2H, OCH_2CH_2), 1.49 – 1.22 (m, 6H, CH_2), 0.93 (t, J = 6.2 Hz, 3H, CH_3). **^{13}C NMR** (100 MHz, CD_3OD): δ (ppm) 181.0 (CS), 157.5, 156.8 (Ar), 126.5 (*Ar*H), 115.1 (*Ar*H), 81.2 (C1), 78.3 (C4), 74.3 (C5), 70.9 (C2), 67.8 (OCH_2), 61.5 (C6), 31.4, 28.9, 25.4, 22.3 (CH_2), 12.9 (CH_3)**. ESI-MS:** m/z 437.1 $(M+Na)^+$, 851.4 ([M-M]+Na)$^+$.

Synthesis of Gold Nanoparticles (AuNPs)

A solution of tetraoctylammonium bromide (2.17g, 3.97 mmol) toluene (80 mL) and a solution of hydrogen tetrachloroaurate (III) (0.30 g, 0.88 mmol) in mQ water (25 mL) were prepared. The two solution were placed in a separating funnel and stirred vigorously. The organic layer was separated and put in a round bottom flask and a solution of $NaBH_4$ (0.334 g, 8.8 mmol) in mQ water (25 mL) was added dropwise. The solution was stirred for an hour then washed with HCl 10 mM (25 mL), NaOH 10 mM (25 mL), water mQ (4x24 mL). The organic solution was stirred overnight then 10mL of dodecanthiol was added and the solution was heated at 65° C for 3 hour. The cooled solution was centrifuged for 5 min at 2000 rpm. Non-aggregated nanoparticles solution is separated from the precipitated nanoparticles and diluted with methanol and centrifuged for 5 min at 2000

rpm, re-disperding the final nanoparticles in chloroform.[13] AuNPs concentration was calculated from UV-Vis spectrum using a calibration line and absorbance peak at 520 nm.

AuNPs functionalization.

Compounds **6** (*cone*–4Man–calix[4]arene), **15** (*cone*–4Gal-calix[4]arene), **16** (*cone*– 4GlcNAc - calix[4]arene), **14** (4-Man-1-hexyloxybenzene) were used to transfer the AuNPs from organic to water phase.

Au@6 NPs. 500 µL of 8.44 µM AuNPs were diluted with 50 mL of chloroform, followed by addition of **6** methanol solution (3.13 mL, 2 mM). The mixture was allowed to react for a few minutes, afterwards the solvents were evaporated giving a red-colored thin film of nanoparticles. 2-3 mL of SBB were added and sonicated for a few minutes resulting in stable water soluble nanoparticles. As-prepared NPs were washed by repeated centrifugation at 7000 rcf for 5 min and re-dispersion in SBB. The final concentration of the AuNPs was calculated from the UV-Vis spectrum using extinction coefficient of 3.07×10^7 $M^{-1}cm^{-1}$ as described by Haiss et al.[32]

Au@15 NPs. 500 µL of 8.44 µM AuNPs were diluted with 50 mL of chloroform, followed by addition of **15** methanol solution (3 mL, 2 mM). The mixture was allowed to react for a few minutes, afterwards the solvents were evaporated giving a red-colored thin film of nanoparticles. 2-3 mL of SBB were added and sonicated for a few minutes resulting in stable water soluble nanoparticles. As-prepared NPs were washed by repeated centrifugation at 7000 rcf for 5 min and re-dispersion in SBB. The final concentration of the AuNPs was calculated from the UV-Vis spectrum using extinction coefficient of 3.07×10^7 $M^{-1}cm^{-1}$ as described by Haiss et al.[31]

***Au@14 NPs*.** 500 uL of 8.06 uM GNPs were diluted with 50 mL of chloroform, followed by addition of **14** methanol solution (1.2 mL, 20 mM). The mixture was allowed to react for a few minutes, afterwards the solvents were evaporated giving a red-colored thin film of nanoparticles. 2-3 mL of SBB were added and sonicated for a few minutes resulting in stable water soluble nanoparticles. As-prepared NPs were washed by repeated centrifugation at 7000 rcf for 5 min and re-dispersion in SBB. The final concentration of the

AuNPs was calculated from UV-vis spectrum using extinction coefficient of 3.07×10^7 $M^{-1}cm^{-1}$ as described by Haiss et al.[16]

Determination of Gold Content by ICP-AES.

HeLa Cells were incubated for 2 h at 37°C with concentration of 50 nM Glycoside-functionalized nanoparticles in 3 cm dishes and were subsequently washed five times with PBS in order to remove excess gold nanoparticles. In order to detach the cells from the dish, 1 mL of aqueous trypsin solution was added and the detached cells were rinsed out with 4 mL of medium, centrifuged and re-dispersed in 2 mL of PBS carefully avoiding any loss. To this suspension was added 5 mL of aqua regia and the mixture was left for 72 h, leading to the complete dissolution of all cellular material. The samples were diluted with water to a final volume of 16 mL before the intracellular amount of gold was determined. Cells were counted manually using a hemacytometer after trypsinization, for each sample.

References

[1] H. Jans, Q. Huo, *Chem. Soc. Rev.*, **2012**, *41*, 2849.
[2] J. M. Nam, C. S. Thaxton and C. A. Mirkin, *Science*, **2003**, *301*, 1884.
[3] J. M. Nam, S. I. Stoeva and C. A. Mirkin, *J. Am. Chem. Soc.*, **2004**, *126*, 5932.
[4] C. You, O.R. Miranda, B. Gider, P.S. Ghosh, I. Kim, B. Erdogan, S.A. Krovi, U.H.F. Bunz, V.M. Rotello, *Nat. Nanotechnol.*,**2007**, *2*, 318.
[5] S. Andrè, F. Sansone, H. Kaltner, A. Casnati, J. Kopitz, H.J. Gabius, R. Ungaro, *ChemBioChem*, **2008**, *9*, 1649.
[6] L. Pescatori, A. Boccia, F. Ciesa, F. Rossi, V. Grillo, A. Arduini, A. Pochini, R. Zanoni, A. Secchi, *Chem. Eur. J.*, **2010**, *16*, 11089.
[7] Q. Liang, C. Li, G. Chen, M. Jiang, *Journal of Colloid and Interface Science*, **2012**, *383*, 82.
[8] T. R. Tshikhudo, D. Demuru, Z. Wang, M. Brust, A. Secchi, A. Arduini, A. Pochini, *Angew. Chem. Int. Ed.*, **2005**, *44*, 2913.
[9] A. Arduini, D. Demuru, A. Pochini, A. Secchi, *Chem. Commun.*, **2005**, 645.
[10] F. Ciesa, A. Plech, C. Mattioli, L. Pescatori, A. Arduini, A. Pochini, F. Rossi, A. Secchi, *J. Phys. Chem. C*, **2010**, *114*, 13601.
[11] A. Wei,*Chem. Commun.*, **2006**, 1581.
[12] J.-M. Ha, A. Solovyov, A. Katz, *Langmuir*, **2009**, *25*, 153.
[13] G. Han, C.C. You, B.J. Kim, R.S. Turigan, N.S. Forbes, C.T. Martin, V.M. Rotello, *Angew. Chem.*, **2006**, *118*, 3237; *Angew. Chem. Int. Ed.*, **2006**, *45*, 3165.
[14] A. Boccia, F. D'Orazi, E. Carabelli, R. Bussolati, A. Arduini, A. Secchi, A.G. Marrani, R. Zanoni, *Chem. Eur. J.*, **2013**, *19*, 7999.
[15] Adapted from J.C. Rutledge, K.F. Ng, H.H. Aung, D.W. Wilson, *Nature Reviews Nephrology*, 2010, *6*, 361.
[16] S. Andrè, F. Sansone, H. Kaltner, A. Casnati, J. Kopitz, H.J. Gabius, R. Ungaro, *ChemBioChem*, **2008**, *9*, 1649.
[17] J.M. Garcia Fernández, C. Ortiz Mellet, *Adv. Carbohydr. Chem. Biochem.*, **2000**, *55*, 35.
[18] F. Sansone, L. Baldini, A. Casnati, R. Ungaro, *New J. Chem.*,**2010**, *34*, 2715.
[19] S. Bernardi, *PhD thesis*, **2011**, Università degli Studi di Parma.
[20] F. Sansone, E. Chierici, A. Casnati, R. Ungaro, *Org. Biomol. Chem.*, **2003**, *1*, 1802.
[21] M.G. Dhonde, A.V. Wankhade, S.P. Deshmukh, *J. Chem. Pharm. Res.*, **2010**, *2*, 518.
[22] D.L. Worthley et al., *Internal Medicine Journal*, **2005**, *35*, 548.
[23] K.P. Ravindranathan Kartha, H.J. Jennings, *J. Carbohydrate Chem.*, **1990**, *9*, 777.

[24] J. Camarasa, P. Fernandez-Resa, M.T. Garcia-Lopez, F.G. De Las Heras, P.P. Mendez-Castrillon, A. San Felix, *Synthesis*, **1984**, 509.
[25] G. Zemplén, E. Pascu, *Ber. Dtsch. Chem. Ges.*, **1929**, *62*, 1613.
[26] M. Faraday, *Philos. Trans. R. SOC. London*, **1857**, *147*, 145.
[27] M.D. Porter, T.B. Bright, D.L. Allara, C.E.D. Chidsey, J. Am. Chem. Soc., **1987**, *109*, 3559; P.E. Libinis, R.G. Muzzo, G.M. Whitesides, *J. Phys. Chem.*, **1992**, *96*, 5097.
[28] M. Brust, M. Walker, D. Bethell, D.J. Schiffrin, R. Whyman, J. Chem. Soc., Chem. Commun., **1994**, 801.
[29] H.-J. Kim, I.-G. Do, H.-K. Jeon, Y. J. Cho, Y. A. Park, J.-J. Choi, C. O. Sung, Y.-Y. Lee, C. H. Choi, T.-J. Kim, B.-G. Kim, J.-W. Lee, D.-S. Bae, *Human Pathology*, **2013,** *44*, 62;
[30] W.-S. Chung et al., *Eur. J. Org. Chem.* **2011**, 1472.
[31] M.J. Jeong, J.H. Park, C. Lee, J.Y. Chang, *Org. Lett.*, **2006**, *8*, 2221.
[32] W. Heiss, N.T.K. Thanh, J. Aveyard, D.G. Fernig, *Anal. Chem.*, **2007**, *79*, 4215.

Chapter 4:

Luminescent Glucosylated Platinum(II) Complexes

4.1 Introduction[♣]

With the development of life science, the research on the intracellular active species, cell signal transduction and apoptosis has become more and more significant in the field of biomedical research and clinical diagnostics. Molecular imaging is playing an increasingly important role in this research. Fluorescent bioimaging, among all kinds of molecular imaging methods, provides a high spatial resolution, which is widely used for cell and tissue imaging in biomedical research and is an effective analytical technique to solve the problems that cannot be resolved by other conventional imaging methods. [1]

Therefore, fluorescent bioimaging has become a very active research field in recent years. Among various classes of fluorophores, phosphorescent heavy-metal complexes possess excellent photophysical properties, as explained in chapter 1, such as evident Stokes shifts and relatively long emission lifetime (μs to ms). This long emission lifetimes permit to avoid the interference from short-lived autofluorescence (background fluorescence) and scattered light by using a time-resolved imaging technique. Thus, it is anticipated that such a class of phosphorescent materials could be used as appealing candidates for bioimaging. Compared with other fluorophores, however, limited examples have been reported about the application of phosphorescent heavy-metal complexes in bioimaging to date.[2]

For application in bioimaging, the phosphorescent probes should be water-soluble because the interaction media is water or a buffered solution. However, the water-solubility of most reported phosphorescent heavy-metal complexes for bioimaging is very poor, and the addition of organic solvents (such as DMSO) is often required in the imaging experiments to improve the solubility of heavy-metal complexes in the aqueous media. However, the addition of organic solvents in sufficient amounts to warrant solubility is usually toxic to cell life and/or destroy the cell membrane, thus limiting the real application of phosphorescent probes. Therefore, it is necessary to develop new phosphorescent probes endowed with a high or complete solubility in water. [3]

In this chapter the synthesis and characterization of luminescent Platinum (II) complexes functionalized with sugars on the ancillary ligand in order to make these complexes,

[♣] *The synthesis and the photo-physical measurements of the complexes presented in this chapter were carried out during my three months stage period the ISIS of Strasbourg (France) under the supervision of Prof. Luisa De Cola.*

usually liphophilic and soluble only in organic solvents, water soluble and to study their facilitated uptake by the cells, is described. These compounds could potentially be able to efficiently enter and selectively stain cells or particular compartments inside cell (such as cytoplasm, organelles or the nucleus) thanks to the interaction of the sugar units with lectins or other carbohydrate binding proteins.[4] Moreover, such kind of complexes could also produce a supramolecular structures such as chiral fibres or aggregates that can enhance the emission intensity. [5]

4.2 Results and discussion

Platinum (II) complexes have a planar-squared geometry, and those studied herein have a tridentate bis-(1,2,4-triazolyl)-pyridine chelating ligand, carrying CF_3 groups on the free 3-positions of the triazole rings. A monodentate ligand, usually called ancillary ligand, complete the coordination around the metal ion. The ancillary ligand is frequently a substituted pyridine, and is well-known that the photophysical properties of these complexes are mainly characterized by the tridentate ligand (fig. 4.1). Several of the tested complexes have been shown to be able to cross the cell membranes and localize in specific cell compartments, depending on their chemical structure. Due to the emitting characteristics of these complexes, mainly related to the change of the emission upon aggregation, it was also shown to be possible to follow their distribution and pathways within cells.

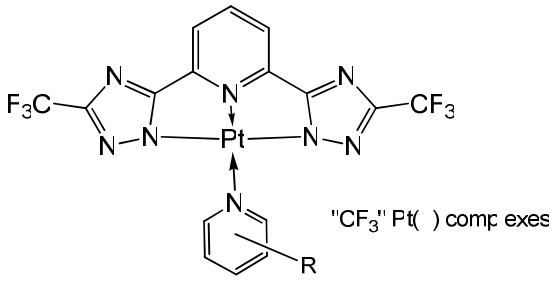

Figure 4.1 Schematic representation of platinum(II) complexes.

We planned therefore to functionalize these complexes with D-glucose, due to the relevance of such saccharide in the interaction with bio-medical important carbohydrate-

binding proteins (lectins). This will possibly influence the uptake of the complex by the different cell-lines and modulate the formation of aggregates, by the different environment provided by the cell or by the proteins (lectins) where the complexes will be localized. D-glucose is also one of the most hydrophilic pyranosidic monosaccharides and this should ensure a higher solubility in water of its conjugates. However, once demonstrated the proof-of-principle that conjugation of glycosides to these Pt-complexes enhances the efficiency and/or selectivity of uptake by the cells, it could be easily planned to insert other and more biologically relevant mono- or oligosaccharides.

Of the different positions where the carbohydrate could be introduced, we choose the ancillary ligand (para position) for different reasons. First of all, since the photophysics of these complexes mainly depend from the tridentate bis-triazolyl-pyridine, we decided not to change this unit and to leave the -CF_3 groups in 3-positions which ensure excellent emission properties. Second, the functionalization of the pyridine ancillary ligand should result much easier and simply by mixing the glycosylated pyridine with the Pt-bis-triazolyl-pyridine would result in the formation of the final desired glycosylated Pt complexes. Finally, even if the single final Pt complexes bear only one carbohydrate unit, the known possibility to aggregate in fibers of these complexes[5,6] might result in the formation of a polyglycosylated noncovalent assemblies potentially able to exploit a glycoside cluster effect in the recognition of lectins.

4.2.1 Synthesis of the glycosylated ancillary ligands

Two different pyridine-based sugar functionalized ancillary ligands were synthesized using the same sugar (D-glucose) but different way to link the sugar to the pyridine ring and different distance between the sugar and the pyridine (fig. 4.2).

The different spacers were also chosen for the easy and straightforward way of conjugation and for their polarity that should also help the solubility in water. Quite different are the synthetic pathways to obtain compounds **8** and **12**. A synthetic strategy consisting in a three-step, for the former, and two-step, for the latter, convergent approach before conjugation, was planned (fig. 4.3 and 4.4).

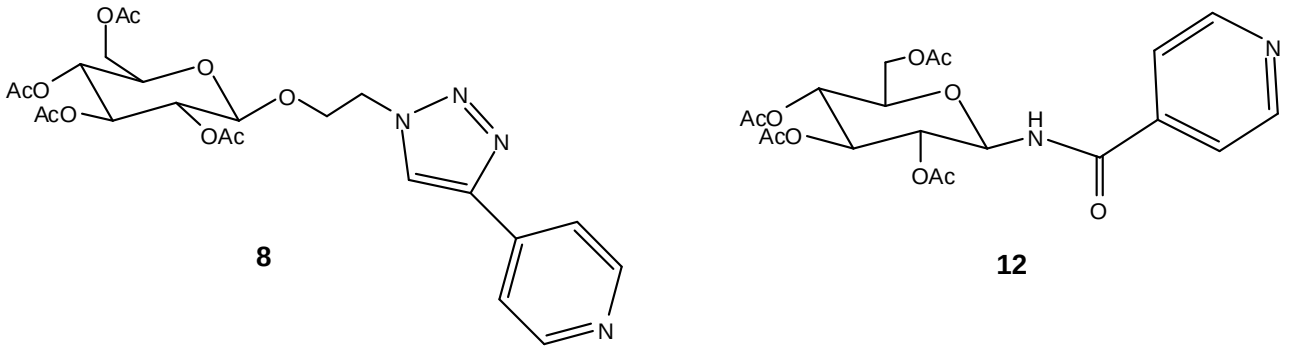

Figure 4.2 The two pyridine-based ancillary ligands.

For obtaining the triazole linked **8**, in fact, a CuAAC (Copper-catalyzed Azido-Alkyne Cycloaddiction) was used and, for this reason, an azido sugar and an alkyne pyridine were synthesized (fig. 4.3 and 4.4). The synthesis started with the functionalization of the glucose (fig. 4.3). The sugar was fist totally acetylated using acetic anhydride and sodium acetate obtaining the pentaacetate **2**.[7] Then using 2-bromo ethanol and boron trifluoride diethyl etherate as Lewis acid for the glycosylation, the anomeric position was functionalized obtaining, after purification, the compound **3**[8] having a terminal bromoalkoxy group on the sugar C_1 position. Compound **4** is then obtained thanks to the reaction of **3** with sodium azide at 65 °C in dry DMF and high yield without any purification needed.

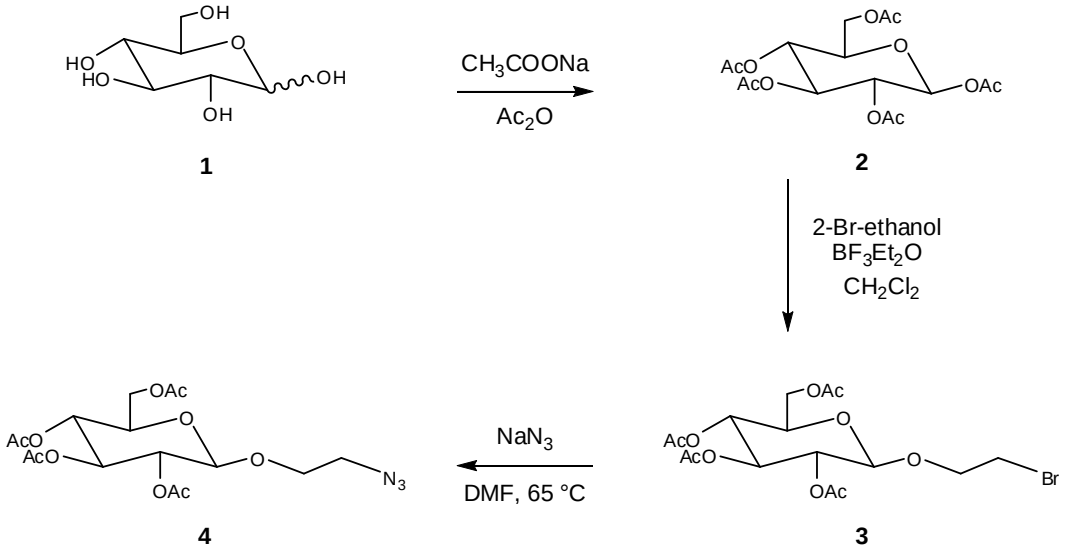

Figure 4.3 Synthesis of the azido sugar **4**.

For what concerns the pyridine moiety (fig. 4.4) the synthesis started from the commercially available 4-iodo-pyridine. Carrying out a Sonogashira reaction with trimethylsilylacetylene as alkyne donator and diisopropylamine as base, compound **6**[9] was obtained after column chromatography purification. At this point the alkyne moiety was deprotected using potassium hydroxide in methanol/dicloromethane obtaining the 4–ethynylpyridine **7**.[5] This compound was then used, together with **4,** in a CuAAC reaction, that generates the triazole nucleus as linker between the sugar and the pyridine**.** This reaction was carried out using copper (II) sulfate pentahydrate and sodium ascorbate in DMF/H_2O, upon microwave irradiation (150W at 80 °C, t = 20 min.). Compound **8**, the first of the two ancillary ligands, was obtained pure after column chromatography that is needed simply to remove the excess of sugar used; no other by-products were in any case detected. The successful outcome of this click reaction was confirmed from ^{1}H-NMR spectroscopy where it is well visible the signal at 8.13 ppm of the CH of the triazole ring, together with all the signal of the sugar between 3.5 and 5.5 ppm and the two doublets of the pyridine ring at 8.72 and 7.97 ppm (fig. 4.5). The identity of compound **8** was also confirmed from ESI-MS where it is present the $[M+Na]^+$ peak at 543 m/z.

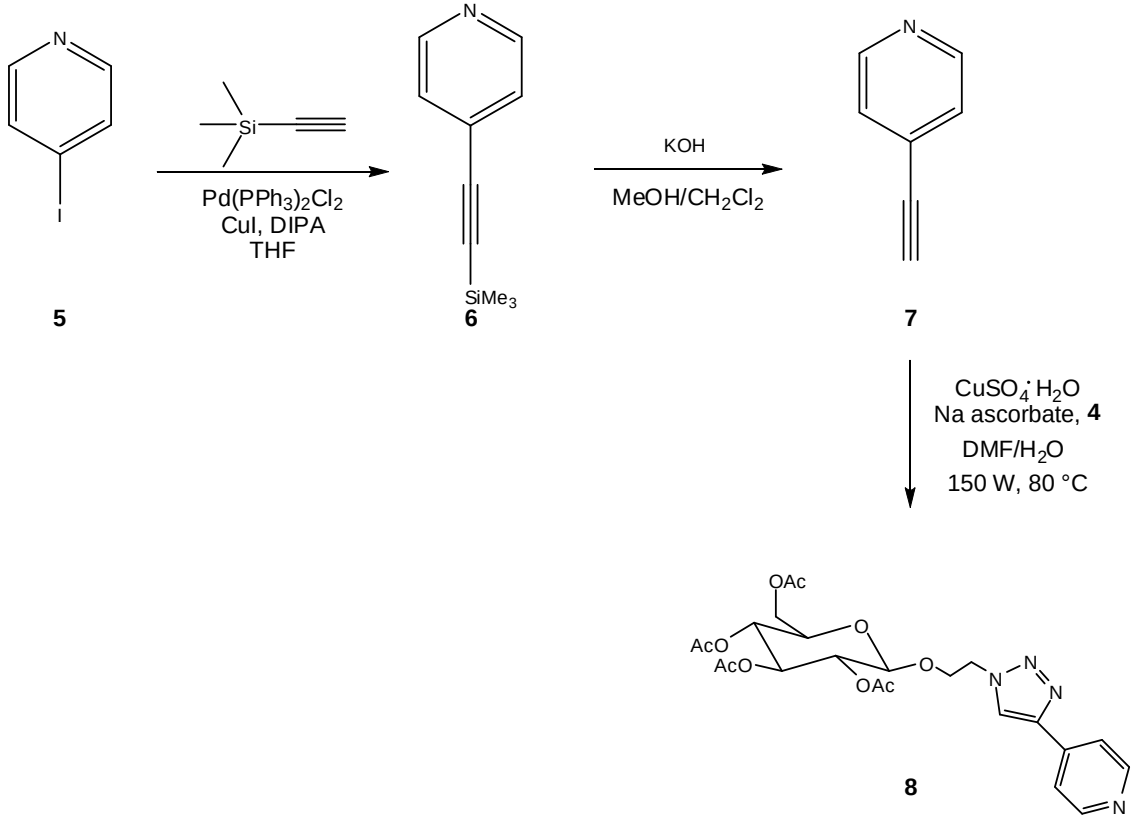

Figure 4.4 Synthesis of the ethynylpyridine **7** and of the protected ancillary ligand **8**

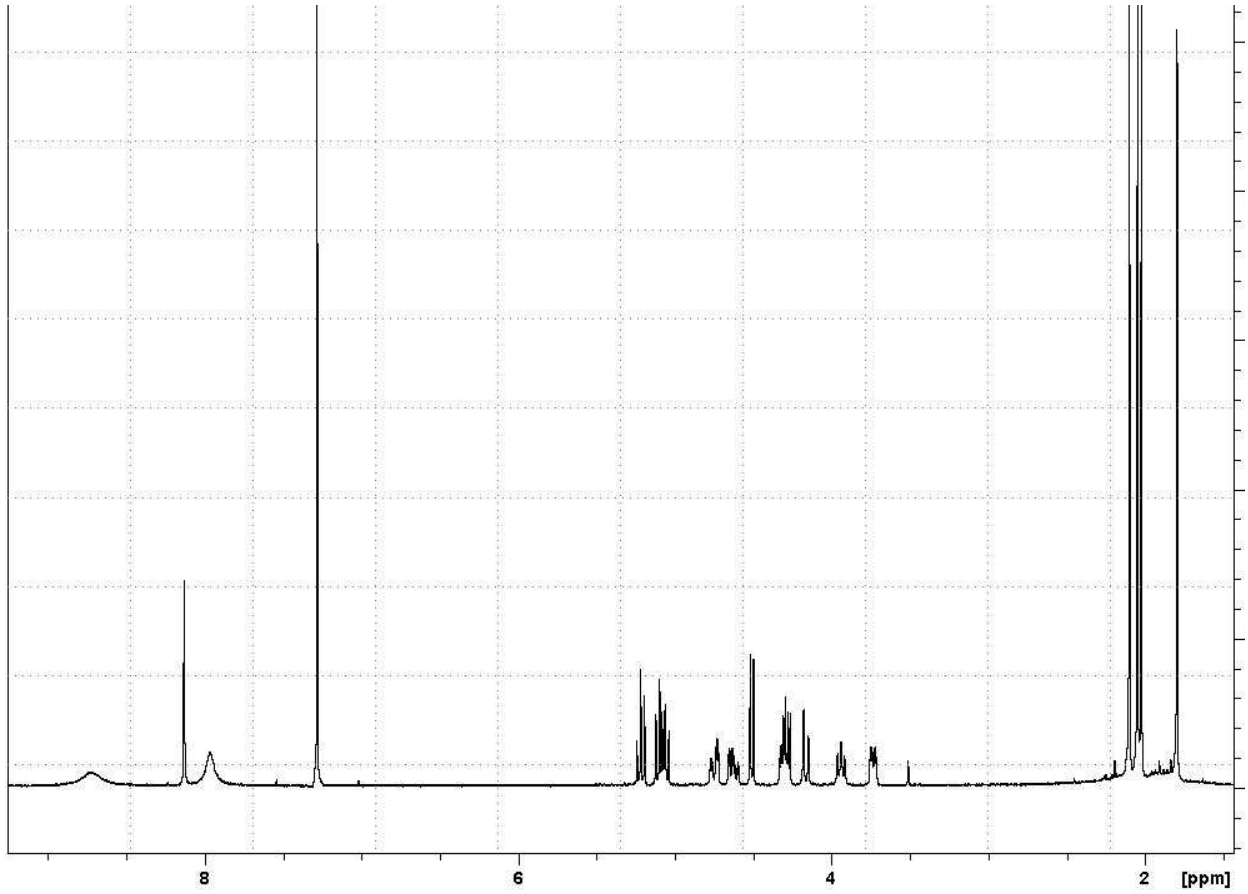

Figure 4.5 ^{1}H-NMR (400 MHz, $CDCl_3$) of **8**

To obtain the amido linked ligand **12** the synthesis started from the commercially available α-D-bromo tetraacetylglucose (fig. 4.6) that thanks to an S_N2 reaction on the anomeric position under phase transfer catalysis condition using sodium azide as nucleophile and tetrabutylammonium hydrogen sulfate, was transformed in the β-D-azido tetraacetylglucose **10**. The success of the reaction was confirmed from ^{1}H-NMR spectra, where the signal of the anomeric proton is shifted to higher fields (lower ppm), as expected from the change in its stereochemistry. Compound **10** was then reduced using H_2 and palladium on carbon, as catalyst, to give β-D-amino tetraacetylglucose **11**. Also in this case ^{1}H-NMR spectroscopy and ESI-MS spetrometry confirm the identity and purity of the product. At this point this sugar could be used for the condensation with commercially available isonicotinic acid to give product **12**, the second ancillary ligand. The reaction was carried out in presence of 1-ethyl-3-(3-dimethylaminopropyl) carbodiimide (EDC) in dry THF (5mL) for 12 hour. A proper integration between the signals of the aromatic protons and those of the sugar in the ^{1}H-NMR spectra together with the presence of the signal of

the NH of the amido group at 7.55 ppm confirmed that conjugation properly took place and that the amino group was formed (fig. 4.7).

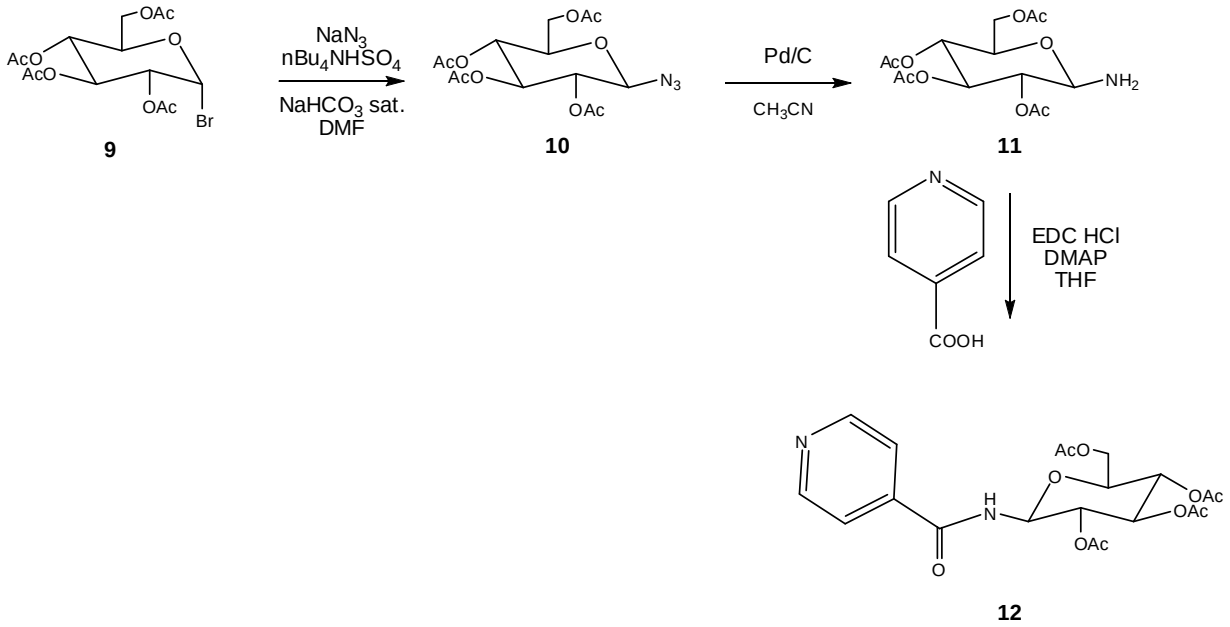

Figure 4.6 Synthesis of the ancillary ligand **12.**

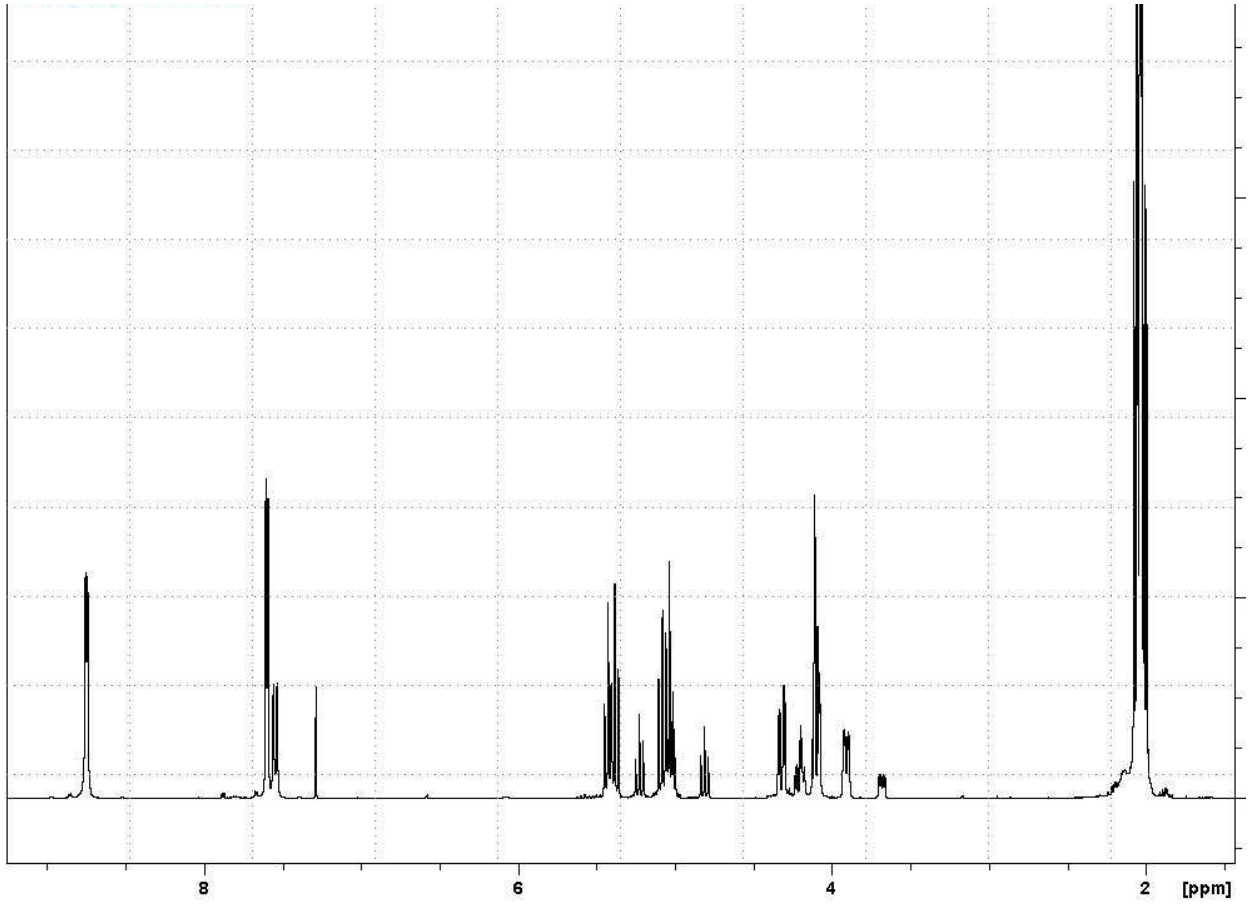

Figure 4.7 ^{1}H-NMR ($CDCl_3$, 400 MHz) of compound **12.**

4.2.2 Synthesis of the platinum (II) complexes and their deprotection

The synthesis of the complexes was carried out using well-known procedures in the group of Prof. De Cola at ISIS in Strasbourg during my period of stage abroad. The complex of Platinum used as a precursor was a dichloride bis-dimetysulfoxide complex and as the tridentate ligand we used a pyridine functionalized with two 1,2,4-triazole bearing a CF_3 group in 3-position. The choice of those N^N^N ligand was driven by the knowledge that this ligand was proved to give quite high emissive complexes, that in some cases tend to form supramolecular aggregates, such as fibres. This aggregation results to be important in terms of emission. In fact, it is experimentally proved that when those N^N^N Platinum complexes form fibers, or aggregates in general, the emission results to be improved and sometimes also red shifted, thanks to the Pt-Pt interaction.[6]

The complexation reactions is always carried out using two subsequent steps: the first one in order to obtain the chelate complexes and the second one to introduce the ancillary ligand (fig. 4.8).

For the first step Platinum complex precursor was dissolved under nitrogen in $CHCl_3$ with the tridentate ligand, and a non-coordinating and non-nucleofilic base, such as DIPEA or K_2HPO_4, was added. The reaction was stirred until the formation of the complex is evident from turning the solution to yellowish. At this point the ancillary ligand can be added to the solution that was then heated at 60 °C. The complex was formed after one night reaction and purification was carried out by column chromatography. While complex **14** is well soluble in $CHCl_3$ and CH_2Cl_2, complex **13** is only slightly soluble in most organic solvent, but is well soluble in hexafluoroisopropanol.

To characterize ad confirm the presence of these compounds both NMR (^1H and ^{19}F) and ESI-MS were used. In both cases in ^1H-NMR of **13** and **14** spectra is easy to verify the complete formation of the complexes thanks to the appearance of the doublet of the pyridine *ortho* proton, that due to the coordination to platinum are shifted to lower fields (9-10 ppm depending on the complex and solvents). In the aromatic region, the singlet of the triazole ring proton at 8.33 ppm (for **13**) or the doublet of NH at 8.01 ppm (for **14**), together with the pattern and integration of the signals of glucose unit between 3.5 and 5.5 ppm, gave other proofs of the effective coordination of the ancillary ligand. The presence

of the chelating ligand is confirmed by the presence of a triplet and a doublet related to the pyridine protons between 7.50 and 8.22 ppm.

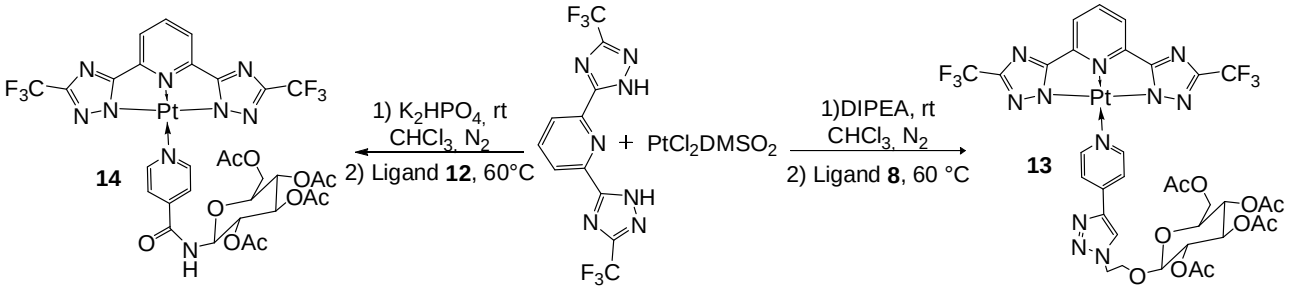

Figure 4.8 Synthesis of the of the complexes **13** and **14**.

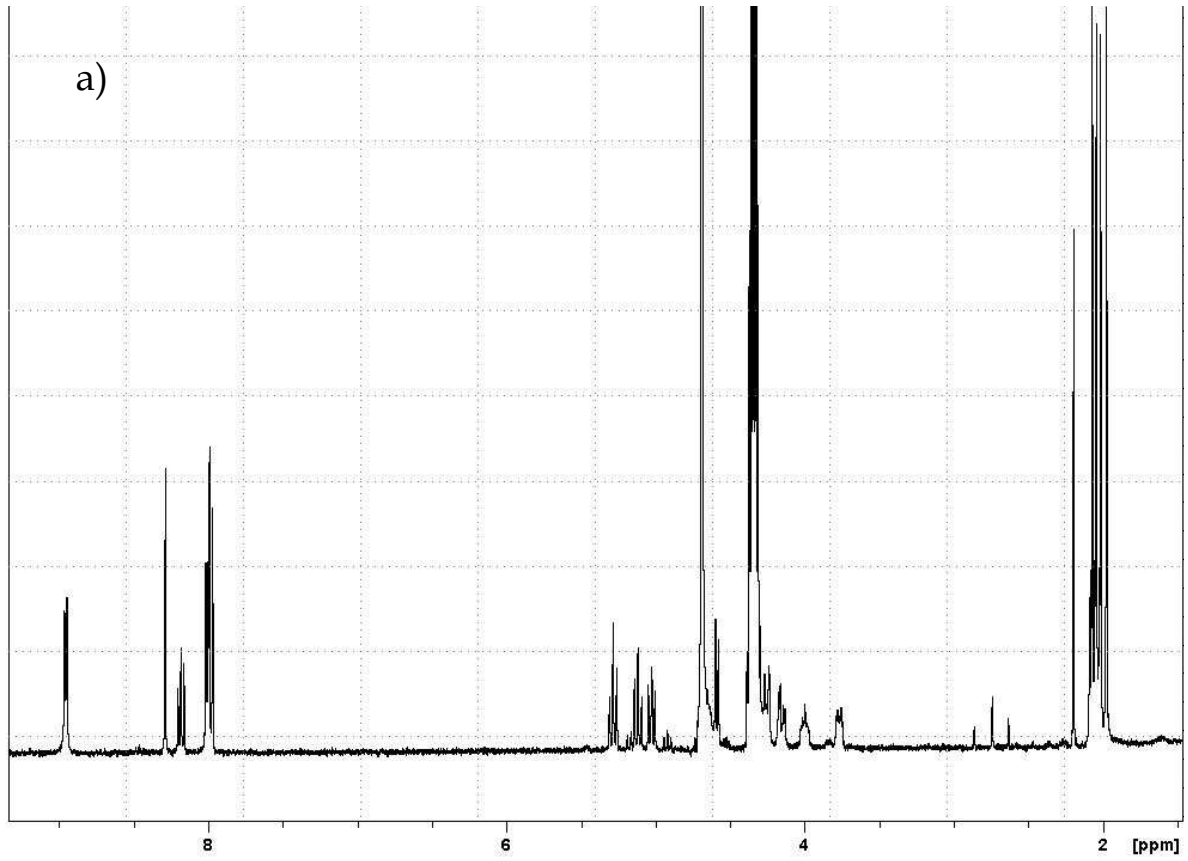

Figure 4.9 ^{1}H-NMR (hexafluoroisopropanhol-d_2, 400 MHz) of the complex **13**.

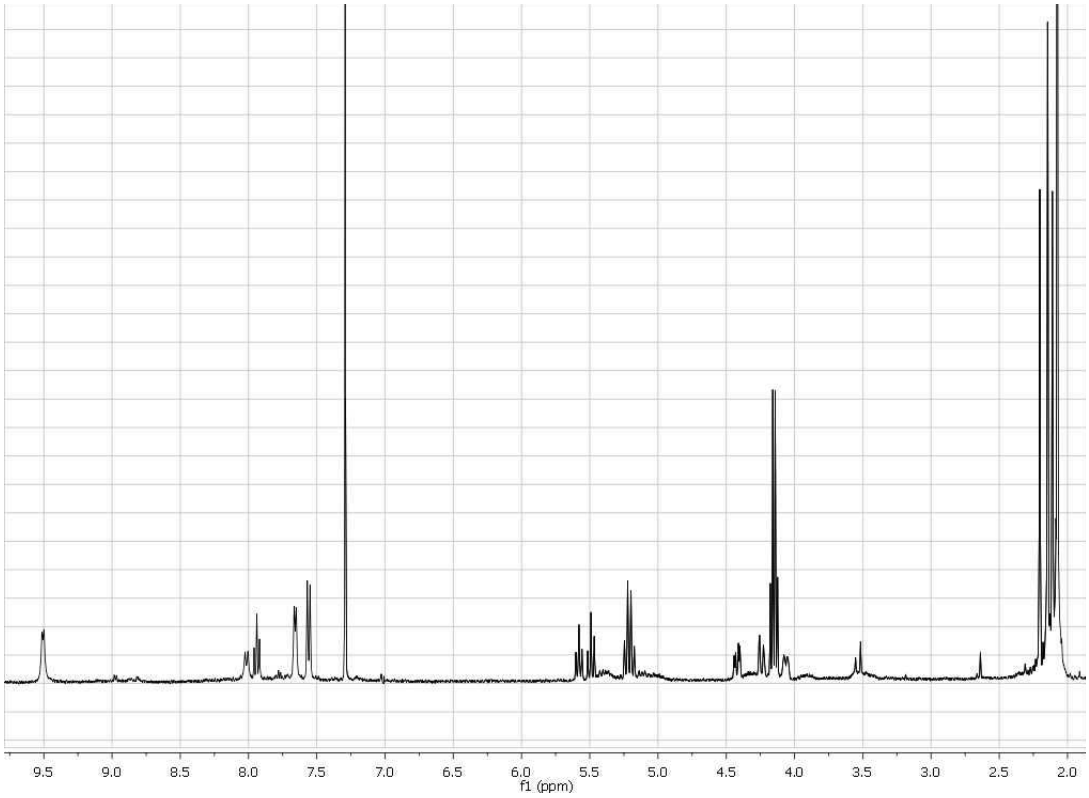

Figure 4.10 ^{1}H-NMR ($CDCl_3$, 400 MHz) of the complex **14**.

Interestingly, the synthesis of complexes **13** and **14** could therefore been easily achieved despite the presence of several C=O groups and bulky carbohydrate unit on the ancillary ligand.

The sugar moiety of the so obtained complexes were then deprotected using the usual Zemplen condition (fig. 4.11): the compounds **13** and **14** ware suspended in MeOH and a 1M solution of sodium methoxide in MeOH was added dropwise until pH 9 was reached. The reaction is stirred from two up to four hours until complete deprotection was achieved as determined from TLC and ESI-MS. As in the previous case, the ESI-MS confirmed the presence of the deprotected complexes. In the ^{1}H-NMR spectra the disappearance of the signals of the CH_3 of the acetyl groups between 1.90 and 2.00 ppm confirm the complete deprotection of the compounds **13** and **14** (fig. 4.12 and 4.13 respectively).

The deprotection of the ancillary ligands before complexation with platinum was also tried, but in this case, the reaction does not lead to the desired compound. So, seeing that the complexes survive the deprotection reaction, we decided to carry out only the deprotection on the Pt complexes.

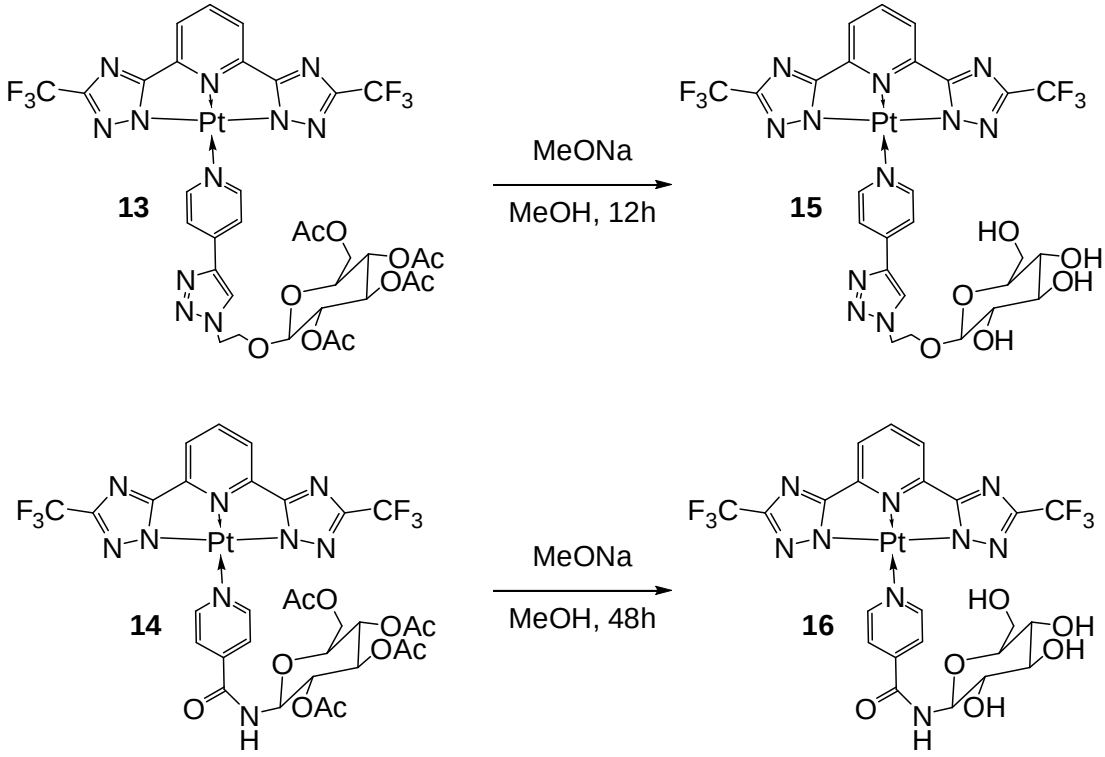

Figure 4.11 Deprotection of the complexes **13** and **14**.

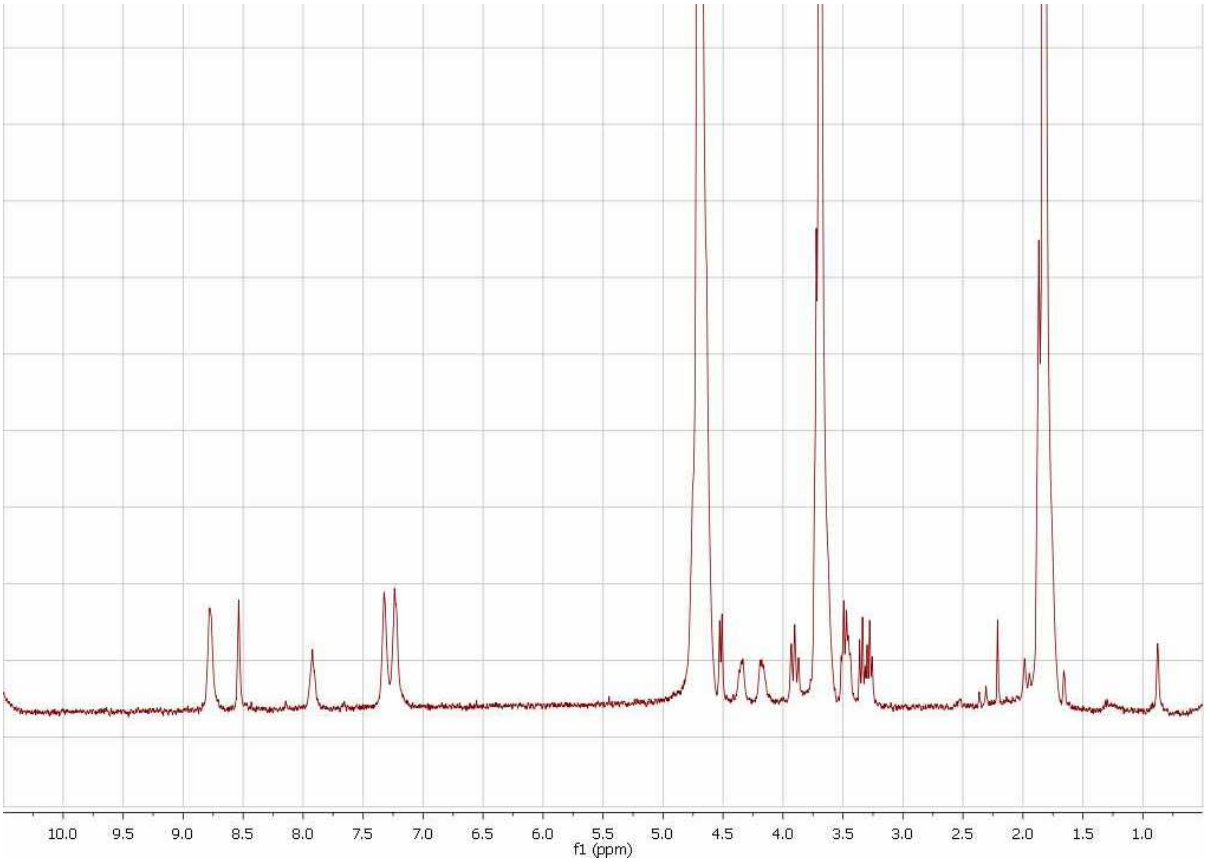

Figure 4.12 ^{1}H-NMR (D_2O/THF-d_8 2/1, 400 MHz) of the complex **15**.

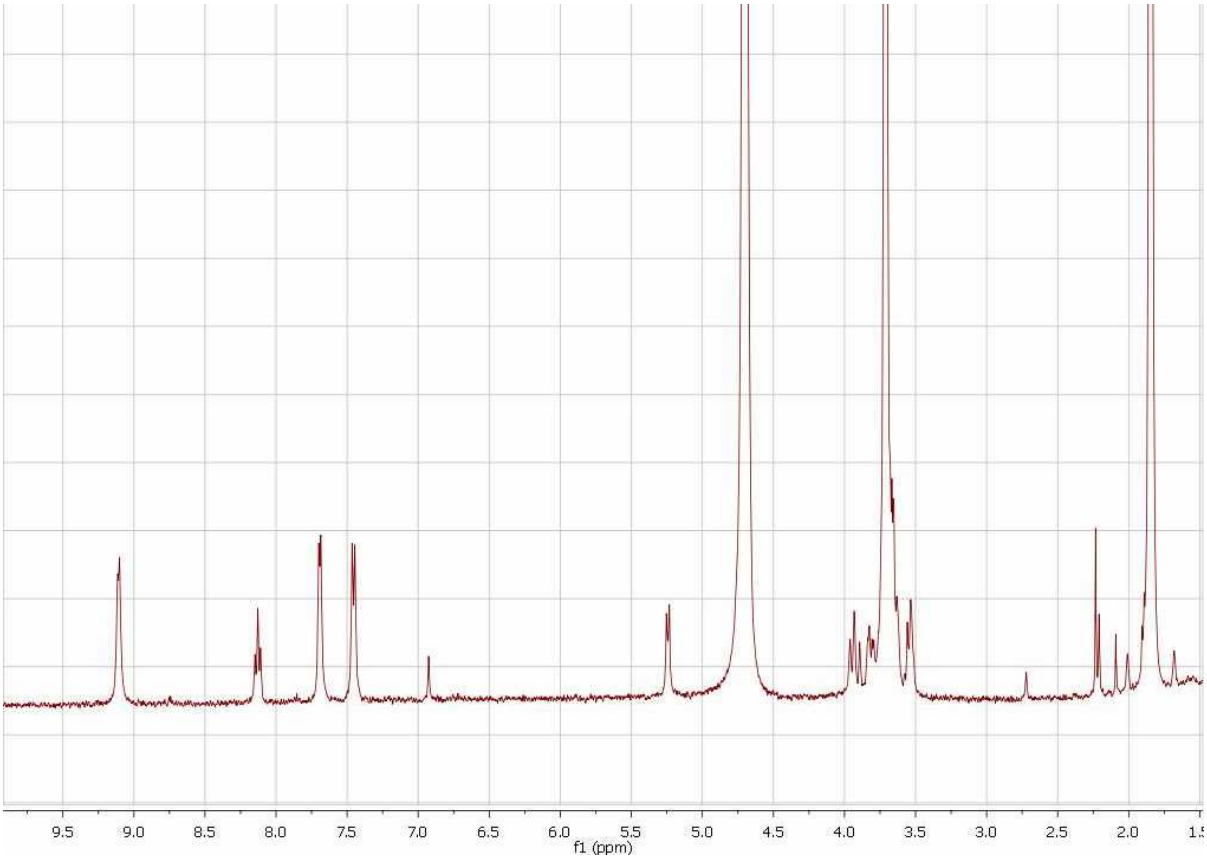

Figure 4.13 ^{1}H-NMR (D_2O/THF-d_8 2/1, 400 MHz) of the complex **16**.

.

4.2.3 Photophysics

The photophysical data are listed in table 4.1 and the absorption and emission spectra displayed in figure 4.12 and 4.13. In diluted solution, the complexes exhibit strong absorption bands (ε = 3.0 – 1.0 × 10^4 M^{-1} cm^{-1} and ε = 2.0 – 0.1 × 10^4 M^{-1} cm^{-1} for **13** and **14**, respectively) at high energy (λ < 350 nm). On the basis of closely related platinum complexes reported in literature,[10] these bands mainly correspond to convolution of singlet-manifold ligand-centered (^{1}LC) transitions involving the tridentate chromophoric ligand (π – π^*) with a minor contribution of metal-centered d orbitals. The low energy (λ = 350–500 nm), broader, featureless and less intense band ($\varepsilon \leq 10^3$ M^{-1} cm^{-1}) represents the S0 → S1 transition, and mainly involves the platinum d orbitals (partially mixed with the π orbitals of the tridentate ligand) and π^* orbitals of the chelate. This transition can be ascribed to the spin-allowed singlet-manifold metal-ligand-to-ligand charge-transfer (^{1}MLLCT). Upon excitation at 300 nm, at room temperature, both complexes **13** and **14**

showed structured emission at 464, 483 and 528 nm in hexafluoroisopropanol and chloroform, respectively, with a clear vibronic progression of 848-1765 cm^{-1}, as shown in figure 4.13a for **13** and figure 4.13b for **14**. Such finding suggests an emitting state with sizeable LC character. In solution, in both degassed and air-equilibrated conditions, the compounds emit with rather low quantum yield (Φ_{em} = 3–4%) and the excited-state decays display relatively fast bi-exponential kinetics in the order of hundred of nanoseconds and few nanoseconds for the longer and shorter component, respectively, which are only slightly sensitive to dioxygen quenching.

Going from room temperature to 77 K in $CHCl_3$/MeOH 1/3 glassy matrix, for both complexes the emission spectra display a more pronounced vibronic structure and only a slight hypsochromic shift (see fig. 4.14), with a concomitant prolongation of the excited-state lifetimes, that reach values as long as about 9 μs. All these findings are indicative of an emissive excited state with a mainly ^{3}LC character and a weak ^{3}MLCT nature.

Complex	**λ_{em} rt [nm]**	**λ_{em} 77K [nm]**	**Φ_{em} aer**	**Φ_{em} degas**	**τ (rt) aer [μs]**	**τ (rt) degas [μs]**	**τ (77K) [μs]**
13	464, 483, 528	454, 484, 521, ~600sh	0.03	0.04	0,316 (93%) 0,0028 (7%)	0,433	9,36 (54,4%) 3,042 (45,6%)
14	464, 483, 528	454, 484, 521, ~560sh	0.03	0.04	0,405 (83,14%) 0,004 (16,86%)	0,515 (69,3%) 0,005 (30,7%)	9,39 (8,25%) 0,009 (91,75%)

Table 4.1 Photophysical properties of complexes **13** and **14**, "sh" denotes a shoulder.

The studied compounds show similar properties to the Pt complexes present in literature.[10]

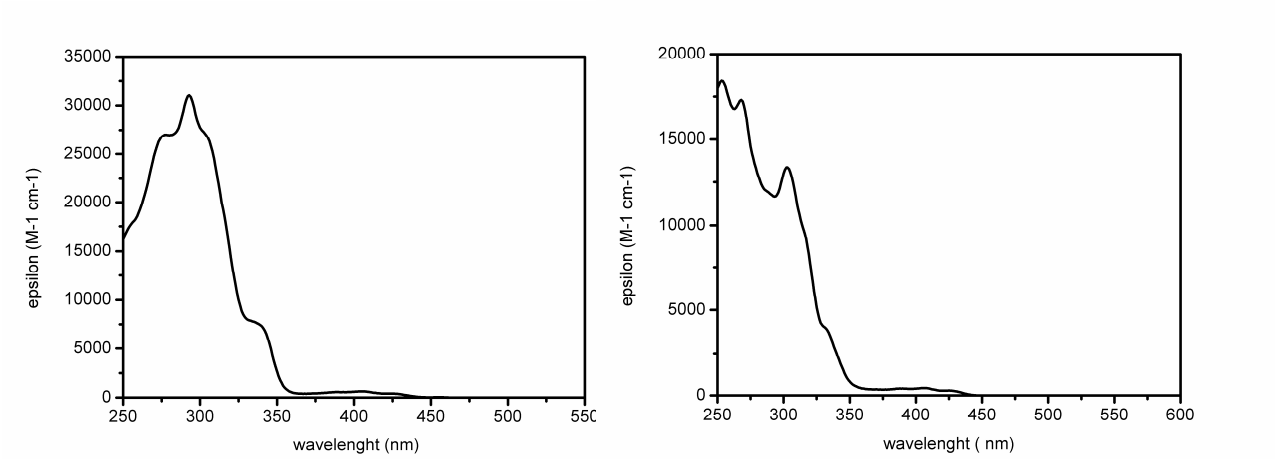

Figure 4.12 Absorption spectra (at concentration of 5*10^{-5} M) of **13** (hexafluoroisopropanol, left) and **14** ($CDCl_3$,right).

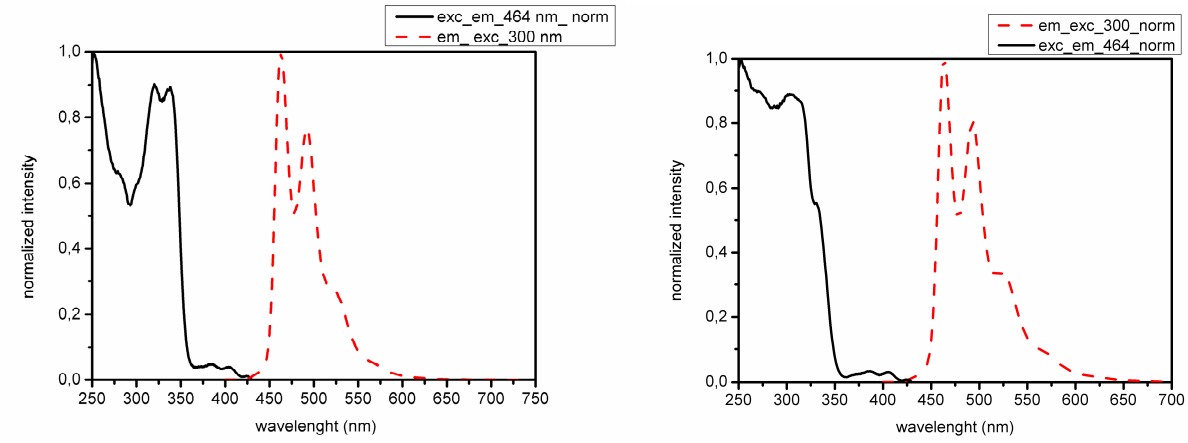

Figure 4.13 Excitation (black lines) and emission (red broken lines) spectra (at concentration of 5*10^{-5} M) of **13** (hexafluoroisopropanol, left) and **14** ($CDCl_3$, right). The samples were excited at λ_{exc} = 300 nm. The excitation spectra were recorded at λ_{em} = 464 nm.

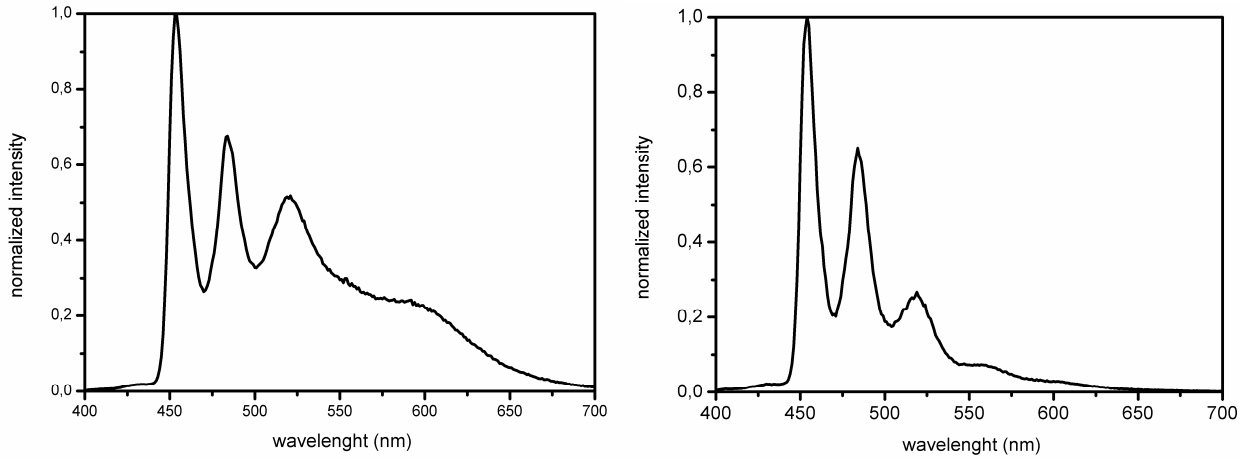

Figure 4.13 Emission spectra (at concentration of 1*10^{-6} M) of **13** (hexafluoroisopropanol, left) and **14** ($CDCl_3$,right) at 77 K in $CHCl_3$/MeOH 1/3 glassy matrix. The samples were excited at □$_{exc}$ = 300 nm..

The photophysical property of the deprotected compounds are now under study.

4.3 Conclusion

Four different luminescent N^N^N platinum complexes with a pyridine-based sugar functionalized ancillary ligand were synthesized using the same sugar (D-glucose) but different way to link the sugar to the pyridine ring and different distance between the sugar and the pyridine. Two complexes (**13** and **14**) present protected glucoside units and are soluble in organic solvents, and two others (**15** and **16**) present the deprotected glucoside moiety and are soluble in acqueous solvents. The different spacers were also chosen on the basis of easy and straightforward methods of conjugation and for their polarity that should also help the solubility in water of the deprotected compounds.

The photophysical properties of these complexes were studied up to now only on the protected compounds but the photophysical behaviour of the deprotected complexes is under investigation. From the absorption spectra of **13** and **14** in diluted solution is possible to underline two different contributions, one stronger, involving the tridentate chromoforic lingand (^{1}LC) and one less intense that can be ascribed to the spin-allowed singlet-manifold metal-ligand-to-ligand charge-transfer (^{1}MLLCT). Both complexes **13** and **14** showed structured emission with a clear vibronic progression, that suggests an emitting state with sizeable LC character. In solution, in both degassed and air-equilibrated conditions, the compounds emit with rather low quantum yield (Φ_{em} = 3–4%). Going from room temperature to 77 K for both complexes the emission spectra display a more pronounced vibronic structure and only a slight hypsochromic shift, with a concomitant elongation of the excited-state lifetimes, that reach values as long as about 9 μs. All these findings are indicative of an emissive excited state with a mainly ^{3}LC character and a weak ^{3}MLCT nature.

4.4 Experimental Part

General Information. All moisture sensitive reactions were carried out under nitrogen atmosphere, using previously oven-dried glassware. Dry $CHCl_3$ and dry DMF were prepared according to standard procedures, distilled before use and stored over 3 or 4 Å molecular sieves, respectively, while dry THF was obtained from commercial sources. Most of the solvents and reagents were obtained from commercial sources and used without further purification. Analytical TLCs were performed using prepared plates of silica gel (Merck 60 F-254 on aluminum) and then, according to the functional groups present on the molecules, revealed with UV light or using staining reagents: H_2SO_4 (5% in EtOH), basic solution of $KMnO_4$ (0.75% in H_2O). Merck silica gel 60 (70-230 mesh) was used for flash chromatography and for preparative TLC plates. ^1H NMR spectra were recorded on Bruker AV300 and Bruker AV400 spectrometers (observation of ^1H nucleus at 300 MHz and 400 MHz respectively) and ^{19}F NMR spectra on Bruker AV400 spectrometer (observation of ^{19}F nucleus at 376 MHz). All chemical shifts are reported in part per million (ppm) using the residual peak of the deuterated solvent, whose values are referred to tetramethylsilane (TMS, $\delta_{TMS} = 0$), as internal standard. Electrospray ionization (ESI) mass analyses were performed with a Waters spectrometer. Microwave reactions were performed using a CEM Discovery System reactor. Absorption spectra were measured on a Shimadzu UV-3600 spectrophotometer double-beam UV–VIS–NIR spectrometer and baseline corrected. Steady-state emission spectra were recorded on a Horiba Jobin−Yvon IBH FL-322 Fluorolog 3 spectrometer equipped with a 450 W xenon arc lamp, double-grating excitation, and emission monochromators (2.1 nm mm^{-1} of dispersion; 1200 grooves mm^{-1}) and a TBX-4-X single photon-counting detector. Emission and excitation spectra were corrected for source intensity (lamp and grating) and emission spectral response (detector and grating) by standard correction curves. Solution state time-resolved measurements were performed using the time-correlated single-photon counting (TCSPC) option of a Picoquant FluoTime 300 (PicoQuant GmbH, Germany). A pulsed laser diode LDH-P-C-375 (l = 375 nm, pulse FWHM <70ps, repetition rate 200 kHz – 40 MHz) was used to excite the sample and mounted directly on the sample chamber at 90°. Data analysis was performed using the commercially available software (FluoFit, PicoQuant).

1,2,3,4,6-penta-*O*-acetyl-β-D-glucopyranoside 2

In a two neck round bottom flask 6.32 g of sodium acetate (0.077 mol) were suspended in 28 mL of acetic anhydride (0.27 mol) and heated to 130 °C. At this temperature D-glucose (2.0 g, 0.011 mol) was slowly added. The mixture was stirred at 130°C for 2 h and checked via TLC (eluent: AcOEt/hexane 1:1). When the reaction was complete it was poured into a flask containing 150 mL of ice and water (5 times the amount of acetic anhydride). The mixture was then stirred at room temperature overnight. The solid formed was recovered by filtration on a Buchner funnel. Product **2** was obtained as white solid in 65% yield. **^{1}H NMR** (300 MHz, $CDCl_3$): δ (ppm) 5.71 (d, J = 8.1 Hz, 1H, H1), 5.25 (t, J = 9.3 Hz, 1H, H3), 5.16 – 5.09 (m, 2H, H2, H4), 4.29 (dd, J = 4.5, 12.6 Hz, 1H, H6), 4.11 (dd, J = 2.1, 12.6 Hz, 1H, H6'), 3.86 – 3.80 (m, 1H, H5), 2.10, 2.08, 2.03, 2.01 (4s, 12H, CH_3). The product shows the same physical-chemical properties reported in the literature. [2]

1-(2-Bromoethoxy)-2,3,4,6-tetra-*O*-acetyl-β-D-glucopyranoside 3

In a two neck round bottom flask 1.0 g of **2** (2.56 mmol) were suspended in 20 mL of dry CH_2Cl_2 and cooled with ice bath to 0 °C. At this temperature were added first bromoethanol (0.24 mL, 3.48 mmol), then borontrifluoride etherate (1.20 mL, 10.2 mmol). The mixture was slowly heated at room temperature. The reaction is stirred for 24h and checked via TLC (eluent: hex/AcOEt 6:4). When the reaction was complete, it was quenched with a saturated solution of NaCl (20mL). The organic layer was extracted and the water phase washed with CH_2Cl_2 (3x20mL). The combined organic phases were dried on anhydrous Na_2SO_4, filtered and evaporated under reduced pressure. The crude was purified by flash chromatography (eluent: hex/AcOEt 6:4) giving the product **3** as yellowish solid in 60% yield. **^{1}H NMR** (300 MHz, $CDCl_3$): δ (ppm) 5.20 (t, J = 11.7 Hz, 1H, H3), 5.09 – 4.96 (m, 2H, H2, H4), 4.55 (d, J = 7.8 Hz, 1H, H1), 4.24 (dd, J = 4.5, 12.3 Hz, 1H, H6), 4.15 – 4.10 (m, 2H, H6', BrCH_2aCH_2), 3.83 – 3.76 (m, 1H, BrCH_2bCH_2), 3.72 – 3.66 (m, 1H, H5), 3.46 – 3.41 (m, 2H, CH_2CH_2Br), 2.09, 2.05, 1.99, 1.98 (4s, 12H, CH_3). The product shows the same physical-chemical properties reported in the literature. [3]

1-(2-Azidoethoxy)-2,3,4,6-tetra-*O*-acetyl-β-D-glucopyranoside 4

In a two neck round bottom flask, 0.228 g of **3** (0.5 mmol) were suspended in 4 mL of dry DMF. Then sodium azide (0.097 g, 1.5 mmol) was added. The mixture was heated at 65 °C

and stirred for 24h, checked via TLC (eluent: hex/AcOEt 6:4). When the reaction was complete, it was quenched with water (5mL) and extracted with AcOEt (5mL). The water was washed with water (2x5mL). The combined organic phases were dried on anhydrous Na_2SO_4, filtered and evaporated under reduced pressure. The product **4** was obtained as white solid in 87% yield. **^{1}H NMR** (300 MHz, $CDCl_3$): δ (ppm) 5.12 (t, J = 9.3 Hz, 1H, H3), 5.02 – 4.88 (m, 2H, H4, H2), 4.52 (d, J = 7.8 Hz, 1H, H1), 4.16 (dd, J = 4.8, 12.4 Hz, 1H, H6), 4.05 (dd, J = 2.7, 12.4 Hz, 1H, H6'), 3.97 – 3.90 (m, 1H, CH_2aCH$_2$), 3.72 – 3.66 (m, 1H, H5), 3.46 – 3.41 (m, 2H, CH_2aCH$_2$Br) 3.67 – 3.57 (m, 2H, H5, CH_2bCH$_2$Br), 3.43 – 3.35 (m,1H, CH$_2$$CH_2$aBr), 2.23 – 3.16 (m, 1H, CH$_2$$CH_2$bBr), 1.98, 1.95, 1.93, 1.90 (4s, 12H, CH_3). The product shows the same physical-chemical properties reported in the literature.[3]

4-(Trimethylsilylethynyl)pyridine 6

A two neck round bottom flask containing $Pd(PPh_3)_2Cl_2$ (0.03 g, 0.044 mmol), CuI (0.09 g, 0.49 mmol) and 4-iodopyridine (1g, 4.9 mmol) was evacuated and filled with nitrogen three times. Then diisopropylamine (3.56 mL, 25.3 mmol) and THF (20 mL) were added via a syringe while stirring and the solution is bubbled 20 min. with N_2. At this point trimethylsilylacetylene (1.38 mL, 9.76 mmol) was added. The dark brown mixture was stirred for 18 h at room temperature. Reaction mixture was poured into water and extracted with CH_2Cl_2 (20mL×3). The collected organic layers were dried with $MgSO_4$ and filtered. Solvent was removed via rotary evaporation. The product was isolated by column chromatography (eluent: cyclohexane/AcOEt 1/1) which afforded **6** as a dark oil in 87 % yield. **^{1}H NMR** (400 MHz, $CDCl_3$) δ (ppm) 8.62 (bs, 2 H, pyridine CH), 7.33 (bs, 2 H, pyridine CH), 0.26 (s, 9 H, SiCH_3). The product shows the same physical-chemical properties reported in the literature.[4]

4-Ethynylpyridine 7

Compound **6** (0.719 g, 4.10 mmol) was dissolved in MeOH (10 mL) and CH_2Cl_2 (5 mL) in a round bottom flask. Anhydrous KOH (0.460 g, 8.20 mmol) was added to the mixture which was then stirred for 3 h. The reaction was partitioned between CH_2Cl_2 and water, and the aqueous layer was further extracted two times (2x15 mL CH_2Cl_2). The combined organic solution was then dried with anhydrous $MgSO_4$, and the solvent was removed by rotary evaporation which afforded **7** as an off-white solid in 50% yield. **^{1}H NMR** (400

MHz, $CDCl_3$) δ (ppm) 8.60 (dd, J = 1.5, 4.4 Hz, 2 H, pyridine CH), 7.35 (dd, J = 1.5, 4.4 Hz, 2 H, pyridine CH), 3.30 (s, 1 H, CC*H*). The product shows the same physical-chemical properties reported in the literature. [4]

2-(Acetoxymethyl)-6-(2-(4-(pyridin-4-yl)-1H-1,2,3-triazol-1-yl)ethoxy)tetrahydro-2H-pyran-3,4,5-triyl triacetate 8

In a microwave tube **4** (60 mg, 0.150 mmol), **7** (10 mg, 0.097 mmol), $CuSO_4$ (7 mg, 0.029 mmol) and sodium ascorbate (11mg, 0.058 mmol) were dissolved in 1mL of DMF and 5 drops of water. The reaction was heated at 80 °C by microwave irradiation (150W) for 20 min. When the reaction was complete (checked with TLC eluent CH_2Cl_2/MeOH 95/5) the mixture is poured into water and extracted with CH_2Cl_2 (2x2mL). The combined organic layer were dried on anhydrous $MgSO_4$, filtered and the solvent is removed under reduced pressure. The crude was purified via column cromatography (eluent CH_2Cl_2/MeOH 9/1) giving the pure product as a yellowish oil in 75% yield. **^{1}H-NMR** (400 MHz, $CDCl_3$): δ (ppm) 8.79 (bs, 2H, pyridine CH), 8.20 (s, 1H, triazole CH), 7.84 (bs, 2H, pyridine CH), 5.15 (t, 1H, J = 9.52 Hz, H3), 5.06 – 5.97 (m, 2H, H4, H2), 4.70 – 4.66 (m, 1H, H8), 4.58 – 4.52 (m, 1H, H8'), 4.44 (d, 1H, J = 7.8 Hz, H1), 4.26 – 4.20 (m, 2H, H6, H7), 4.11 – 4.07 (m, 1H, H6'), 3.91 – 3.85 (m, 1H, H7'), 3.69 – 3.65 (m, 1H, H5), 2.03, 1.97, 1.93, 1.71 (4s, 12H, CH_3). **^{13}C-NMR** (100 MHz, $CDCl_3$): δ (ppm) 170.5, 170.1, 169.7, 169.4 (CO), 144.7 (triazole C), 143.3 (pyridine C), 125.4 (triazole CH), 121.4, 121.3 (pyridine CH), 100.3 (C1), 72.1 (C3, C5), 71.1 (C2), 68.2 (C4), 67.0 (OCH_2), 61.7 (C6), 50.5 (NCH_2), 20.7, 20.5 (CH_3). **ESI-MS**: m/z 521.19 $(M+H)^+$, 543.17 $(M+Na)^+$.

Complex 13

In a two neck round bottom flask $PtCl_2DMSO_2$ (105 mg, 0.25 mmol) and CF_3 ligand (86 mg, 0.25 mmol) was dissolved in $CHCl_3$ (11.3 mL) and DIPEA (104μL, 0.59 mmol) under N_2. The solution was stirred for 20 min. Compound **8** (150mg, 0.30 mmol) was added and the solution was heated at 60 °C overnight. When the reaction was complete (checked with TLC eluent AcOEt/Acetone 8/2) the solvent is removed by rotary evaporation. The compound was purified by precipitation from CH_2Cl_2. **^{1}H-NMR** (400MHz, hexafluoro isopropanol-d_2): δ (ppm) 8.99 (d, 2H, J = 6.8 Hz, pyridine CH), 8.33 (s, 1H, triazole H), 8.22 (t, 1H, J = 8 Hz, ligand CH), 8.05 – 8.01 (m, 4H, ligand and pyridine CH), 5.32 (t, 1H, J = 9.4

Hz, H3), 5.16 (t, 1H, J = 9.4 Hz, H4), 5.06 (t, 1H, J = 8 Hz, H2), 4.63 (d, 1H, J = 8 Hz, H1), 4.42 – 4.28 (under the solvent peak, 4H, CH_2), 4.21 – 4.17 (m, 1H, H6), 4.05 – 3.99 (m, 1H, H6'), 3.82 – 3.79 (m, 1H, H5), 2.13, 2.07, 2.04, 1.91 (4s, 12H, CH_3). **^{19}F-NMR** (376 MHz, hexafluoro isopropanol-d2): δ (ppm) -60.82 (C*F*$_3$). **ESI-MS**: m/z 1063.17 $(M+Na)^+$.

1-Azido-2,3,4,6-tetra-*O*-acetyl-β-D-glucopyranoside 10

In a round bottom flask α-bromoglucose (1g, 2.52 mmol),NaN_3 (0.33 g, 5.03 mmol) and tetrabutylammonium hydrogen sulfate (0.85 g, 2.52 mmol) were dissolved in CH_2Cl_2 (10mL). A saturated solution of $NaHCO_3$ (10mL) is added and the solution is vigorously stirred for 2 hr. The reaction is monitored with TLC (eluent AcOEt/CH_2Cl_2 1/1). The mixture was poured in AcOEt (4 times the volume of CH_2Cl_2) and extracted. The organic layer is washed with water, a saturated solution of $NaHCO_3$ and brine, then dried on anhydrous $MgSO_4$. The solvent was removed by rotary evaporation giving **10** in 91% yield. **^{1}H-NMR** (400 MHz, $CDCl_3$): δ (ppm) 5.19 (t, 1H, J = 9.6 Hz, H3), 5.07 (t, 1H, J = 6 Hz, H4), 4.91 (t, 1H, J = 9.2 Hz, H2), 4.64 (d, 1H, J = 9.2 Hz, H1), 4.24 (dd, 1H, J_1 = 4.8 Hz, 12.4 Hz, H6), 4.15 – 4.05 (m, 1H, H6'), 3.80 – 3.77 (m, 1H, H5), 2.06, 2.05, 2.00, 1.97 (4s, 12H, CH_3). The product shows the same physical-chemical properties reported in the literature. [11]

1-Amino-2,3,4,6-tetra-*O*-acetyl-β-D-glucopyranoside 11

In a Parr reactor, compound **10** (1.7 g, 4.55 mmol) was dissolved in CH3CN (60ml) and Pd/C (catalytic amount) was added. The reaction was stirred at room temperature overnight (H_2 pressure = 2bar). When the reaction was complete (checked with TLC, eluent CH_2Cl_2/MeOH 9/1) the catalyst was filtered off and the solvent was removed by rotary evaporation. The product **11** was obtained as a white solid in a 90% yield. **^{1}H-NMR** (400 MHz, $CDCl_3$): δ (ppm) 5.27 (t, 1H, J = 9.6 Hz, H3), 5.06 (t, 1H, J = 9.6 Hz, H4), 4.85 (t, 1H, J = 9.6 Hz, H2), 4.27 – 4.21 (m, 2H, H2, H6), 4.13 (dd, 1H, J = 2.4, 12.4, H6'), 3.74 – 3.69 (m, 1H, H5), 2.12, 2.09, 2.05, 2.03 (4s, 12H, CH_3). The product shows the same physical-chemical properties reported in the literature. [12]

N-(2,3,4,6-tetra-*O*-acetyl-β- D -Glucopyranosyl)-pyridine-4-carboxamide 12

In a round bottom flask isonicotinic acid (50 mg, 0.4 mmol), EDC (78 mg, 0.4 mmol) and DMAP (50 mg, 0.4 mmol) were dissolved in dry THF (5mL) and the reaction is stirred at 0 °C for 5 min. Then the sugar **11** was added and the mixture was stirred ad room temperature overnight. The reaction was checked with TLC (eluent AcOEt). When the reaction was complete was poured into AcOEt and washed with water (5mL) and brine (5mL). The organic phase is dried over anhydrous Na_2SO_4 and the solvent was removed via rotary evaporation. The crude was purified via column chromathography giving the product as a white solid in 50% yield. **^{1}H-NMR** (400 MHz, $CDCl_3$): 8.75 (d, 2H, J = 5.6 Hz, pyridine CH), 7.60 (d, 2H, J = 5.6 Hz, pyridine CH), 7.55 (d, 1H, J = 6.6 Hz, N*H*), 5.45 – 5.36 (m, 2H, H3, H1), 5.11 – 5.00 (m, 2H, H4, H2), 4.32 (dd, 1H, J = 4.4, 14.2Hz, H6), 4.13 – 4.08 (m, 1H, H6'), 3.93 – 3.89 (m, 1H, H5), 2.06, 2.05, 2.04, 2.03 (4s, 12H, CH_3). The product shows the same physical-chemical properties reported in the literature. [9]

Complex 14

In a two neck round bottom flask $PtCl_2DMSO_2$ (46 mg, 0.1 mmol) and CF_3 ligand (38 mg, 0.1 mmol) was dissolved in $CHCl_3$ (7 mL) and K_2HPO_4 (57 mg, 0.33 mmol) under N_2. The solution was stirred for 20 min. Compound **12** (59mg, 0.13 mmol) was added and the solution was stirred ad room temperature overnight. When the reaction was complete (checked with TLC eluent AcOEt/Acetone 8/2) the mixture is diluted into $CHCl_3$ and extracted with water. The solvent is removed by rotary evaporation. **^{1}H-NMR** (400MHz, $CDCl_3$): δ (ppm) 9.50 (d, 2H, J = 5.6 Hz, pyridine CH), 8.01 (d, 1H, J = 8.0 Hz, N*H*), 7.94 (t, 1H, J = 8.0 Hz, ligand CH), 7.66 (d, 2H, J = 5.6 Hz, pyridine CH), 7.56 (d , 2H, J = 8 Hz, ligand CH), 5.58 (t, 1H. J = 8.8 Hz, H3), 5.49 (t, 1H, J = 9.2 Hz, H4), 5.21 (m, 2H, H2, H1), 4.42 (dd, 1H, J = 4.4, 12.8 Hz), 4.24 (d, 1H, J = 12.8 Hz, H6'), 4.08 – 4.05 (m, 1H, H5), 2.20, 2.14, 2.11, 2.08 (4s, 12H, CH_3). **^{19}F-NMR** (376 MHz, $CDCl_3$): δ (ppm) 61,03 (CF_3) **ESI-MS**: m/z 1017.15 $(M+Na)^+$.

Complex 15

In a round bottom flask, complex **13** (80mg, 0.075) was suspended in MeOH and a solution 1M of MeONa was added dropwise until pH 9. The reaction was stirred ad room temperature for four hours and checked with TLC (eluent AcOEt/acetone 8/2). The

reaction was centrifuged and the solid was dried under vacuum. **^{1}H-NMR** (400 MHz, D_2O/THF-d_8 = 2/1): δ (ppm) 8.78 (bs, 2H, pyridine CH), 8.54 (bs, 1H, triazole CH), 7.92 (bs, 1H, ligand CH), 7.32 (bs, 2H, pyridine CH), 7.24 (bs, 2H, ligand CH), 4.52 (d, 1H, J = 8 Hz, H1), 4.35 – 4.33 (m, 2H, CH_2), 4.19 – 4.16 (m, 2H, CH_2), 3.93 – 3.87 (m, 1H, H4), 3.72 – 3.68 (under solvent peak, H3), 3.51 – 3.46 (m, 2H, H5, H6') 3.36 – 3.26 (m, 2H, H2 H6). **ESI-MS:** m/z 895 $(M+H)^+$, 917 $(M+Na)^+$.

Complex 16

In a round bottom flask, compound **14** (15mg, 0.015) was suspended in MeOH and a solution 1M of MeONa was added drop by drop until pH 9. The reaction was stirred ad room temperature for two hours and checked with TLC (eluent AcOEt). The reaction was centrifuged and the solid was dried under vacuum. **^{1}H-NMR** (400 MHz, D_2O/THF-d_8 = 2/1): δ (ppm) 9.10 (d, 2H, J = 5.6 Hz, pyridine CH), 8.12 (t, 1H, J = 8 Hz, ligand CH), 7.69 (d, 2H, J = 5.6 Hz, pyridine CH), 7.45 (d, 2H, J = 8 Hz, ligand CH), 6.92 (NH), 5.24 (d, 1H, J = 8.4 Hz, H1), 3.92 – 3.91 (m, 1H, H4), 3.81– 3.80 (m, 1H, H3), 3.71 -3.69 (under solvent peak, m, 2H, H5, H6), 3.64 – 3.63 (m, 1H, H2), 3.55 – 3.53 (m, 1H, H6') . **ESI-MS**: m/z 849 $(M+Na)^+$.

References

[1] E. Baggaley, J.A. Weinstein, J.A.G. Williams, *Coordination Chemistry Reviews*, **2012**, *256*, 1762.

[2] Y. Ma, H. Yang, Y. Wu, C. Yang, X. Liu, Q. Zhao, H. Wu, J. Liang, F. Li, W. Huang, *J. Mater. Chem.*, **2011**, *21*, 18974 and references therein.

[3] Q. Zhao, C. Huang, F. Li, *Chem. Soc. Rev.*, **2011**, *40*, 2508.

[4] L. De Cola, M. Mauro, N. Seda Kehr, C.A. Strassert, *PCT Int. Appl.*, **2012**, WO 2012117082 A1 20120907.

[5] C.A. Strassert, C.-H. Chien, M.D. Galvez Lopez, D. Kourkoulos, D. Hertel, K. Meerholz, L. De Cola, *Angew. Chem. Int. Ed.*, **2011**, *50*, 946.

[6] N. Kumar Allampally, C.A. Strassert, L. De Cola, *Dalton Trans.*, **2012**, *41*, 13132.

[7] M.L. Wolfrom, A. Thompson, *Methods Carbohydr. Chem.*, **1963**, *2*, 2112.

[8] J. Dahmen, T. Frejd, G. Grönberg, T. Lave, G. Magnusson, G. Noori, *Carbohyd. Res.*, **1983**, *116*, 303.

[9] M.A. Bartucci, P.M. Wierzbicki, C. Gwengo, S. Shajan, S.H. Hussain, J.W. Ciszek, *Tetrahedron Letters*, **2010**, *51*, 6839.

[10] M. Mydlak, M. Mauro, F. Polo, M. Felicetti, J. Leonhardt, G. Diener, L. De Cola, C-A. Strassert, *Chem. Mater.*, **2011**, *23*, 3659.

[11] S. Deng, U. Gangadharmath, C.-W.T. Chang, *J. Org. Chem.* **2006**, *71,* 5179.

[12] H. Paulsen, K.-W. Pflughaupt, *2nd ed. In The Carbohydrates*, Chemistry and Biochemistry, Vol. IB, Academic: New York, **1980**, 881.